THE UNIVERSITY OF QUEENSLAND

SCHOOL OF CIVIL ENGINEERING

REPORT CH84/11

PHYSICAL AND NUMERICAL MODELLING OF NEGATIVE SURGES IN OPEN CHANNELS

AUTHOR: Martina REICHSTETTER and Hubert CHANSON

HYDRAULIC MODEL REPORTS

This report is published by the School of Civil Engineering at the University of Queensland. Lists of recently-published titles of this series and of other publications are provided at the end of this report. Requests for copies of any of these documents should be addressed to the Civil Engineering Secretary.

School of Civil Engineering
The University of Queensland
Brisbane QLD 4072
AUSTRALIA

Telephone: (61 7) 3365 4163
Fax: (61 7) 3365 4599

URL: http://www.eng.uq.edu.au/civil/

First published in 2011 by
School of Civil Engineering
The University of Queensland, Brisbane QLD 4072, Australia

ISBN No. 9781742720388

The University of Queensland, St Lucia QLD

Physical and Numerical Modelling of Negative Surges in Open Channels

by

Martina REICHSTETTER

MPhil student, The University of Queensland, School of Civil Engineering, Brisbane QLD 4072, Australia

and

Hubert CHANSON

Professor, The University of Queensland, School of Civil Engineering, Brisbane QLD 4072, Australia, Email: h.chanson@uq.edu.au

REPORT No. CH84/11

ISBN 9781742720388

School of Civil Engineering, The University of Queensland, October 2011

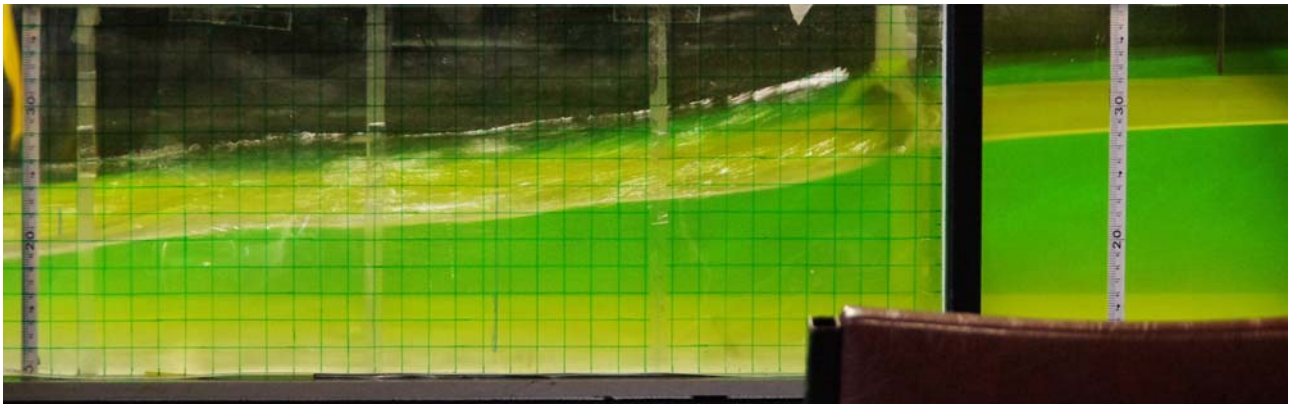

Negative surge generation immediately upstream of the gate about 0.6 s after gate opening - Negative wave leading edge propagating from left to right

ABSTRACT

Negative surges are caused by a sudden change in flow resulting from a decrease in water depth. New experiments were conducted in a horizontal channel (L = 12 m, W = 0.5 m) to record the unsteady water depth and turbulence in negative surges propagating upstream against an initially-steady flow. The data were collected using video-imagery, acoustic displacement meters and acoustic Doppler velocimetry (ADV). The physical observations showed that the leading edge of negative surge propagated upstream with a celerity which varied with time. During the first initial instants following the surge formation, the negative surge leading edge accelerated ad its celerity increased with time up to x_{Gate}-x = $4d_o$. After the acceleration phase, the negative surge propagation was more gradual: the surge leading edge was very flat and barely perceptible, and its celerity tended to decrease slowly with increasing distance from the gate. The data implied some deceleration in a manner which is contrary to theoretical considerations. The physical measurements highlighted that the negative surges were associated with some flow acceleration. The turbulent velocity data highlighted some increased turbulence occurring beneath the negative surge with large velocity fluctuations and large Reynolds stress components. The velocity fluctuations and turbulent stresses were significantly larger than in the initially steady flow and in the final flow motion. The physical data were used to test an analytical solution of the Saint-Venant equations (the simple wave solution) and some 1-D and 2-D numerical model results. The findings showed that the negative surge propagation was relatively little affected by the boundary friction. For a relatively simple geometry such as the prismatic rectangular flume used in the present study, the physical data were best modelled by the simple wave theory, although the numerical model results were qualitatively in agreement with the experimental observations. The present results suggested that the negative surge remains a challenging topic for the computational modellers.

Keywords: Negative surges, Unsteady open channel flow, Physical modelling, Numerical modelling, Turbulence, Turbulent Reynolds stress tensor, Negative waves.

TABLE OF CONTENTS

LIST OF SYMBOLS

The following symbols are used in this report:

A flow cross-section area (m^2);

B channel width (m);

C celerity (m/s) of a small distance in a shallow water: $C = \sqrt{g\,d}$ in a rectangular channel;

C_c dimensionless coefficient of contraction;

d water depth (m) measured above the invert;

d_c critical flow depth: $d_c = \sqrt[3]{Q^2/(gB^2)}$ in a rectangular channel;

E specific energy (m) defined as:

$$E = d + \frac{V_x^{\,2}}{2g};$$

Fr Froude number locally defined as:

$$Fr = \frac{V}{\sqrt{g\,d}};$$

f Darcy-Weisbach friction factor;

g gravity constant: g = 9.80 m/s^2 in Brisbane QLD, Australia;

H total head (m);

h initial undershoot gate opening (m);

i integer;

N integer;

P pressure (Pa);

Q water discharge (m^3/s);

R_s free-surface radius (m) of curvature;

S_f friction slope:

$$S_f = -\frac{\partial H}{\partial x}$$

S_o bed slope: $S_o = \sin\theta$;

t time (s);

U celerity (m/s) of negative surge leading edge for an observer standing on the bank;

V 1- flow velocity: V = Q/A;

2- instantaneous velocity component (m/s);

V_x instantaneous longitudinal velocity component (m/s);

V_y instantaneous transverse velocity component (m/s);

V_z instantaneous vertical velocity component (m/s);

V_* shear velocity (m/s): $V_* = \sqrt{\tau_o/\rho}$;

$\overline{V}$ ensemble-average velocity component (m/s);

v turbulent velocity fluctuation (m/s): $v = V - \overline{V}$;

v_x longitudinal turbulent velocity fluctuation (m/s);

v_y transverse turbulent velocity fluctuation (m/s);

v_z vertical turbulent velocity fluctuation (m/s);

v'	standard deviation of the turbulent velocity fluctuation (m/s);
w_o	particle fall velocity (m/s);
x	longitudinal distance (m) positive downstream, with x = 0 at test section upstream end;
x_{Gate}	longitudinal co-ordinate (m) of the tainter gate (x_{Gate} = 11.15 m herein);
x_s	longitudinal co-ordinate (m) of negative surge leading edge;
y	transverse co-ordinate (m) positive towards the left sidewall;
z	vertical distance (m) positive upwards, with z = 0 at the bed;

α	angle between tainter gate and horizontal;
δ	boundary layer thickness (m);
Γ	dimensionless parameter;
μ	dynamic viscosity (Pa.s) of water;
θ	angle between channel bed and horizontal;
ρ	water density (kg/m^3);
σ	surface tension between air and water (N/m);
τ_o	boundary shear stress (Pa);

Subscript

Gate	flow properties of tainter gate;
G1	flow properties immediately upstream of tainter gate;
G2	flow properties immediately downstream of tainter gate;
max	maximum value;
min	minimum value;
o	initial flow conditions: i.e., upstream of the negative surge leading edge;
x	longitudinal direction positive downstream;
y	transverse direction positive towards the left;
z	vertical direction positive upwards;
25	first quartile: i.e., value for which 25% of data are smaller;
75	third quartile: i.e., value for which 75% of data are smaller;

Abbreviations

ADV	acoustic Doppler velocimeter;
EA	ensemble-average;
PDF	probability density function;
Std	standard deviation;
s	second.

1. INTRODUCTION

A negative surge, also called negative wave, is an unsteady open channel flow motion characterised by a decrease with time of the flow depth (Jaeger 1956, Henderson 1966, Montes 1998). Negative surges may occur downstream of a control structure when the discharge is reduced or upstream of a gate that is opened suddenly. For a stationary observer the negative surge appears to be a gentle lowering of the free surface (Fig. 1-1).

The knowledge into the hydraulics of negative surges in open channels remains limited despite the classical experiments of Favre (1935) and some well-detailed presentations in textbooks (Montes 1998, Sturm 2001, Chanson 2004). The present study investigates physically and numerically the unsteady flow properties of negative surges. Both one-dimensional and two-dimensional modelling results are compared with physical data and an analytical solution based upon the method of characteristics. It is the aim of this work to characterise the unsteady open channel flow motion including free-surface properties and velocity field in negative surges.

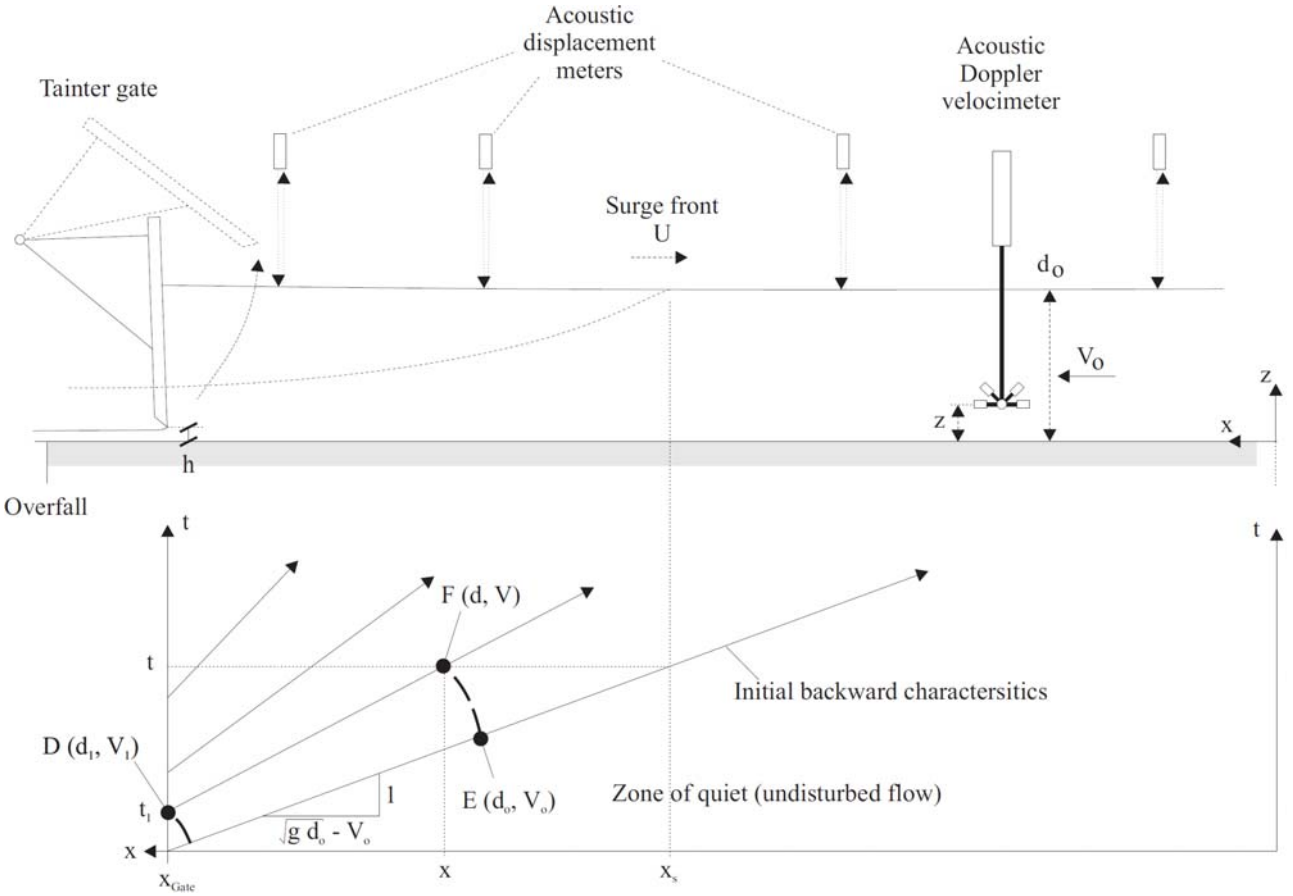

Fig. 1-1 - Sketch of a negative surge propagating upstream and characteristic diagram for the simple wave solution

Some basic theoretical developments are presented in section 2. Section 3 describes the

experimental apparatus and procedures. The results are presented in sections 4 to 5. Appendix A shows some photographs of the physical experiments. Appendix B describes the initial and final flow conditions. Appendices C and D present some turbulent velocity and Reynolds stress results respectively. Appendix E describes the CFD model application.

2. BASIC ANALYSIS OF NEGATIVE SURGES

A negative surge is an unsteady open channel flow which may be solved using the one-dimensional unsteady open channel flow equations called the Saint-Venant equations:

$$B\frac{\partial d}{\partial t} + A\frac{\partial V}{\partial x} + BV\frac{\partial d}{\partial x} + V\left(\frac{\partial A}{\partial x}\right)_{d=constant} = 0 \quad (2\text{-}1)$$

$$\frac{\partial V}{\partial t} + V\frac{\partial V}{\partial x} = -g\frac{\partial d}{\partial x} + g(S_o - S_f) \quad (2\text{-}2)$$

where d and V are respectively the water depth and flow velocity, x is the longitudinal co-ordinate positive downstream, B is the free-surface width, g is the gravity acceleration, S_o is the bed slope and S_f is the friction slope (Montes 1998, Chanson 2004). Equation (2-1) is the continuity equation and Equation (2-2) is the dynamic equation. The Saint-Venant equations may be transformed into a characteristic system of equations. For a negative surge generated by the rapid opening of a downstream gate, the characteristic diagram forms a series of diverging lines as illustrated in Figure 1-1.

The characteristic system of equations may be solved analytically for the simple wave approximation when the initial flow conditions (d_o, V_o) are constant along a channel, and $S_o = S_f$ at any time and space. This includes the case $S_o = S_f = 0$. The simple wave solution expresses the velocity and flow depth (V, d) at any point (x, t) along a forward characteristic line as a function of the initial flow properties (V_o, d_o) and the flow depth d_1 at $x = x_{Gate}$ for $t = t_1$ (Fig. 1-1):

$$V = V_o + 2(\sqrt{gd_o} - \sqrt{gd_1}) \qquad x_s < x < x_{Gate} \quad (2\text{-}3)$$

$$d = d_1 \quad (2\text{-}4)$$

where V is positive in the downstream direction. Equations (2-3) and (2-4) provide the complete simple wave solution when the boundary condition is the time-variations of water depth at the gate ($x = x_{Gate}$). Since $d_1 < d_o$, Equation (2-3) implies a flow acceleration. The longitudinal free-surface profile may be derived from the equation of the characteristics D-F issued from the gate:

$$x_{Gate} - x = \left(3\sqrt{gd} - 2\sqrt{gd_o} - V_o\right)(t - t_1) \qquad x_s < x < x_{Gate} \quad (2\text{-}5)$$

which is a parabola. The negative surge propagates upstream at a celerity of $U = (gd_o)^{1/2} - V_o$ in a rectangular channel with U the celerity positive upstream (Montes 1998, Chanson 2004). The location of the surge leading edge is:

$$x_s = x_{Gate} - \left(\sqrt{gd_o} - V_o\right)t \qquad t > 0 \quad (2\text{-}6)$$

Effect of flow resistance

The effects of flow resistance on negative surge propagation may be tested using a linear

development of small perturbation theory. The following development derives from Henderson (1966). Let us consider a rectangular prismatic channel along which the initial flow conditions (d_o, V_o) are constant and $S_o = S_f$ at t = 0. The latter condition implies that:

$$S_o = \frac{f}{8} Fr_o^{\,2} \tag{2-7}$$

where f is the Darcy-Weisbach friction factor assumed constant independent of time and $Fr_o = V_o/C_o$. The difference (S_o-S_f) is then:

$$S_o - S_f = \frac{f}{8}\left(Fr_o^{\,2} - Fr^2\right) \tag{2-8}$$

where Fr = V/C. Equations (2-1) and (2-2) may be rewritten as a characteristic system of equations:

$$\frac{d(C(Fr+2))}{dt} = g\frac{f}{8}\left(Fr_o^{\,2} - Fr^2\right) \qquad \text{along } \frac{dx}{dt} = V + C \tag{2-9a}$$

$$\frac{d(C(Fr-2))}{dt} = g\frac{f}{8}\left(Fr_o^{\,2} - Fr^2\right) \qquad \text{along } \frac{dx}{dt} = V - C \tag{2-9b}$$

Along the initial backward characteristics (Fig. 1-1), $V = V_o$ and $C = C_o$. Considering a backward characteristics D-F located very close to the initial forward characteristics (i.e. $t_1\sqrt{g/d_o} \ll 1$ in Fig. 1, Bottom), the following approximation holds: $Fr \approx Fr_o + \Delta Fr$, and Equation (2-9b) becomes:

$$(Fr-2)\frac{dC}{dt} + C\frac{dFr}{dt} = -g\frac{f}{4}Fr_o^{\,2}\Delta Fr \qquad \text{along } \frac{dx}{dt} = V - C \text{ \& for } t_1\sqrt{\frac{g}{d_o}} \ll 1 \tag{2-10}$$

For $t\sqrt{g/d_o} \ll 1$, the backward characteristics D-F issued from (x_{Gate}, t_1) diverges slowly from the initial characteristic line along which $V = V_o$ and $C = C_o$. Hence the rate of change of C(Fr+2) is negligible yielding

$$(Fr+2)\frac{dC}{dt} + C\frac{dFr}{dt} \approx 0 \qquad \text{along } \frac{dx}{dt} = V - C \text{ \& for } t_1\sqrt{\frac{g}{d_o}} \ll 1 \tag{2-11}$$

along E-F (Fig. 1, Bottom). Subtracting (2-11) out of (2-10), it yields:

$$4\frac{dC}{dt} = g\frac{f}{4}Fr_o^{\,2}\Delta Fr \tag{2-12}$$

Along the characteristic line E-F, and for $t_1\sqrt{g/d_o} \ll 1$, the following relationship holds:

$$\Delta Fr = \frac{2+Fr}{C\left(1 + g\frac{f}{8}\frac{Fr_o}{C}\Delta t\right)}\Delta C \tag{2-13}$$

where $\Delta C = C - C_o$ and Δt is the time increment from E to F. Equation (2-13) links ΔFr and ΔC, noting that $C = C_o(1+\varepsilon)$ and $Fr = Fr_o(1+\varepsilon')$ where ε and ε' are negligibly small quantities since $t_1\sqrt{g/d_o} \ll 1$. The combination of Equations (2-12) and (2-13) gives the following differential

equation:

$$\frac{dC}{dt} = g\frac{f}{4}\frac{Fr_o}{C_o}(Fr_o + 2)(C - C_o) \qquad (2\text{-}14)$$

With the appropriate boundary conditions $C(x=0, t_1) = C_1$, the integration along the backward characteristics D-F yields:

$$C = C_o + (C_1 - C_o)\exp\left(g\frac{f}{4}\frac{Fr_o}{C_o}(Fr_o + 2)(t - t_1)\right) \qquad t \geq t_1 \quad (2\text{-}15)$$

The trajectory of the characteristic D-F is given by:

$$\frac{dx}{dt} = V - C = V_o + 2C_o - 3C \qquad (2\text{-}16)$$

using Equation (2-11). Inserting Equation (2-15), the integration of the D-F characteristic trajectory yields:

$$x_{Gate} - x = (V_o - C_o)(t - t_1) + \frac{3(C_1 - C_o)}{g\frac{f}{4}\frac{Fr_o}{C_o}(Fr_o + 2)}\left[\exp\left(g\frac{f}{4}\frac{Fr_o}{C_o}(Fr_o + 2)(t - t_1)\right) - 1\right]$$

for $x \geq 0$ and $t \geq t_1$ (2-17)

Equation (2-17) is the equation of the backward characteristics D-F in presence of friction. It shows that the divergence between the characteristics D-F and the initial characteristics decreases with increasing bed friction. The slope dt/dx decreases with increasing time for a given friction coefficient. The characteristics D-F is flatter as shown in Figure 2-1.

For a negative surge as illustrated in Figures 1-1 and 2-1, it is worth to note that $d_1 < d_o$ and hence $C_1 < C_o$. Along the backward characteristics D-F, the following holds: $C_1 < C < C_o$. The sign of Fr is the sign of V and the sign of S_o is the sign of Fr_o. For $S_f = S_o = 0$, the backward characteristics is a straight line whose equation is:

$$x - x_{Gate} = (V_o + 2C_o - 3C_1)(t - t_1) \qquad (2\text{-}18)$$

The above considerations suggest that the flow resistance will make a negative surge less dispersive. Henderson (1966) argued however that the development has some physical limitation.

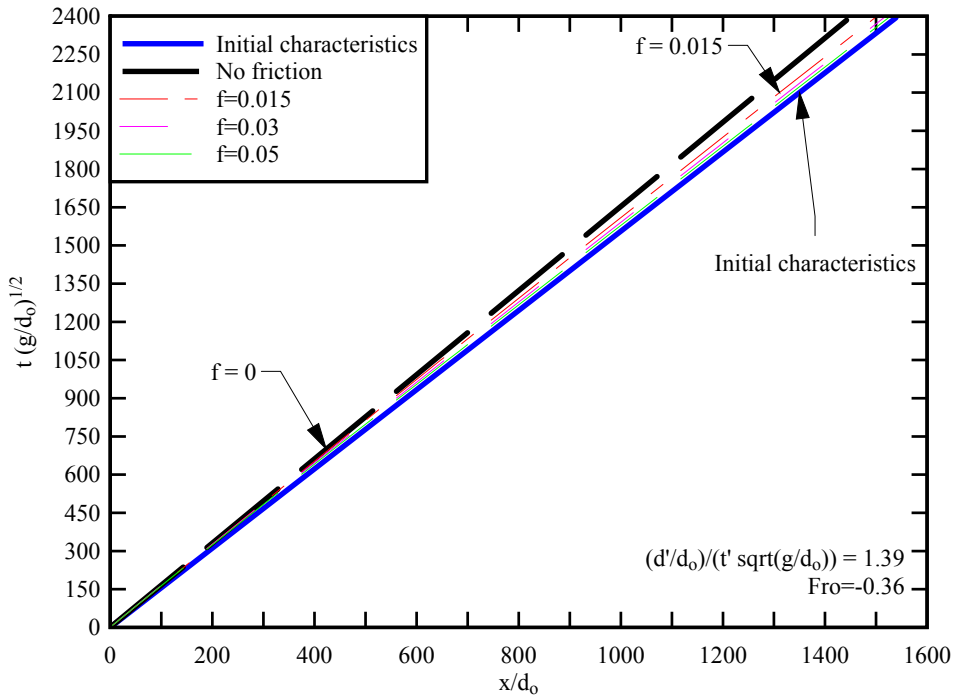

Fig. 2-1 - Effects of flow resistance on a negative surge - Calculations performed for $(d_1/d_o)/(t_1(g/d_o)^{1/2}) = 1.39$ and $Fr_o = 0.36$

3. PHYSICAL MODELLING OF NEGATIVE SURGES

3.1 PRESENTATION

The physical studies of negative surges are performed with geometrically similar models, and the modelling requires the selection of the relevant similitude. For the simple case of a negative surge propagating in a rectangular, horizontal channel after a sudden and complete gate opening, a dimensional analysis yields:

$$d, V_x, V_y, V_z = F_1(x, y, z, t, d_o, V_o, \delta, B, g, \rho, \mu, \sigma...) \quad (3\text{-}1)$$

where d is the flow depth, V_x, V_y, V_z are respectively the longitudinal, transverse and vertical velocity components at a location (x, y, z), x is the coordinate in the flow direction, y is the horizontal transverse coordinate measured from the channel centreline, z is the vertical coordinate measured from channel bed, t is the time, d_o and V_o are the initial flow depth and velocity respectively, δ is the initial boundary layer thickness at x, B is the channel width, g is the gravity acceleration, ρ and μ are the water density and dynamic viscosity respectively, and σ is the surface tension between air and water. Equation (3-1) expresses the unsteady flow properties (left handside terms) at a point in space (x, y, z) and time t as functions of the initial flow conditions, channel geometry and fluid properties.

Some basic considerations show that the relevant characteristic length and velocity scales are respectively the initial flow depth d_o and velocity V_o. Equation (3-1) may be rewritten in dimensionless terms:

$$\frac{d}{d_o}, \frac{V_x}{V_o}, \frac{V_y}{V_o}, \frac{V_z}{V_o} = F_2\left(\frac{x}{d_o}, \frac{y}{d_o}, \frac{z}{d_o}, t\sqrt{\frac{g}{d_o}}, \frac{V_o}{\sqrt{g d_o}}, \rho\frac{V_o\, d_o}{\mu}, \frac{\delta}{d_o}, \frac{B}{d_o}, \frac{g\,\mu^4}{\rho\,\sigma^3}, ...\right) \quad (3\text{-}2)$$

In Equation (3-2) right handside, the fifth and sixth terms are the Froude and Reynolds numbers respectively, and the ninth term is the Morton number.

In a geometrically similar model, a true dynamic similarity is achieved only if each dimensionless parameter has the same value in both model and prototype. Scale effects may exist when one or more Π-terms have different values between the model and prototype. In free-surface flows including negative surges, the gravity effects are important and a Froude similitude is commonly used (Henderson 1966, Chanson 1999). This is also the case in the present study.

3.2 EXPERIMENTAL FACILITY AND INSTRUMENTATION

The experiments were performed in a 12 m long, 0.5 m wide tilting flume (Fig. 3-1). The channel was made of smooth PVC bed and glass walls. The water was supplied by a constant head tank to a large intake chamber with a smooth convergent feeding into the glass-walled channel. A fast-

opening gate was located at the channel downstream end: x = 11.15 m where x is the longitudinal distance from the channel upstream end (Fig. 1-1). (The gate was identical to that used by Koch and Chanson (2005,2009).) A number of experimental flow conditions were tested. Table 3-1 summarises the range of experimental flow conditions where Q is the initially steady flow rate, h is the undershoot gate height before fast-opening, and S_o is the bed slope.

The water discharge was measured with two orifice meters designed based upon the British Standards (1943) and calibrated on site with a volume per time technique. The percentage of error was less than 2%. In steady flows, the water depths were measured using rail mounted pointer gauges. The unsteady water depth was measured using a series of acoustic displacement meters Microsonic^{TM} Mic+25/ IU/TC. The data accuracy and response of the acoustic displacement meters were 0.18 mm and 50 ms, respectively. The turbulent velocity components were measured using an acoustic Doppler velocimeter (ADV) Nortek^{TM} Vectrino+ (Serial No. VNO 0436) equipped with a side-looking head. The velocity rate was set to 1.0 m/s and the sampling rate was 200 Hz for all the experiments with an estimated data accuracy of 0.01 m/s (Nortek 2009). The translation of the ADV probe in the vertical direction was controlled by a fine adjustment travelling mechanism connected to a Mitutoyo^{TM} digimatic scale unit with an error less than 0.1 mm. Herein all the measurements were taken on the channel centreline, and the ADV and displacement sensors were synchronised and sampled simultaneously at 200 Hz.

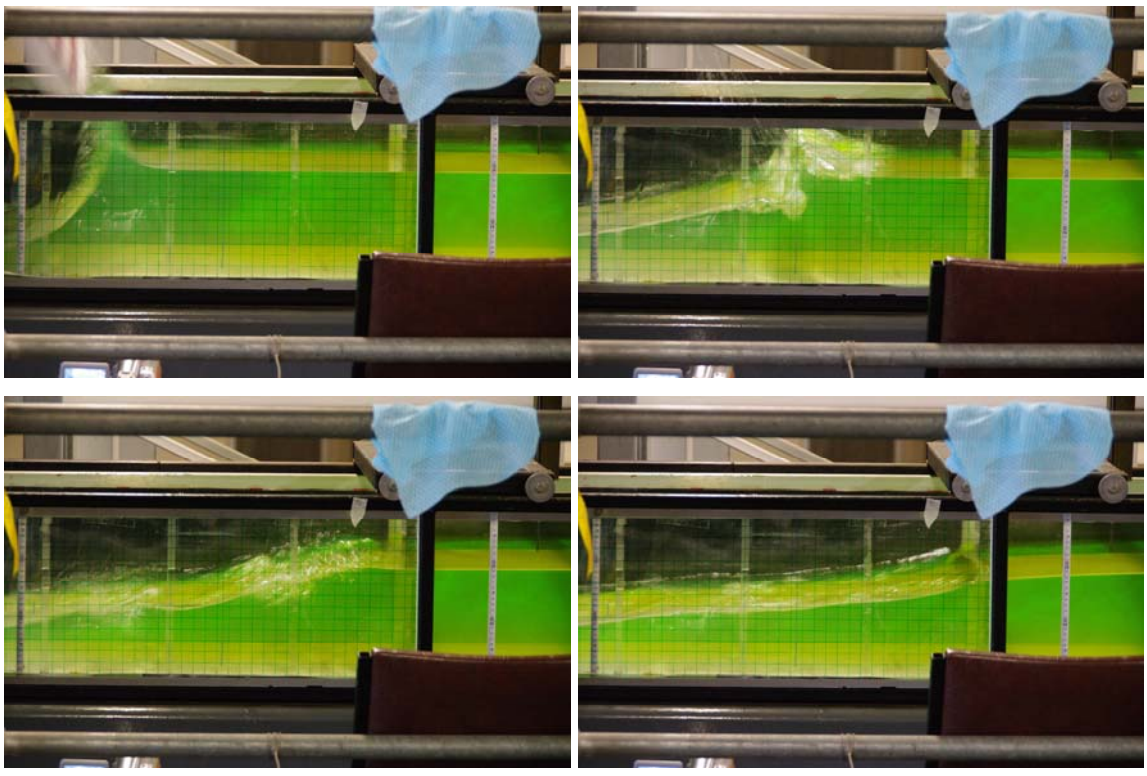

(A) Negative surge generation next to the gate - Initial flow conditions: Q = 0.020 m^3/s, h = 0 - Photographs after lens distortion corrections - From Top Left to Bottom Right, Left to Right, t = 0,

0.19, 0.385, 0.577 s

(B) Negative surge propagating upstream - Initial flow conditions: Q = 0.020 m^3/s (from right to left), h = 0.030 m - The photograph covers 11 m > x > 7 m, and the gate is fully opened (left handside)

Fig. 3-1 - Photographs of the negative surge experiments - Negative surge propagation from left to right

A video camera Panasonic™ NV-H30 (25 fps) was used to record the instantaneous free-surface profile at two different locations along the channel. The camera was placed about 0.5 m from the channel sidewall. A 20 mm squared grid was placed on the side wall for reference and lens distortion correction. Some coloured vegetable dye was added to the water to improve the visibility of the surface edge in the images (Fig. 3-1). The focal plan of the camera was placed slightly beneath the initial free-surface for the recorded image to show the free surface close to the wall rather than on the channel centreline. Additional informations were recorded with a Pentax™ K-7 camera with a 14Mp resolution. Further photographs of the experiments are presented in Appendix A.

3.3 INFLOW CONDITIONS AND NEGATIVE SURGE GENERATION

The displacement meters were located at x = 5.6, 6.0, 6.2, 10.2, 10.5, 10.8 m where x is the longitudinal distance from the channel upstream end. The video-camera was centered either at x = 6.0 m covering 5.8 < x < 6.3 m or x = 10.8 m covering 10.5 < x < 11.2 m (incl. the gate). The ADV unit was mounted at x = 6 or 10.5 m, and at z = 0.0067, 0.025, 0.124, 0.135 m where z is the elevation above the bed. At each sampling location, the experiments were repeated 25 times and the results were ensemble-averaged. For the two upper locations, the sampling was stopped when the ADV head became out of water.

For each experimental run, the steady gradually-varied flow conditions were established prior to the first measurements. The negative surge was produced by opening rapidly a tainter gate (Fig. 3-1).

The gate was operated manually and the opening times were less than 0.15 to 0.2 s. Such an opening time was small enough to have a negligible effect on the surge propagation as shown by Lauber (1997). After the rapid gate opening, the gate did not intrude into the flow as sketched in Figure 3-1A. The experimental flow conditions are summarised in Table 3-1 where Q is the initially steady flow rate, d_o and V_o are the initial flow depth and velocity recorded at x = 6 m, and h is the undershoot gate height before opening.

Table 3-1 - Experimental investigations of negative surges

Ref.	S_o	Q	h	d_o (at x=6m)	U (at x=6m)	Instrument(s)
		(m^3/s)	(m)	(m)	(m/s)	
(1)	(2)	(3)	(4)	(5)	(6)	(7)
20_30mm	0	0.020	0.030	0.24	0.91	Video, ADV, displacement meters.
20_50mm		0.020	0.050	0.10	0.25	Video.
30_40mm		0.030	0.040	0.26	0.33	Video.
30_50mm		0.030	0.050	0.22	0.49	Video.

Notes: h: undershoot gate height before sudden opening.

Boundary conditions

Prior to each experiment, the flow was controlled by the downstream tainter gate. Figure 3-2 shows the arrangement. In the initially steady flow, the continuity equation and Bernoulli principle yield:

$$Q = V_{G1}\, d_{G1}\, B = V_{G2}\, d_{G2}\, B \tag{3-3}$$

$$E = d_{G1} + \frac{{V_{G1}}^2}{2\,g} = d_{G2} + \frac{{V_{G2}}^2}{2\,g} \tag{3-4}$$

where Q is the water discharge, V and d are the flow velocity and depth respectively, the subscripts G1 and G2 refer to the flow properties immediately upstream and downstream of the gate (Fig. 3-2),d B is the channel width and E is the specific energy.

The flow depth downstream of the gate was controlled by the gate opening h and the angle α between the gate and the horizontal:

$$d_{G2} = C_c\, h \tag{3-5}$$

where C_c is the contraction coefficient which may be calculated from ideal fluid flow considerations (Rouse 1946, Chanson 2009). The flow depth immediately upstream of the gate is derived from energy considerations:

$$d_{G1} = E\left(\frac{1}{3} + \frac{2}{3}\cos\left(\frac{\Gamma}{3}\right)\right) \quad (3\text{-}6)$$

where and Γ is defined as (Chanson 1999):

$$\cos\Gamma = 1 - \frac{27}{4}\left(\frac{d_c}{E}\right)^3 \quad (3\text{-}7)$$

with d_c the critical flow depth ($d_c = \sqrt[3]{Q^2/(g\,B^2)}$)

Prior to gate opening, the free-surface followed a M2 profile which was controlled by the tainter gate flow conditions. After gate opening, the final free-surface shape ([1]) was another M2 profile controlled by the overfall at the channel downstream end where critical flow conditions took place. For a series of experiments, the initial and final free-surface profiles are reported in Figure 3-3.

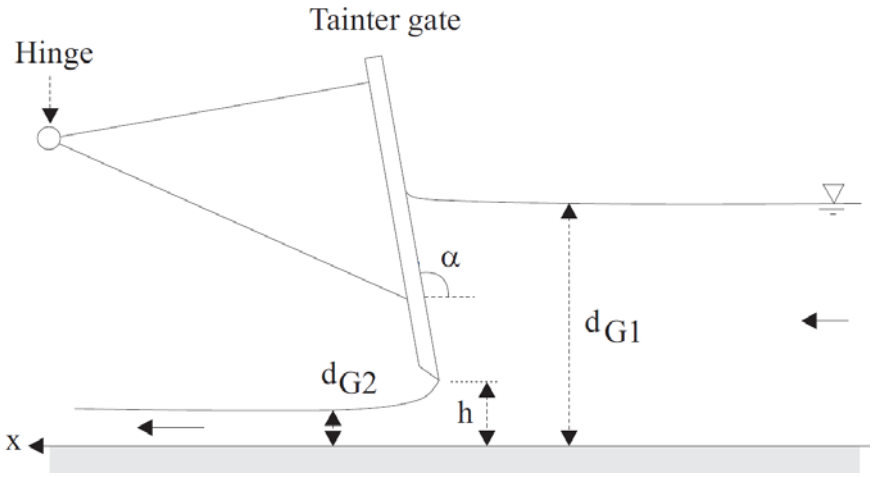

Fig. 3-2 - Definition sketch of the underflow beneath the tainter gate prior to gate opening

Table 3-2 - Experimental flow properties across the tainter gate immediately prior to opening

Ref.	S_o	Q	h	α	C_c	d_{G2} ($^+$)	d_{G1} ($^\$$)	d (at x=10.8m)
		(m^3/s)	(m)	(deg.)		(m)	(m)	(m)
(1)	(2)	(3)	(4)	(5)	(6)	(7)	(8)	(9)
20_30mm	0	0.020	0.030	91.75	0.608	0.0182	0.262	0.243
20_50mm		0.020	0.050	93.92	0.605	0.0302	0.113	0.106
30_40mm		0.030	0.040	92.92	0.606	0.0242	0.335	*0.266*
30_50mm		0.030	0.050	93.92	0.605	0.0302	0.227	0.236

Notes: C_c: contraction coefficient of a two-dimensional flow (von Mises 1917); h: undershoot gate height before sudden opening; ($^+$) calculated using Eq. (3-5); ($^\$$): calculated using equation (3-6);

[1] Recorded 5 minutes after gate opening.

Italic data: possibly incorrect data.

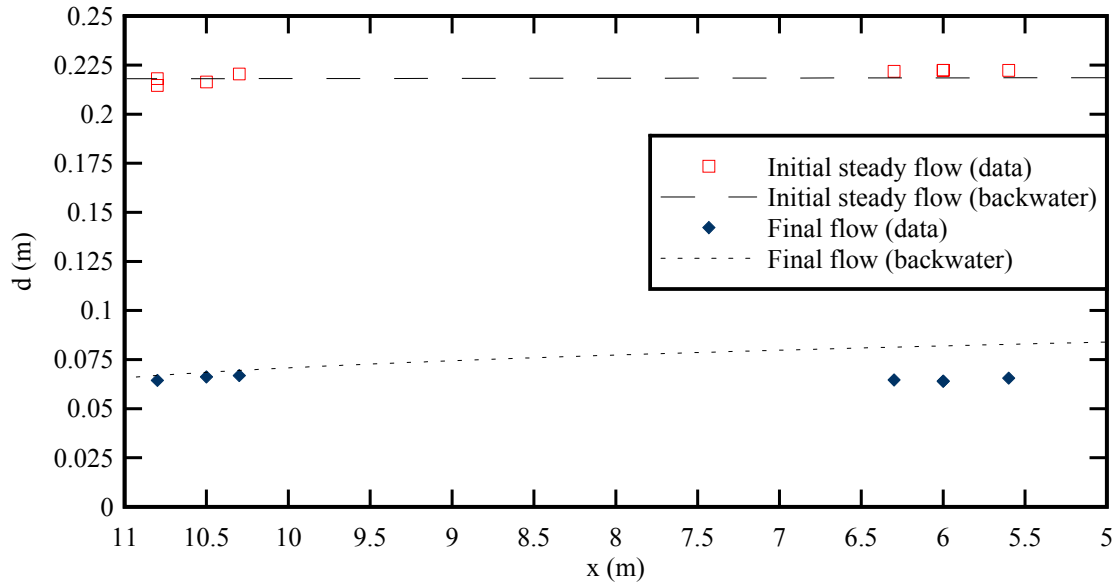

Fig. 3-3 - Initial steady flow free-surface profile prior to negative surge and final free-surface profile after gate opening - Flow conditions: Q = 0.020 m^3/s, h = 0.030 m, steady flow direction from right to left - Comparison between physical data (recorded with acoustic displacement meters) and backwater calculations

4. BASIC OBSERVATIONS

4.1 BASIC FLOW PATTERNS

Both visual observations and water surface profile measurements at the gate showed a steep drop in water depth close to the gate (e.g. 10 < x < 11.15 m) compared to the observations further upstream at 5.5 < x < 6.5 m (Fig. 3-1 & 4-1). Figure 3-1 presents some photographs of the upstream propagation of negative surges. Figure 3-1A shows a series of 4 photographs of surge propagating immediately upstream of the gate within 0.8 s. Figure 3-1B presents an instantaneous shot of the water surface between x = 7 and 11 m. Additional photographs of experiments are presented in Appendix A. Figure 4-1 shows some instantaneous free-surface profiles next to the gate (10.48 < x < 11.2 m, Fig. 4-1A) and further upstream (5.8 < x < 6.3 m, Fig. 4-1B) recorded with the video camera. In Figure 4-1, d_o is the initial flow depth at x = 6 m and the data were recorded at 25 fps. the results illustrate the gradual lowering of the water surface associated with the upstream propagation of the negative surge.

The observations highlighted the rapid gate opening and surge formation (Fig. 3-1A & 4-1A), as well as some interactions of the gate lower lip with the upper flow region. Very rapidly (within a second), the disturbance vanished and the instantaneous free-surface exhibited a smooth shape as shown in Figures 3-1B & 4-1B.

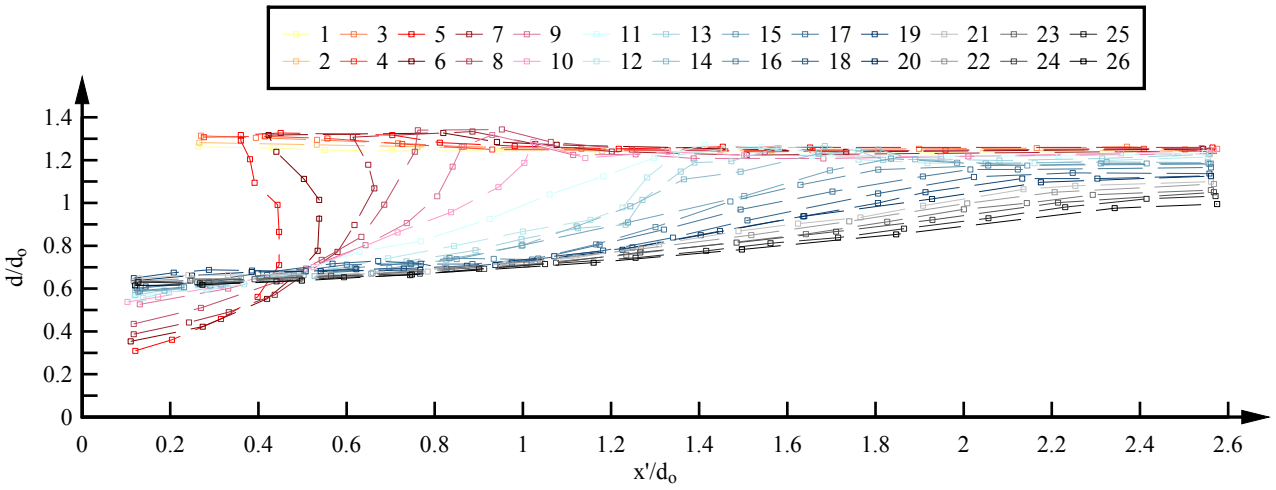

(A) Immediately upstream of the gate (10.48 < x < 11.2 m)

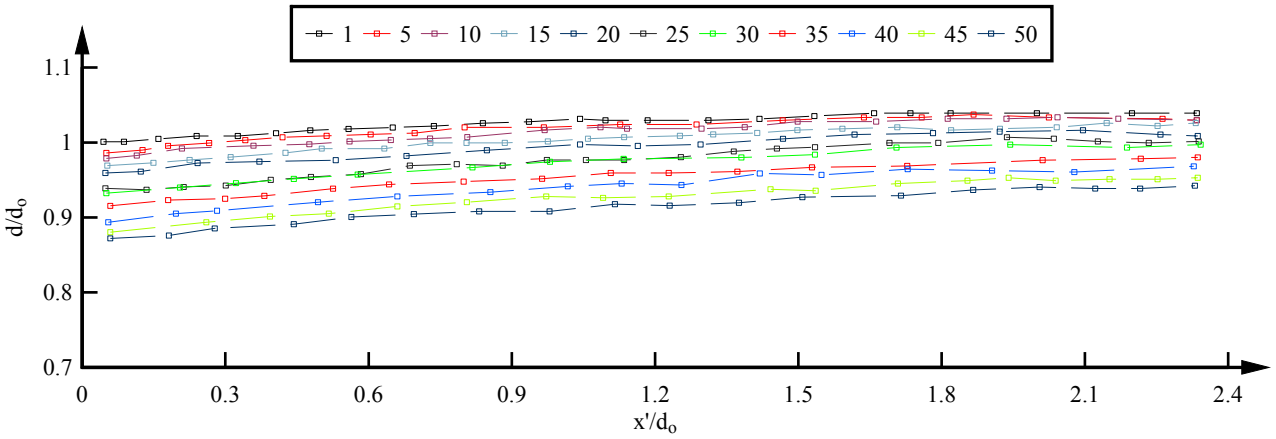

(B) About x = 6 m (5.8 < x < 6.3 m)

Fig. 4-1 - Instantaneous free-surface profiles during the negative surge propagation - Initial flow conditions: Q = 0.030 m^3/s, h = 0.040 m, d_o = 0.26 m - Negative surge propagation from left to right - The legend indicates the video frame number

The observations showed some free-surface curvature immediately after the gate opening as illustrated in Figures 3-1A & 4-1A, typically for $t\sqrt{g/d_o} < 1.5$. For larger times after gate opening, the free-surface was very flat and smooth. The water surface curvature was not discernable by eye and the assumption of hydrostatic pressure was likely valid.

Negative surge celerity

The celerity of the negative surge leading edge was deduced from photographic, video and acoustic displacement meter measurements. Typical results are presented in Figure 4-2 where the downstream gate is shown with a thick dashed line. For all the experimental flow conditions, the celerity data highlighted two distinct phases. Very close to the gate, and immediately after gate closure, the negative surge formation was associated with some local dissipative process illustrated in Figure 3-1A. During this formation phase, the celerity of the negative surge leading edge increased with time. Within the experimental flow conditions (Table 3-1), the present data sets suggested that the acceleration phase took place within a distance $4d_o$ from the gate. After the acceleration/formation phase, the negative surge propagated upstream in a more gradual manner. During this gradually-varied phase, the surge leading edge was very flat and barely perceptible, and its celerity tended to decrease slowly with increasing distance from the gate as shown in Figure 4-2 for $x/d_o < 40$. The data implied some deceleration in a manner which is contrary to the above theoretical development (section 2). At x = 6 m, the dimensionless negative surge celerity $(U+V_o)/(g\ d_o)^{1/2}$ ranged from 0.3 up to 1.0 depending upon the initial steady flow conditions, where

U is the celerity of the surge leading edge positive upstream (Table 3-1).

For comparison, the analytical solution of the Saint-Venant equations for a simple wave predicts that the leading edge of the negative surge propagates with a constant dimensionless celerity $(U+V_o)/(g\ d_o)^{1/2} = 1$. In a rectangular flume, Favre (1935) measured the surge celerity propagating downstream as $(U+V_o)/(g\ d_o)^{1/2} = 1$. Lauber and Hager (1998) performed experiments in a horizontal rectangular channel initially at rest (V_o=0) with a 3.5 m long reservoir and observed $U/(g\ d_o)^{1/2} = 1.4$. Tan and Chu (2009) re-analysed the same data set (V_o=0), and their computational data matched the experimental observations yielding $U/(g\ d_o)^{1/2} = 1$. The present results (Figure 4-2, Table 3-1) suggest that neither the Saint-Venant equations solution nor previous findings are comparable with the present findings. While the negative surge formation might be affected by the gate opening mechanism, the gradually-varied phase associated with a slow deceleration of the negative surge leading edge was possibly linked with the initial flow conditions and the upstream propagation of the surge against a M2 backwater profile with slightly increasing depth with increasing distance from the gate. Further work is required to comprehend the scatter of the surge celerity data.

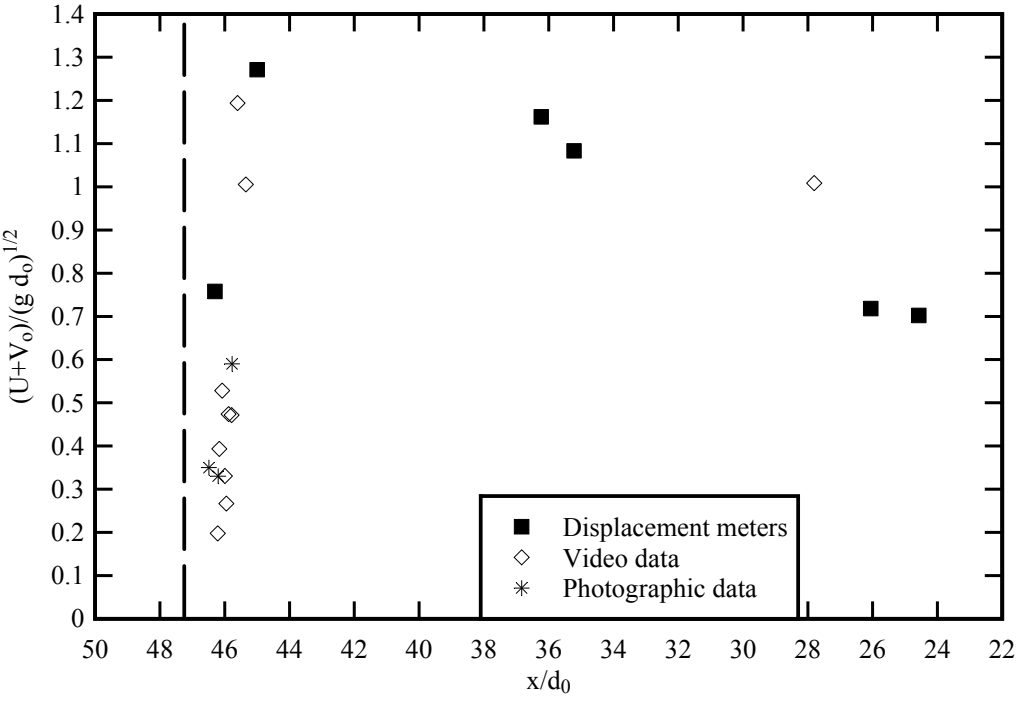

Fig. 4-2 - Dimensionless negative surge celerity as a function of the longitudinal distance - Flow conditions: Q = 0.020 m^3/s, h = 0.030 m, d_o = 0.24 m

4.2 FREE-SURFACE AND TURBULENT VELOCITY MEASUREMENTS

During the negative surge, the water depth decreased relatively gradually after the initial surge formation. The free surface measurements showed some marked curvature near the surge leading edge. The longitudinal velocity component increased at the same time as the water depth decreased. Typical results are presented in Figures 4-3, 4-4 and 4-5. Figure 4-3 presents some free-surface measurements at x = 6 and 10.5 m; both the ensemble-median, the difference between maximum and minimum water depths (d_{max}-d_{min}) and the difference between the 3rd and 1st quartiles (d_{75}-d_{25}) are presented. Figures 4-4 and 4-5 show some velocity measurements at x = 10.5 m and x = 6 m respectively. Each graph includes the ensemble-median water depth, the median velocity components and difference between the 3rd and 1st quartiles (V_{75}-V_{25}) ([2]). Further velocity data are presented in Appendix C.

The free-surface data highlighted the free-surface curvature at the leading edge of the negative wave (Fig. 4-3). Some large fluctuations in free-surface elevations were observed briefly behind the negative surge leading edge: e.g., for $t(g/d_o)^{1/2}$ = 70-75 and 95-105 in Figures 4-3A and 4-3B respectively. The free-surface curvature and slope were both larger close to the gate (x = 10.5 m) than further upstream (x = 6 m) (Fig. 4-3). Based upon the maximum free-surface curvature at the surge leading edge, the vertical pressure distributions were calculated using a solution of the Boussinesq equation (Montes and Chanson 1998). The calculations are summarised in Table 4-1 presenting the radius of curvature of free-surface and deviation from hydrostatic pressure where the free-surface curvature is maximum (Table 4-1, columns 6 & 7). The results implied that the smallest radius of curvature was large: $|(R_s)_{min}|$ = 7 m and 49 m at x_{Gate}-x = 0.65 and 5.15 m respectively (i.e. x = 10.5 & 6 m). The pressures at the leading edge were basically hydrostatic within the approximations of the theoretical model.

Table 4-1 - Maximum free-surface curvature at the leading surge of the negative surge

Q (m3/s)	h (m)	x (m)	$(\partial^2 d/\partial t^2)_{max}$ (m/s^2)	$\partial d/\partial t$ (m/s)	$(R_s)_{min}$ (m)	$1+\frac{(\partial P/\partial z)_{max}}{\rho g}$
(1)	(s)	(3)	(4)	(5)	(6)	(7)
0.020	0.030	6.0	-0.017	-0.007	-48.6 ($^+$)	6×10^{-5} ($^+$)
		10.5	-0.143	-0.066	-6.9 ($^+$)	5.3×10^{-4} ($^+$)

Notes: R_s: radius of curvature; ($^+$): calculations based upon the Boussinesq equation solution of

[2] For a Gaussian velocity distribution around the mean, the difference (V_{75}-V_{25}) would be equal to 0.7v' where v' is the standard deviation of the velocity component.

Montes & Chanson (1998).

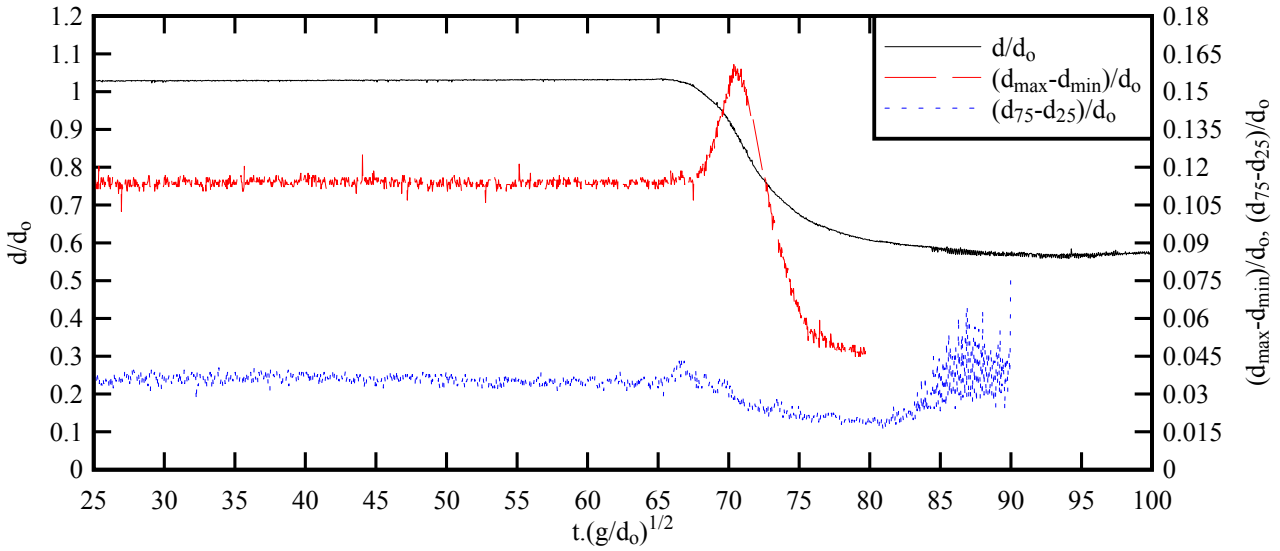

(A) Water depth data recorded at x = 10.5 m (close to the gate)

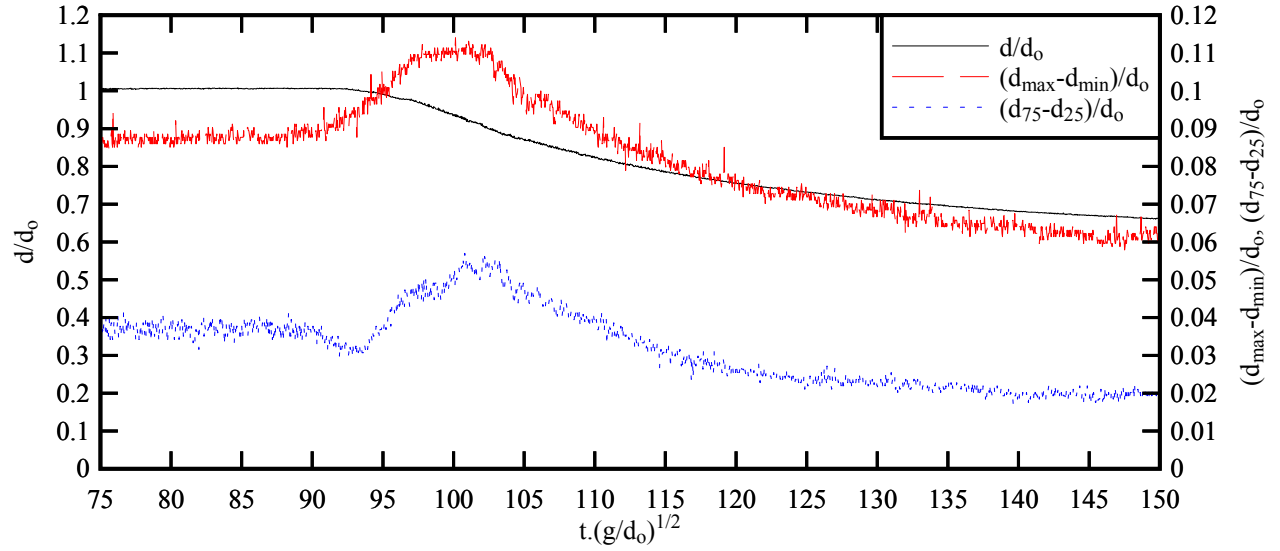

(B) Water depth data recorded at x = 6 m

Fig. 4-3 - Unsteady free-surface measurements beneath a negative surge: time-variations of the median water depth, difference between maximum and minimum water depths (d_{max}-d_{min}) and difference between the 3rd and 1st quartiles (d_{75}-d_{25}) - Flow conditions: Q = 0.020 m^3/s, h = 0.030 m

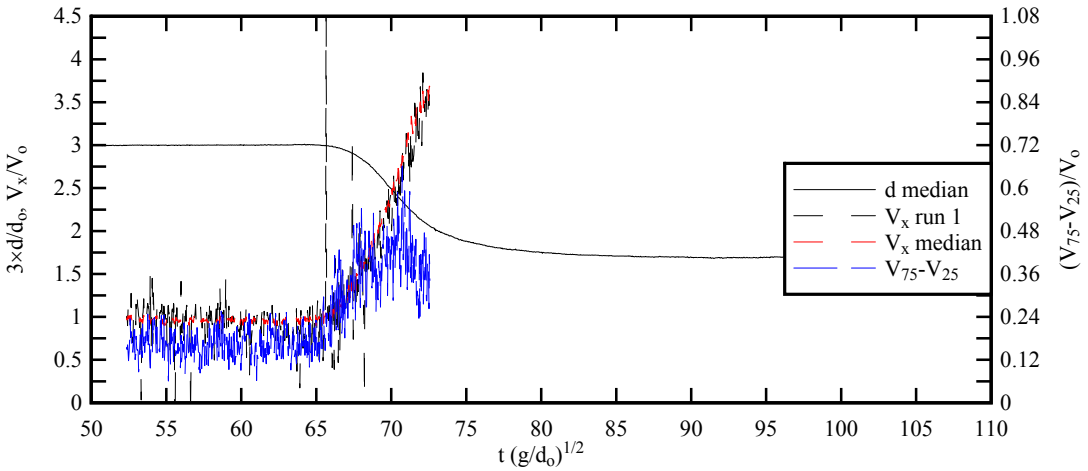

(A) Longitudinal velocity component V_x at $z/d_o = 0.615$

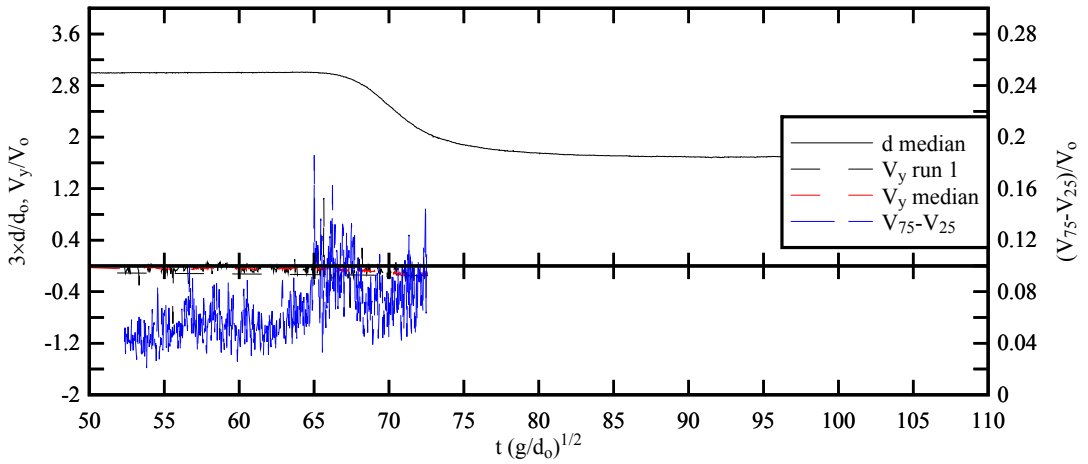

(B) Transverse velocity component V_y at $z/d_o = 0.615$

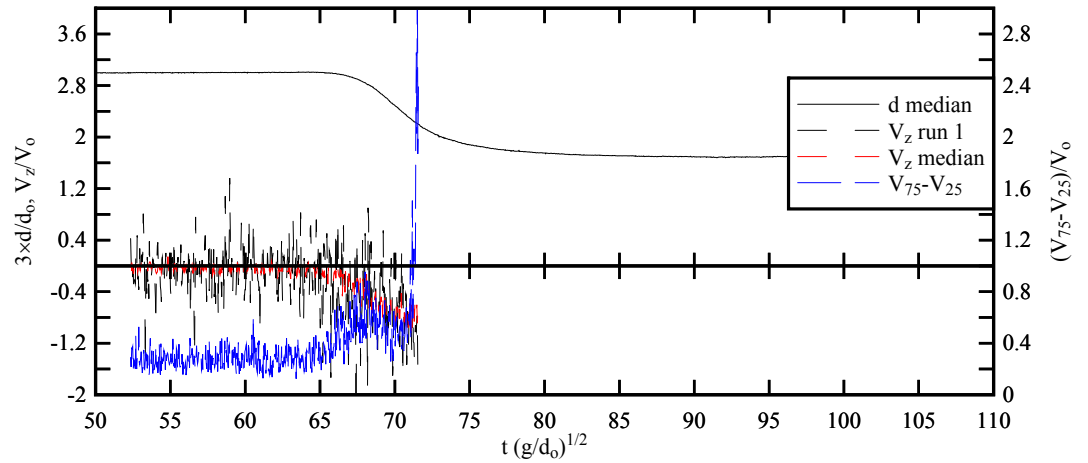

(C) Vertical velocity component V_z at $z/d_o = 0.615$

Fig. 4-4 - Free-surface and velocity data beneath a negative surge at x = 10.5 m (0.65 m upstream of gate): ensemble-median water depth d_{median}, median velocity components and difference between the 3rd and 1st quartiles (V_{75}-V_{25}) - Flow conditions: Q = 0.020 m^3/s, h = 0.030 m, x = 10.5 m - Data truncated when ADV unit was out of water

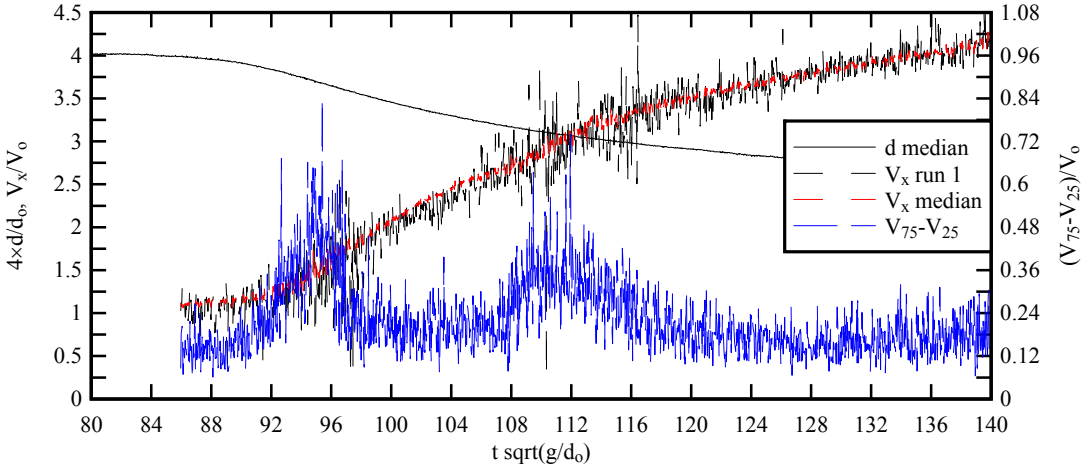

(A) Longitudinal velocity component V_x at $z/d_o = 0.563$

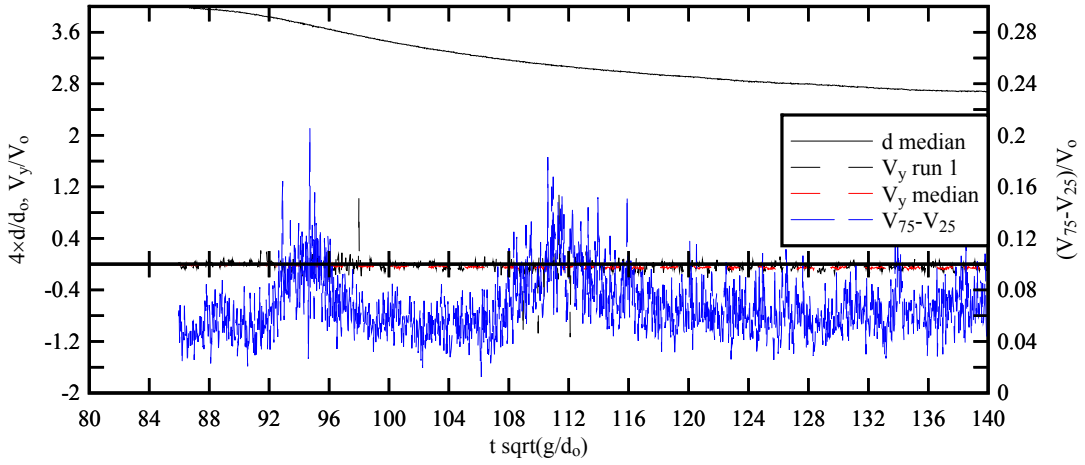

(B) Transverse velocity component V_y at $z/d_o = 0.563$

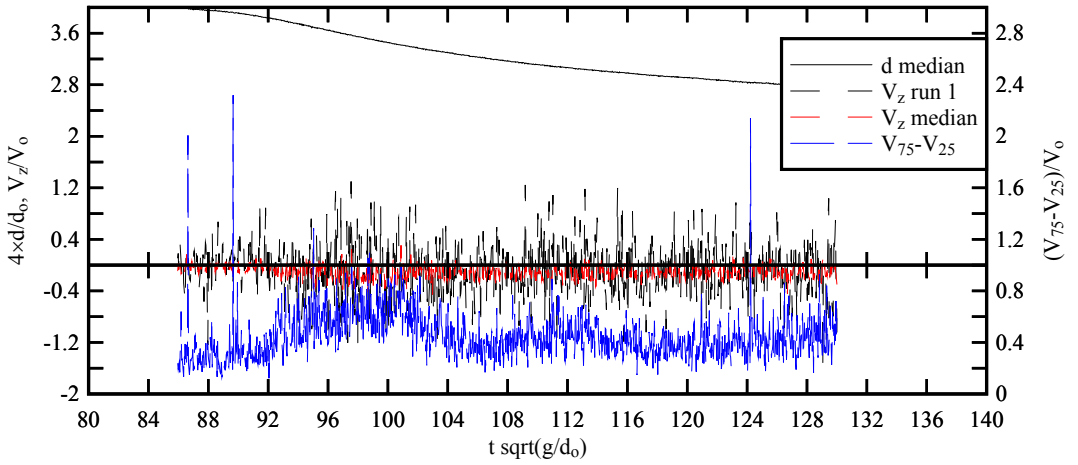

(C) Vertical velocity component V_z at $z/d_o = 0.563$

Fig. 4-5 - Free-surface and velocity data beneath a negative surge at x = 6 m (5.15 m upstream of gate): ensemble-median water depth d_{median}, median velocity components and difference between the 3rd and 1st quartiles (V_{75}-V_{25}) - Flow conditions: Q = 0.020 m^3/s, h = 0.030 m, x = 6.0 m

The unsteady velocity data highlighted a number of basic features beneath the negative surge. The longitudinal velocity measurements showed an acceleration of the flow during the drawdown of the free-surface (Fig. 4-4 & 4-5). This was associated with some increase in all velocity component fluctuations, compared to the steady state and to the final flow conditions (not shown herein). For example, for $t(g/d_o)^{1/2}$ = 65 to 75 and 90 to 120 in Figures 4-4 and 4-5 respectively. The magnitude of the difference between 3rd and 1st quartiles (V_{75}-V_{25}) was about similar at both locations (x = 6 & 10.5 m) as seen in Figures 4-4 and 4-5 drawn with the same horizontal and vertical scales.

The transverse velocity component V_y showed quantitatively lesser fluctuations before, during and after surge formation than in the horizontal and vertical directions. Close to the free-surface (e.g. z/d_o = 0.62), the vertical velocity component was negative on average and its magnitude was comparable to the maximum vertical velocity of the free-surface: that is, $(\partial d/\partial z)_{max}/V_o$ = -1.7 and -0.25 at x = 10.5 and 6 m respectively.

Overall the present data indicated that the negative surge flow was an unsteady three-dimensional turbulent process.

4.3 TURBULENT REYNOLDS STRESS MEASUREMENTS

In a turbulent flow, the flux of x-momentum in the y-direction induces a shear stress term in the x-direction: i.e., the turbulent stress $\rho v_x v_y$. The turbulent stress tensor is a transport effect resulting from turbulent motion induced by velocity fluctuations with the subsequent increase of momentum exchange and of mixing (Piquet 1999). In the present study, the turbulent shear stresses were calculated based upon an ensemble-median technique (median value of 25 runs) (App. D). Some typical results are presented in Figure 4-6. Further results are reported in Appendix D.

The experimental results showed a number of basic properties. Overall the turbulent stress data suggested that the passage of a negative surge was associated with large turbulent stresses and turbulent stress fluctuations at all vertical elevations. That is, the magnitude of turbulent Reynolds stress components was significantly larger than in the initially steady flow and than in the final flow (after the passage of the surge). This was observed with all Reynolds stress components at both x = 6 and 10.5 m. The findings were not unlike some turbulent stress measurements during the ebb tide motion in estuaries (Stacey et al. 1999, Trevethan et al. 2008).

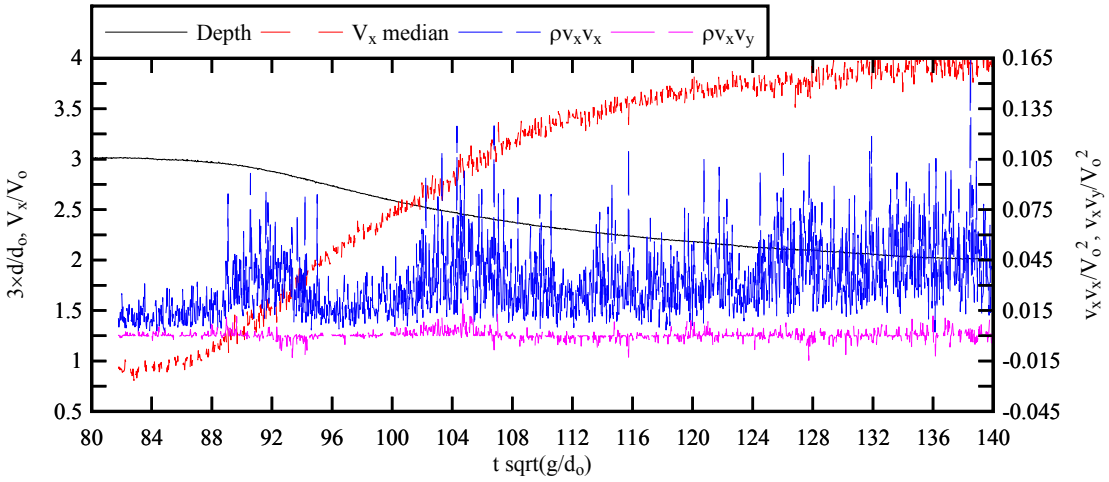

(A) Reynolds stress tensor components ρv_x^2 and $\rho v_x v_y$

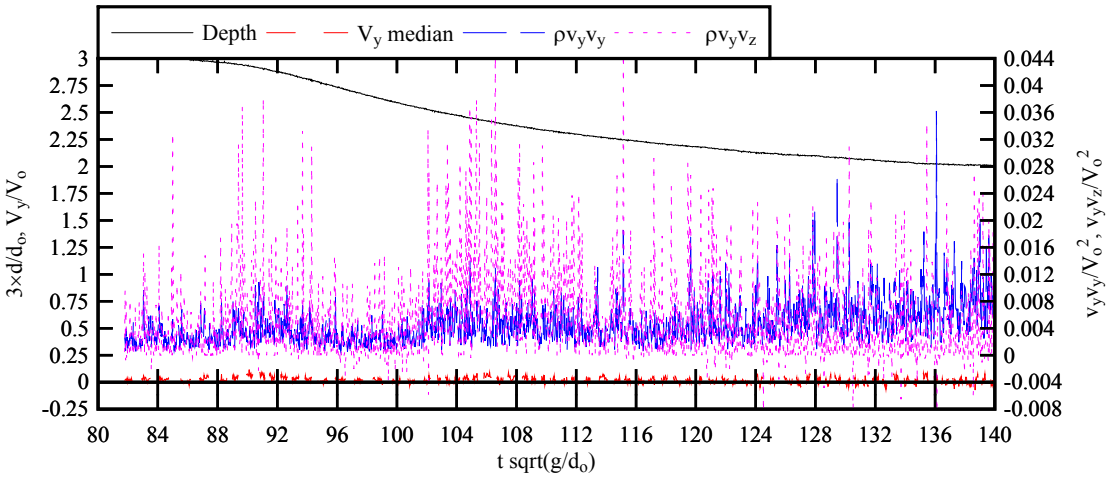

(B) Reynolds stress tensor components ρv_y^2 and $\rho v_y v_z$

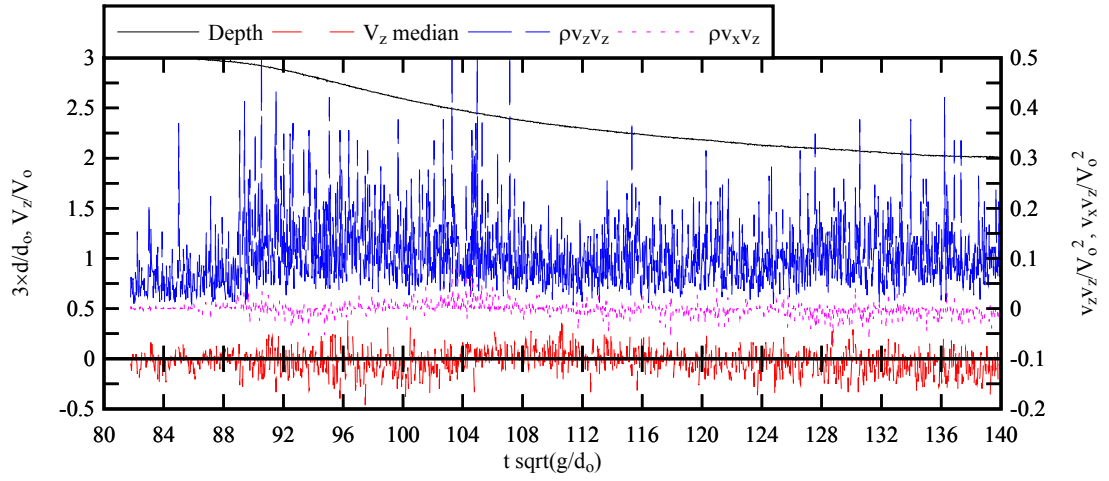

(C) Reynolds stress tensor components ρv_z^2 and $\rho v_x v_z$

Fig. 4-6 - Ensemble-median water depth d_{median} and velocity components, and median turbulent Reynolds stress tensor components beneath a negative surge at x = 6 m (5.15 m upstream of gate) and $z/d_o = 0.030$ - Flow conditions: Q = 0.020 m^3/s, h = 0.030 m, x = 6.0 m, z = 0.0067 m

Although the boundary shear stress in an accelerating flow is lower than that in a steady flow for the same velocity and depth (Johnson 1991, He et al. 2011), the present data highlighted large fluctuations of all velocity components as well as large turbulent stress components in the accelerating flow beneath the negative surge (Fig. 4-6). The unsteady Reynolds stress components were significantly larger in the initially steady and final flow motions. The results implied that negative surges have some potential to induce some significant turbulent mixing.

Some large magnitude and rapid fluctuations of turbulent Reynolds stresses were observed at all elevations. For a non-cohesive sediment material, the Shields diagram gives a critical shear stress for sediment bed load motion about $(\tau_o)_c$ = 0.1 to 0.5 Pa for fine sand particles with sizes between 0.1 and 1 mm (Graf 1971, Julien 1995, Chanson 1999). Herein the instantaneous turbulent shear stress magnitudes ranged up to more than 5 Pa. The Reynolds stress levels were an order of magnitude larger than the critical threshold for sediment motion and transport. For the same fine sand particles with sizes between 0.1 and 1 mm, the ratio of shear velocity to particle fall velocity V_*/w_o ranged from 5 downs to 0.5 and may be compared with the threshold for onset of sediment suspension: $(V_*/w_o)_c > 0.2$ to 2 (van Rijn 1984, Julien 1995, Chanson 1999). The present data implied that the negative surge motion could scour relatively fine sediment particles and advect these in suspension during the drawdown process.

This comparison has some limitations however. The validity of the Shields diagram, critical shear stress estimate and suspension threshold is debatable in a rapidly-varied flow such as a negative surge.

5. COMPARISON WITH ANALYTICAL AND NUMERICAL MODELS

5.1 PRESENTATION

The physical data set was used to test three models: an analytical model and two numerical models of the negative surge (Table 5-1). One numerical model was based upon the one-dimensional equations as for the analytical model, while the second numerical model was a two-dimensional one.

The first model (M1) was an analytical solution of the St Venant equations based upon the simple wave approximation (Eq. (2-3) to (2-6)). The explicit solution assumed $S_f = S_o = 0$: i.e, frictionless flow. The second model (M2) was a numerical integration of the St Venant equations using the Hartree method (Courant et al. 1952, Montes 1998). The one-dimensional model solution was integrated from x = 10.8 m using the measured flow depth for its downstream boundary condition, with an integration time step $\Delta t = 0.05$ s and a grid size $\Delta x = 0.10$ m. The last model (M3) was a two-dimensional ([1]) numerical model using the software Flow-3D™. The classical RNG turbulence model was selected for its robustness and an uniform mesh size was used. A sensitivity analysis was performed with mesh sizes of 5 mm, 15 mm and 30 mm. The 5 mm mesh size results gave the best agreement with the physical data and are presented below. Further details on the CFD modelling and sensitivity analysis results are reported in Appendix E.

Table 5-1 - Summary of analytical and numerical models of the negative surge

Model	Type	Description	Characteristics	Downstream boundary conditions	Flow conditions
(1)	(2)	(3)	(4)	(5)	(6)
M1	Analytical	Simple wave	--	Measured depth at x=10.8 m	$Q = 0.020$ m^3/s, $h = 0.030$ m
M2	Numerical (1D)	Integration of St Venant equations	Hartree method (Δx=0.1m, Δt=0.05s)	Measured depth at x=10.8 m	
M3	Numerical (2D)	Flow-3D™ (v. 9.3)	Uniform mesh size: 5, 15, 30 mm, RNG turbulence model	Sudden gate removal	

5.2 COMPARATIVE RESULTS

The analytical solution and numerical model data were compared with the free-surface physical data (Fig. 6-1). Figure 6-1 presents the free-surface data are x = 6 and 10.8 m, together with the

[1] vertical plane corresponding to the channel centreline.

simple wave solution, the Saint-Venant equation (SVE) integration results for two values of Darcy-Weisbach friction factor and the CDF model results for a 5 mm mesh size. The simple wave method and the numerical integration of Saint-Venant equations compared well with the physical data. The simple wave solution with no friction compared best to the measurements. Indeed the laboratory flume had a rectangular cross-section with PVC bed and glass sidewalls; i.e., the flume was relatively smooth. The CFD results were close to the physical observations at x = 10.8 m. But they underestimated slightly the surge celerity while the water depth predictions at x = 6 m were consistently higher than the observations (Fig. 5-1). The CFD results showed a slight delay in the surge front propagation compared to the physical data and this might be a result of different downstream boundary conditions: i.e., an idealised gate opening for the CFD, versus the measured data at x = 10.8 m for the integration of Saint-Venant equations.

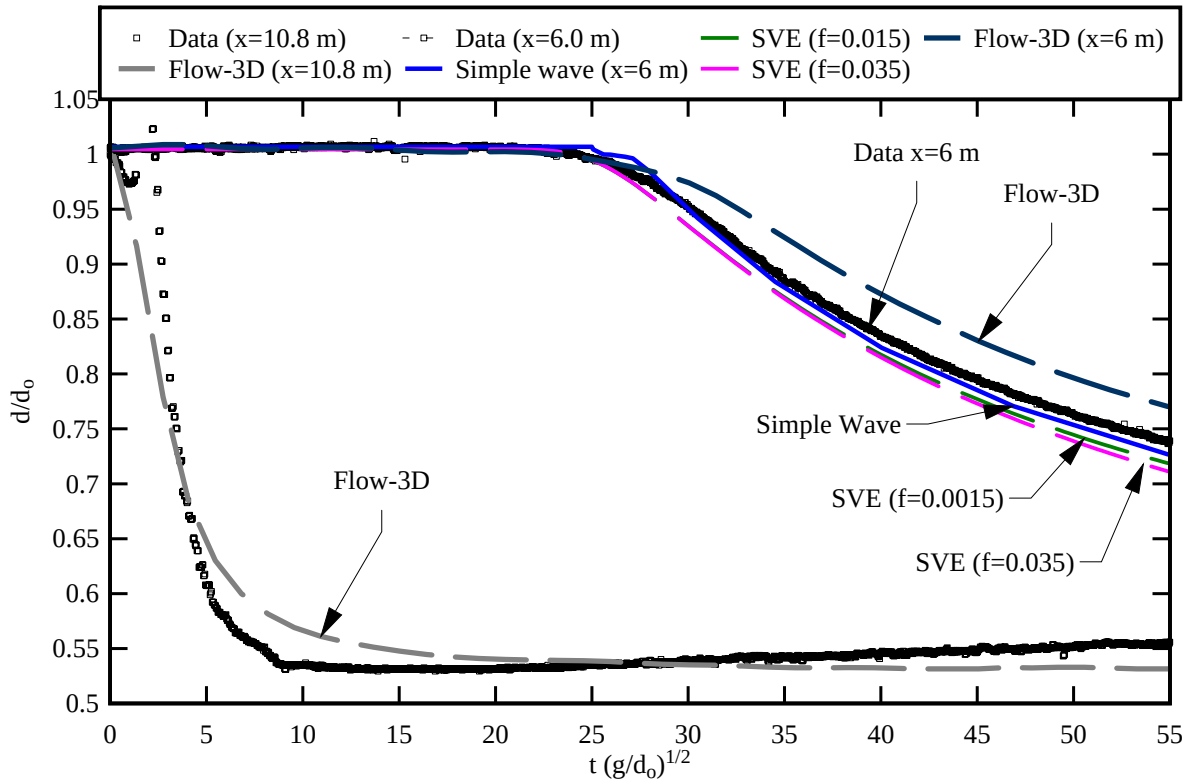

Fig. 5-1 - Dimensionless free-surface profile in a negative surge: comparison between physical, analytical and numerical results - Flow conditions: Q = 0.020 m^3/s, h = 0.030 m, x = 6.0 & 10.8 m

Some comparative results in terms of the longitudinal velocity data are presented in Figure 5-2. The physical data (instantaneous velocity) are compared with the calculations based upon of the simple wave methods, the numerical integration of the Saint-Venant equations and Flow-3D^{TM} simulations. Note that the simple wave and St Venant equation results are depth-averaged velocity data, while the physical data and the CFD results are functions of the relative vertical elevations z/d$_o$ at a given

cross-section. In Figure 5-2, the time-variations of the velocity V_x are presented in dimensionless form and the data were obtained at x = 6 m. The analytical and numerical results compared qualitatively well with the experimental measurements. All the data highlighted the acceleration of the flow beneath the negative surge. However neither the analytical nor numerical solutions can reproduce the turbulent fluctuations in terms of the longitudinal velocity, as indeed the numerical approaches were turbulence averaged. Both the physical observations and CFD results indicated an increase in longitudinal velocity components with increasing vertical elevation at a given time.

The CFD results generally underestimated the longitudinal velocities beneath the negative surge at all vertical elevations. The numerical data tended to compare better with the physical data at z/d_o = 0.6 than at z/d_o = 0.03 suggesting that the numerical model did not represent well the physical processes close to the channel bed.

In general, the simple wave method produced some reasonably good results compared to the experimental data. This was also the least time-consuming method. But both the simple wave method and the numerical integration of the Saint-Venant equations required an initial input time series (water depth) for the downstream boundary to predict the surge propagation.

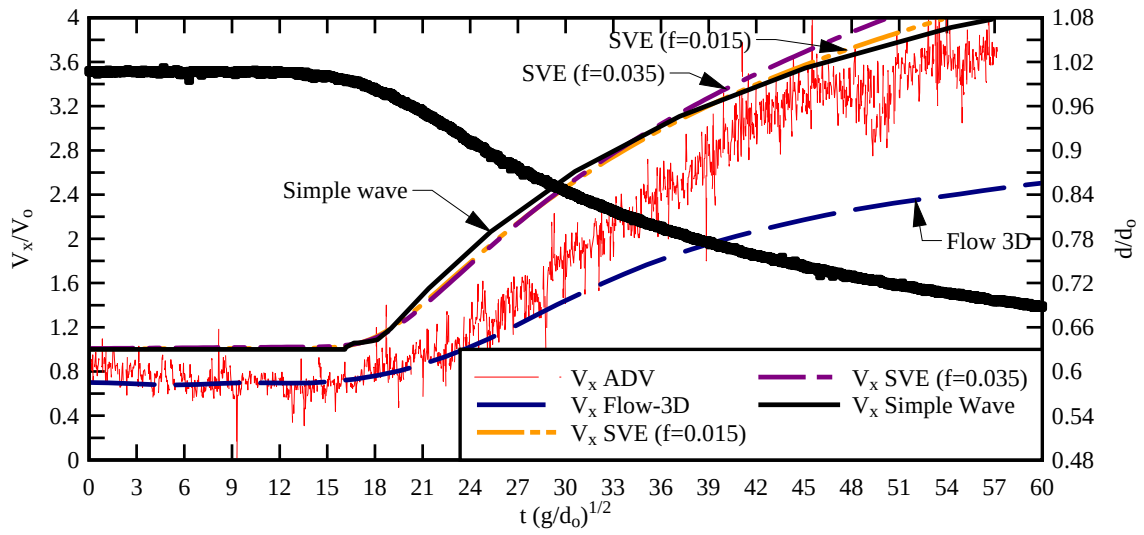

(A) z/d_o = 0.030

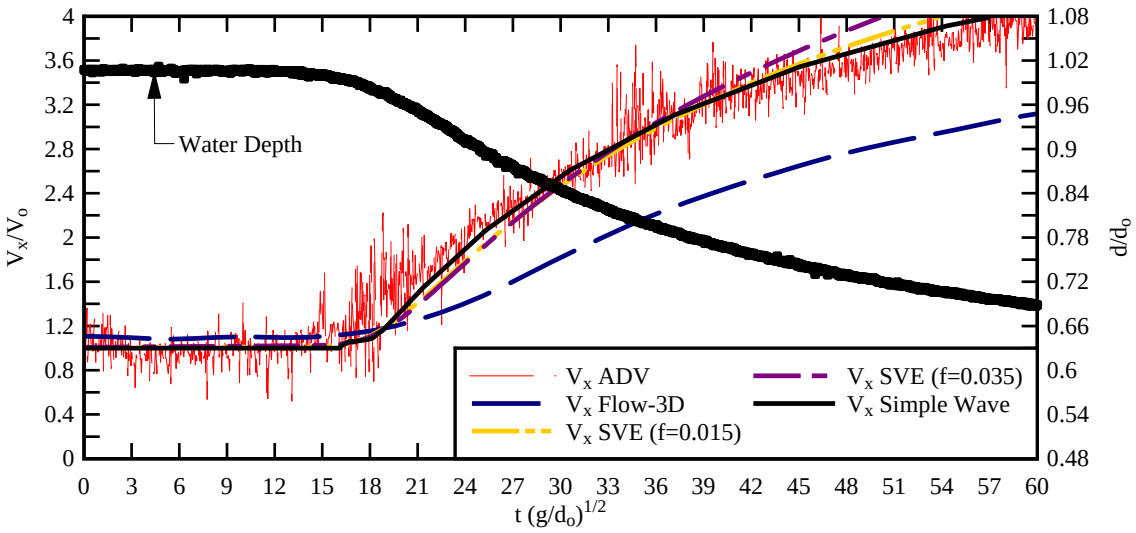

(B) $z/d_o = 0.615$

Fig. 5-2 - Dimensionless free-surface and longitudinal velocity in a negative surge: comparison between physical, analytical and numerical results - Flow conditions: Q = 0.020 m^3/s, h = 0.030 m, x = 6.0, z/d_o = 0.030 & 0.615

6. CONCLUSION

Limited quantitative informations about the characteristics and propagation of negative surges are available to date. In the present study, some new physical experiments were conducted in a large rectangular channel with high temporal and spatial resolution to characterise the unsteady free-surface profile and turbulence characteristics in a negative surge propagating upstream. The detailed velocity measurements were performed using acoustic Doppler velocimetry (ADV) at high frequency (200 Hz), while the free-surface elevations were recorded using non-intrusive techniques, namely acoustic displacement meters (ADM) and video imagery. The physical results were used as benchmark to test some analytical and numerical methods.

The physical observations showed that the leading edge of negative surge propagated upstream with a celerity which varied with time and space. During the first initial instants following the gate opening (formation phase), the celerity of negative surge leading edge increased with time up to x_{Gate}-x = $4d_o$. After the acceleration phase, the negative surge propagated upstream in a more gradual manner: the surge leading edge was very flat and barely perceptible (Fig. 6-1). Its celerity tended to decrease slowly with increasing distance from the gate. The data implied some deceleration in a manner which is contrary to theoretical considerations. At x_{Gate}-x = 5.15 m, the dimensionless negative surge celerity $(U+V_o)/(g\ d_o)^{1/2}$ ranged from 0.3 up to 1.0 depending upon the initial steady flow conditions.

The physical results showed that the propagation of the negative surges was associated with an acceleration of the flow. The velocity data highlighted some increased turbulence occurring beneath the negative surge, with large velocity fluctuations and large Reynolds stress components. The velocity fluctuations and turbulent stresses were significantly larger than in the initially steady flow and in the final flow motion. Further there was some more intense turbulent mixing occurring next to the gate (x_{Gate}-x = 0.35 m) shortly after gate opening than further upstream (x_{Gate}-x = 5.15 m). The rate of water elevation decrease was the largest next to the leading edge of the negative surge, while the longitudinal velocity increased during the initial stages of negative surge.

The physical results were used to test the analytical solution of the Saint-Venant equations and some 1-D and 2-D numerical model results. The findings showed that the negative surge propagation was relatively little affected by the boundary friction within the experimental flow conditions. For a relatively simple geometry such as the prismatic rectangular flume used herein, the physical data were best modelled by the simple wave analytical solution. Both numerical model results were qualitatively in agreement with the experimental observations.

The present results suggested that the negative surge remains a challenging topic for the computational modellers. Yet one must ask: do the results of the negative surge investigated in a

laboratory setting represent the real world? Is the analytical solution of the Saint-Venant equations more applicable to derive the free-surface profile of the surge propagation, as compared to the numerical solutions used in most one-dimensional flow models or derived from two-dimensional CFD models? What is the influence of the boundary conditions on the numerical results?

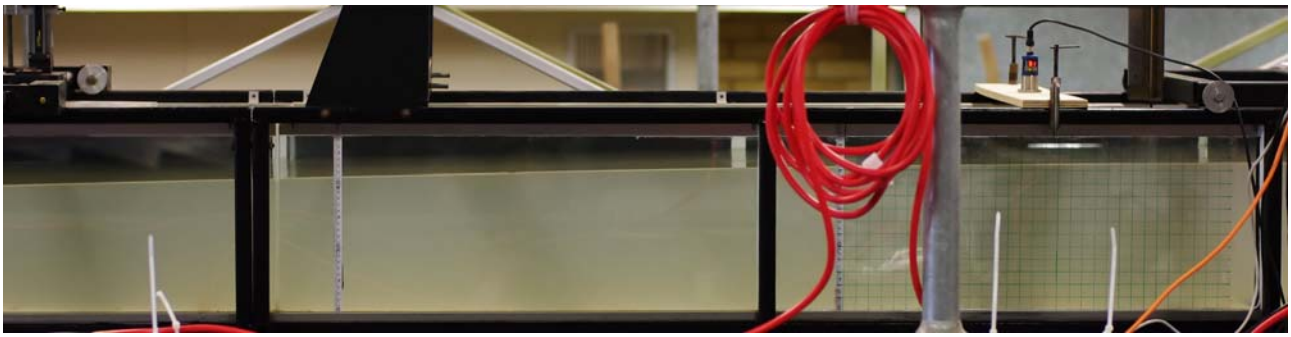

Fig. 6-1 - Negative surge propagation at x_{Gate}-x = 5.15 m - Negative wave leading edge propagating from left to right - The surge leading edge is approximately beneath the acoustic displacement meter in the right handside - Flow conditions: Q = 0.020 m^3/s, h = 0.030 m, x_s ~ 6 m

7. ACKNOWLEDGEMENTS

The authors thank Professor Fabian Bombardelli (University of California Davis) for his detailed review of the report and valuable comments, and Dr Pierre Lubin (University of Bordeaux) for some pertinent advice.

The writers acknowledge the advice of Dr Luke Toombes (Aurecon, Australia) and the assistance of Professor Peter Rutschmann (Technical University of Münich) to perform the numerical modelling with Flow-3D^{TM}. They acknowledge further the helpful inputs during the course of the study by Professor Fabian Bombardelli (University of California Davis), Professor John Fenton (Technical University Vienna) and Dr Pierre Lubin (University of Bordeaux) in alphabetical order.

APPENDIX A - PHOTOGRAPHIC OBSERVATIONS OF NEGATIVE SURGE EXPERIMENTS

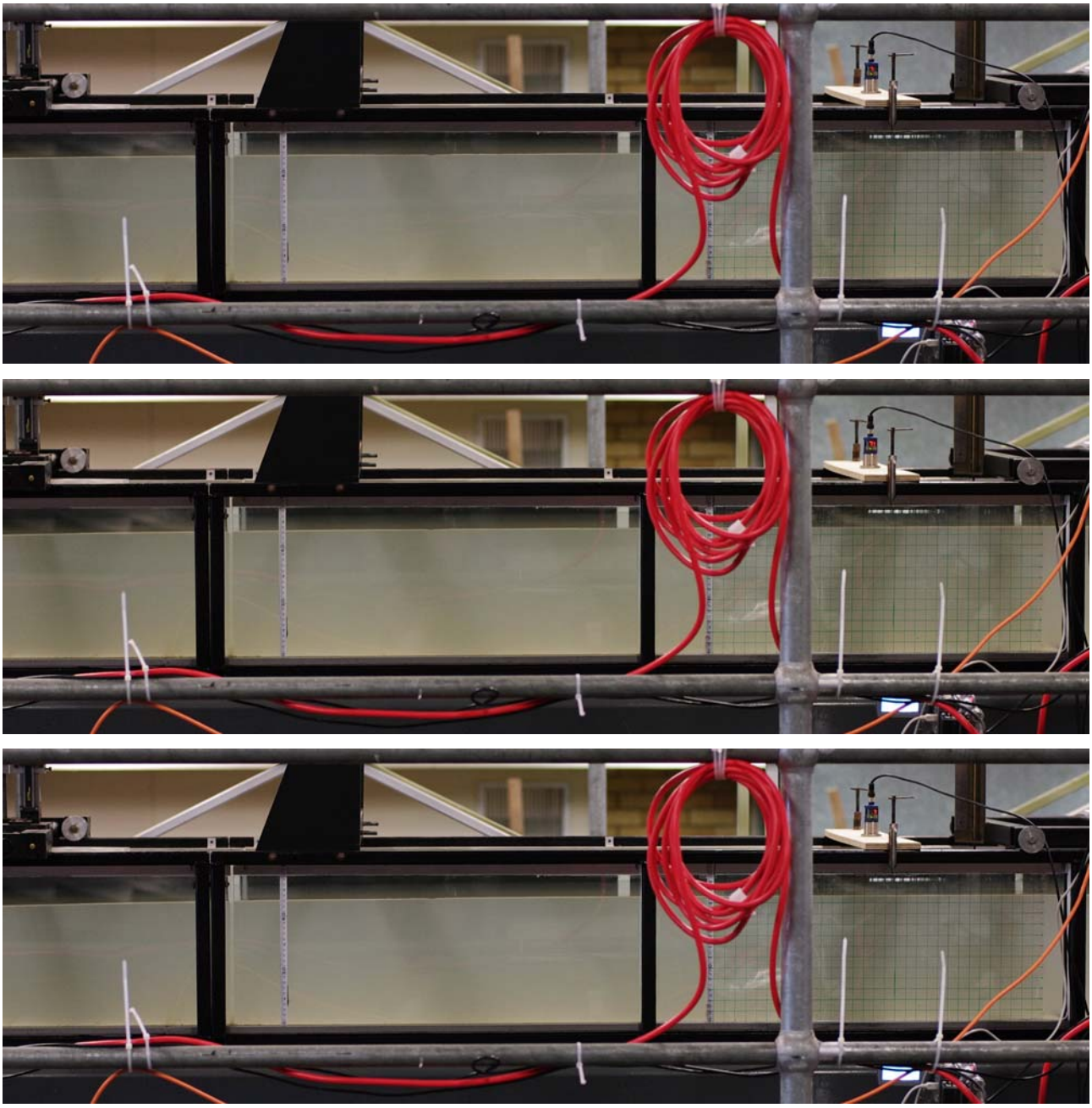

Fig. A-1 - Negative surge propagating upstream (from left to right) - Initial flow conditions: Q = 0.020 m^3/s, h = 0.030 m - From Top to Bottom, t = 0, 0.19, 0.38, 0.58, 0.77, 0.96, 1.15, 1.35, 1.54, 1.73, 1.92, 2.12 s - The photograph covers 8.5 m > x > 5.5 m - The leading edge of the negative surge appears on the far left of the first photograph - Lens: Voigtlander Nokton 58mm f1.4, shutter 1/1,00 s

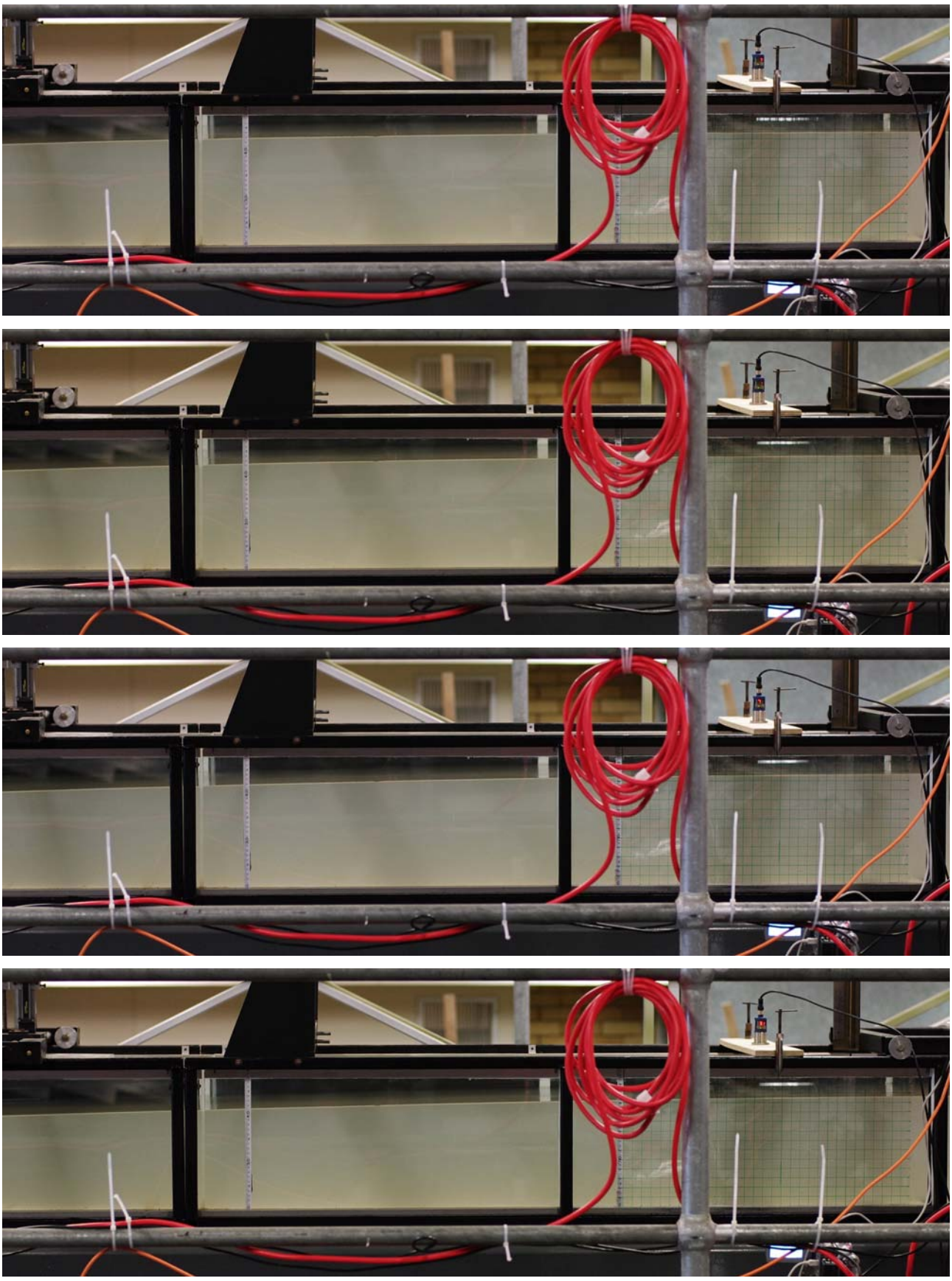

Fig. A-1 - Negative surge propagating upstream (from left to right) - Initial flow conditions: Q = 0.020 m^3/s, h = 0.030 m - From Top to Bottom, t = 0, 0.19, 0.38, 0.58, 0.77, 0.96, 1.15, 1.35, 1.54, 1.73, 1.92, 2.12 s - The photograph covers 8.5 m > x > 5.5 m - The leading edge of the negative

surge appears on the far left of the first photograph - Lens: Voigtlander Nokton 58mm f1.4, shutter 1/1,00 s

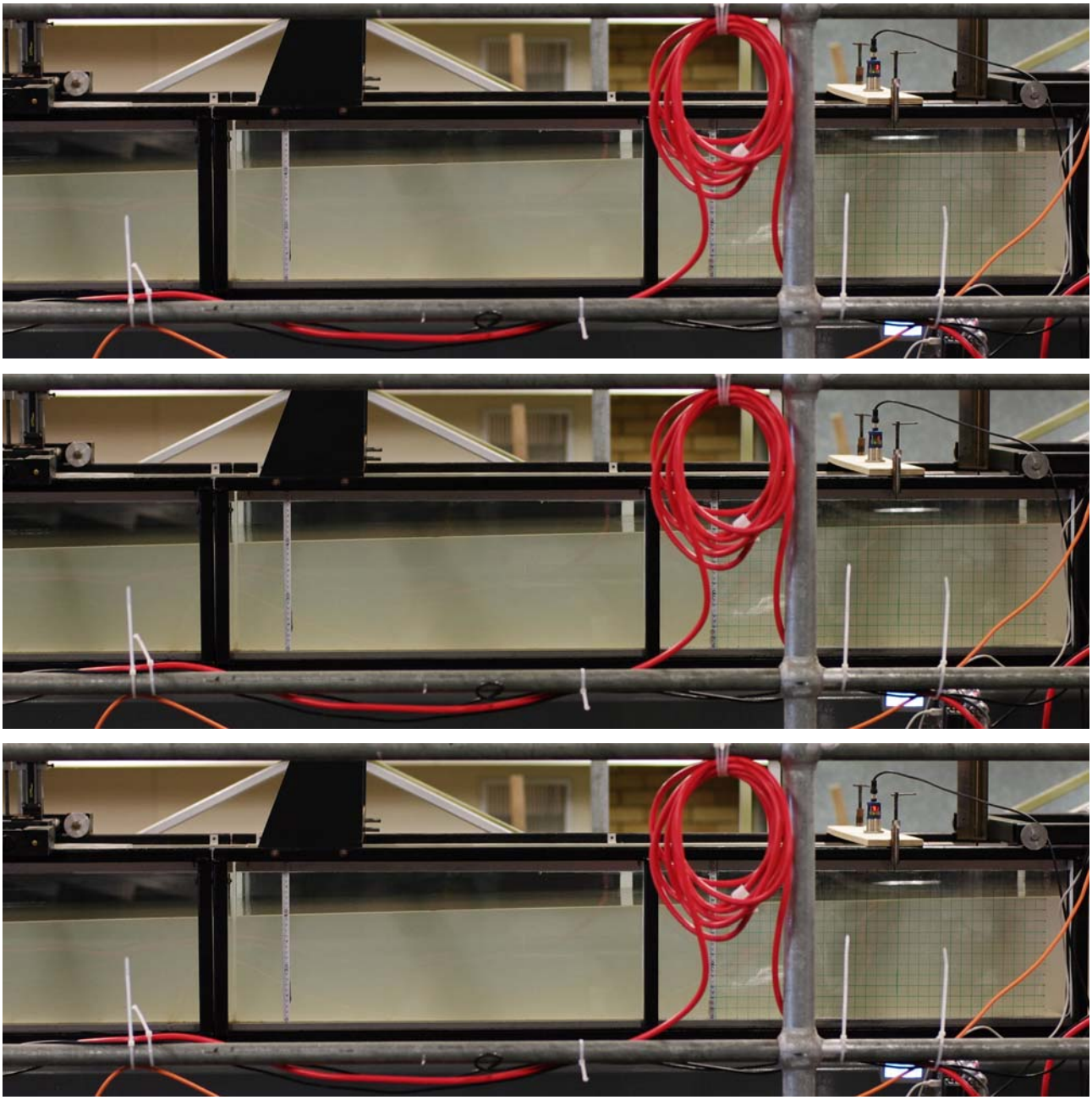

Fig. A-1 - Negative surge propagating upstream (from left to right) - Initial flow conditions: Q = 0.020 m^3/s, h = 0.030 m - From Top to Bottom, t = 0, 0.19, 0.38, 0.58, 0.77, 0.96, 1.15, 1.35, 1.54, 1.73, 1.92, 2.12 s - The photograph covers 8.5 m > x > 5.5 m - The leading edge of the negative surge appears on the far left of the first photograph - Lens: Voigtlander Nokton 58mm f1.4, shutter 1/1,00 s

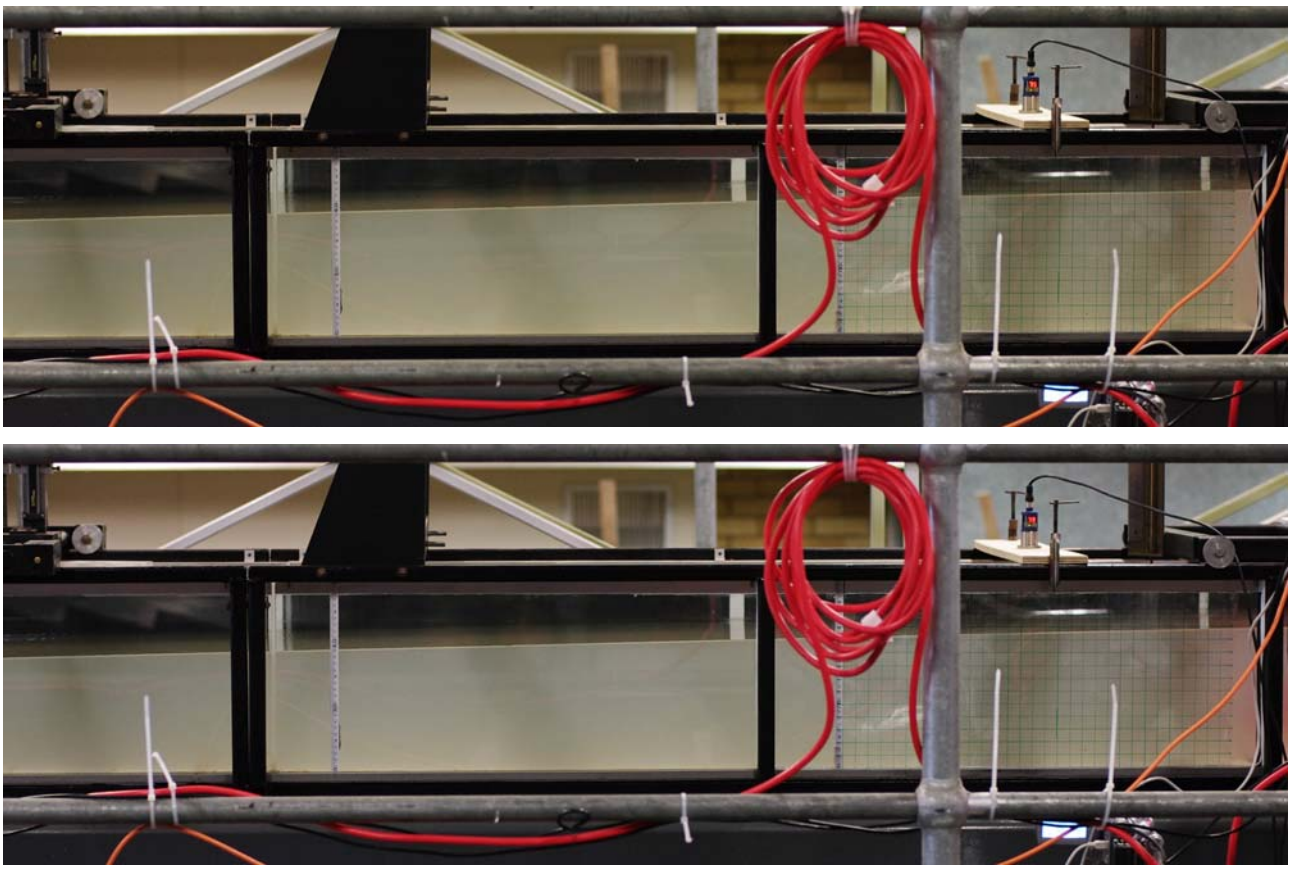

Fig. A-1 - Negative surge propagating upstream (from left to right) - Initial flow conditions: Q = 0.020 m^3/s, h = 0.030 m - From Top to Bottom, t = 0, 0.19, 0.38, 0.58, 0.77, 0.96, 1.15, 1.35, 1.54, 1.73, 1.92, 2.12 s - The photograph covers 8.5 m > x > 5.5 m - The leading edge of the negative surge appears on the far left of the first photograph - Lens: Voigtlander Nokton 58mm f1.4, shutter 1/1,00 s

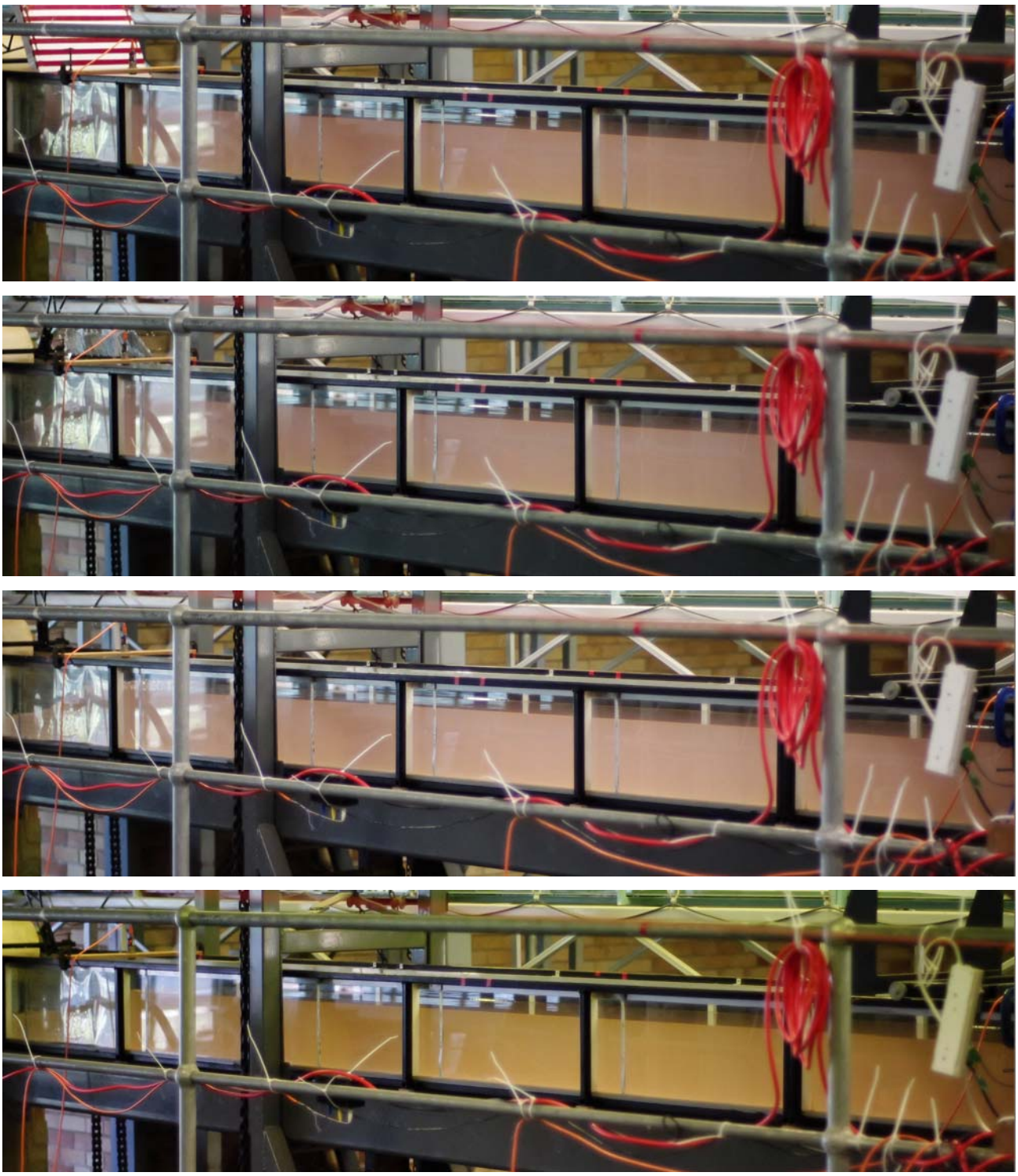

Fig. A-2 - Negative surge propagating upstream (from left to right) - Initial flow conditions: Q = 0.020 m^3/s, h = 0.030 m - From Top to Bottom, t = 0, 0.19, 0.38, 0.58, 0.77, 0.96, 1.15, 1.35, 1.54, 1.73, 1.92, 2.12, 2.31, 2.50, 2.69, 2.88, 3.08 s - The photograph covers 11 m > x > 6 m - The first photograph corresponds to the instant when the gate lower edge (far left) is just above the water surface - Lens: Voigtlander Nokton 58mm f1.4, shutter 1/1,000 s

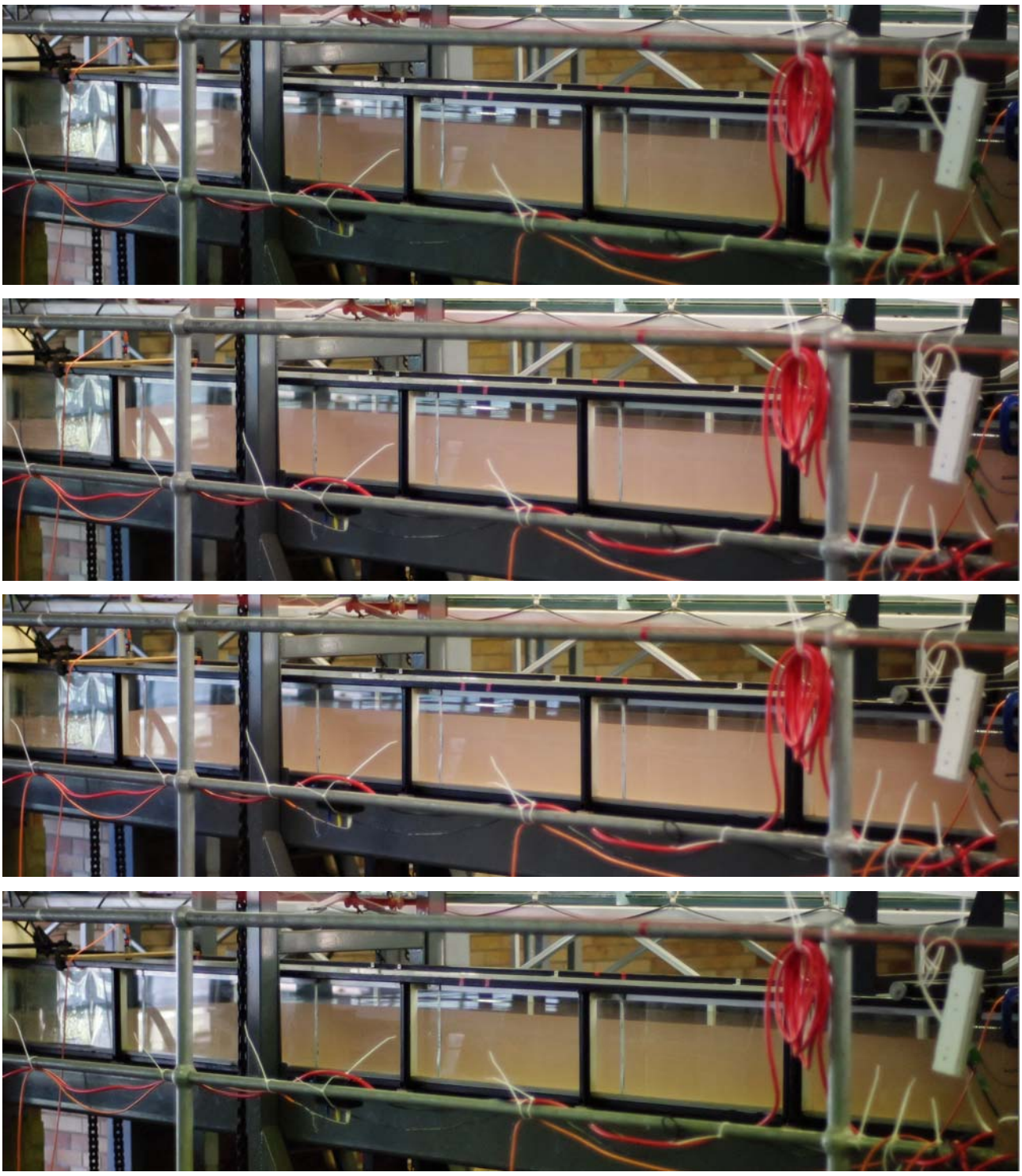

Fig. A-2 - Negative surge propagating upstream (from left to right) - Initial flow conditions: Q = 0.020 m^3/s, h = 0.030 m - From Top to Bottom, t = 0, 0.19, 0.38, 0.58, 0.77, 0.96, 1.15, 1.35, 1.54, 1.73, 1.92, 2.12, 2.31, 2.50, 2.69, 2.88, 3.08 s - The photograph covers 11 m > x > 6 m - The first photograph corresponds to the instant when the gate lower edge (far left) is just above the water surface - Lens: Voigtlander Nokton 58mm f1.4, shutter 1/1,000 s

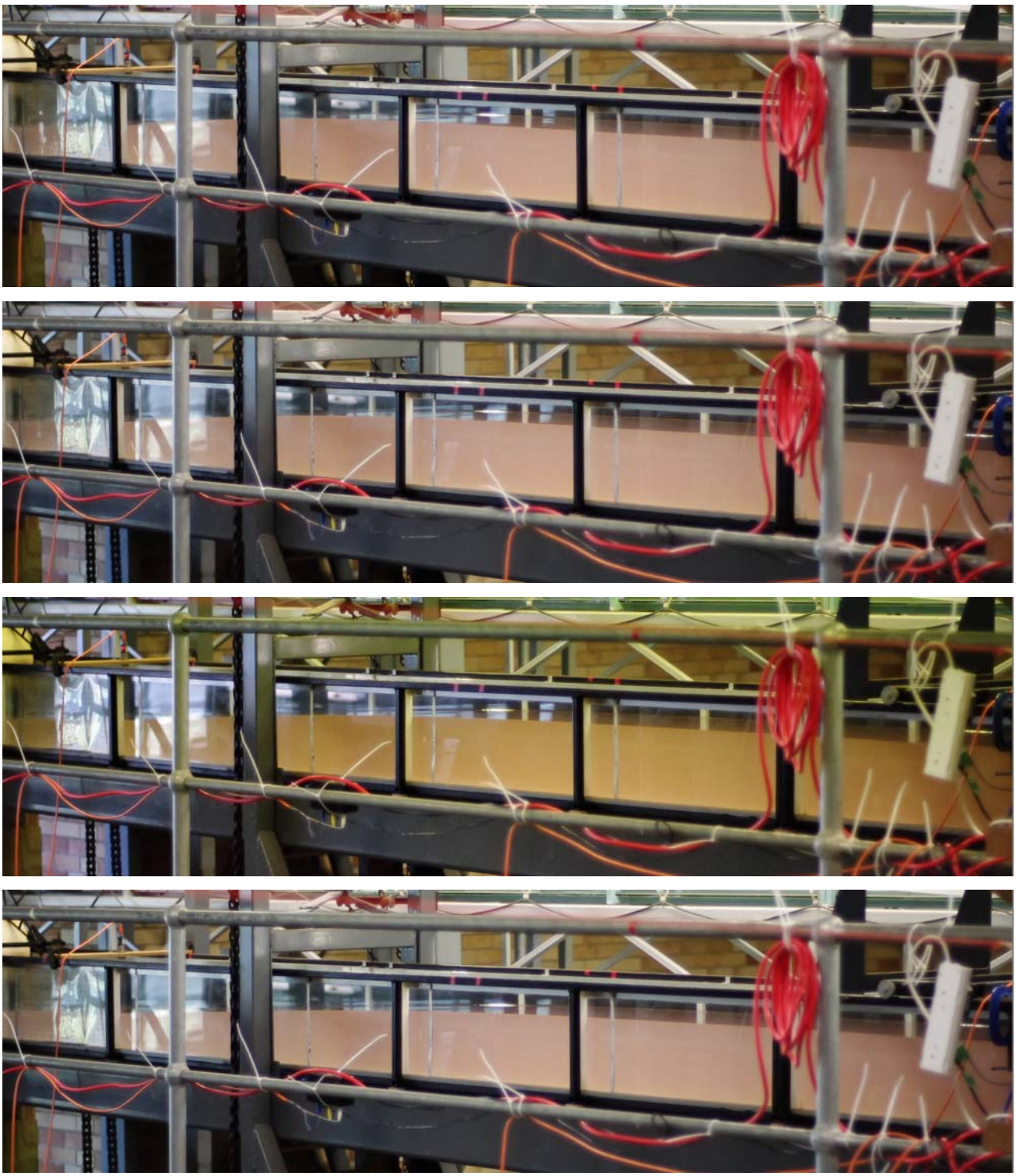

Fig. A-2 - Negative surge propagating upstream (from left to right) - Initial flow conditions: Q = 0.020 m^3/s, h = 0.030 m - From Top to Bottom, t = 0, 0.19, 0.38, 0.58, 0.77, 0.96, 1.15, 1.35, 1.54, 1.73, 1.92, 2.12, 2.31, 2.50, 2.69, 2.88, 3.08 s - The photograph covers 11 m > x > 6 m - The first photograph corresponds to the instant when the gate lower edge (far left) is just above the water surface - Lens: Voigtlander Nokton 58mm f1.4, shutter 1/1,000 s

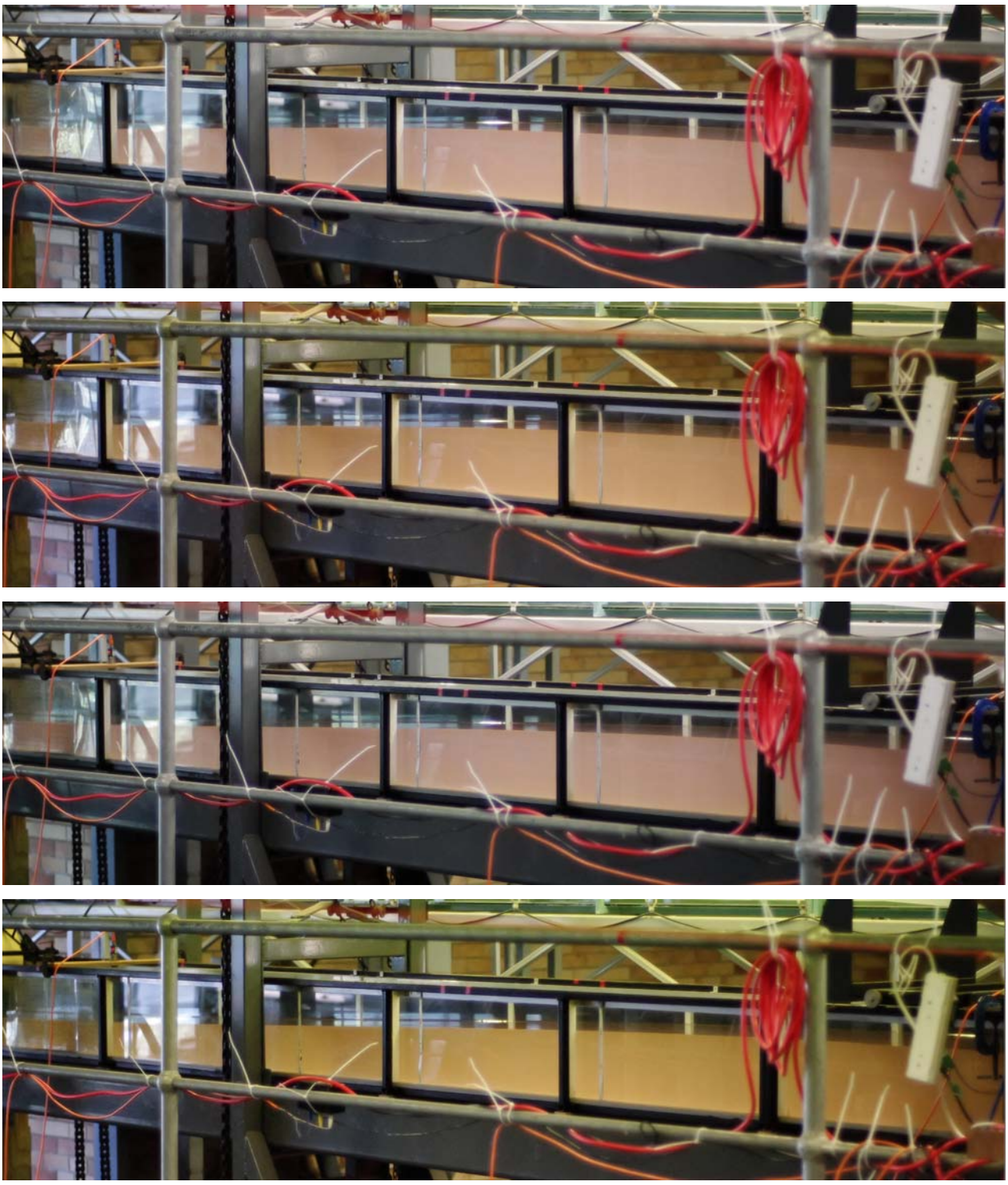

Fig. A-2 - Negative surge propagating upstream (from left to right) - Initial flow conditions: Q = 0.020 m^3/s, h = 0.030 m - From Top to Bottom, t = 0, 0.19, 0.38, 0.58, 0.77, 0.96, 1.15, 1.35, 1.54, 1.73, 1.92, 2.12, 2.31, 2.50, 2.69, 2.88, 3.08 s - The photograph covers 11 m > x > 6 m - The first photograph corresponds to the instant when the gate lower edge (far left) is just above the water surface - Lens: Voigtlander Nokton 58mm f1.4, shutter 1/1,000 s

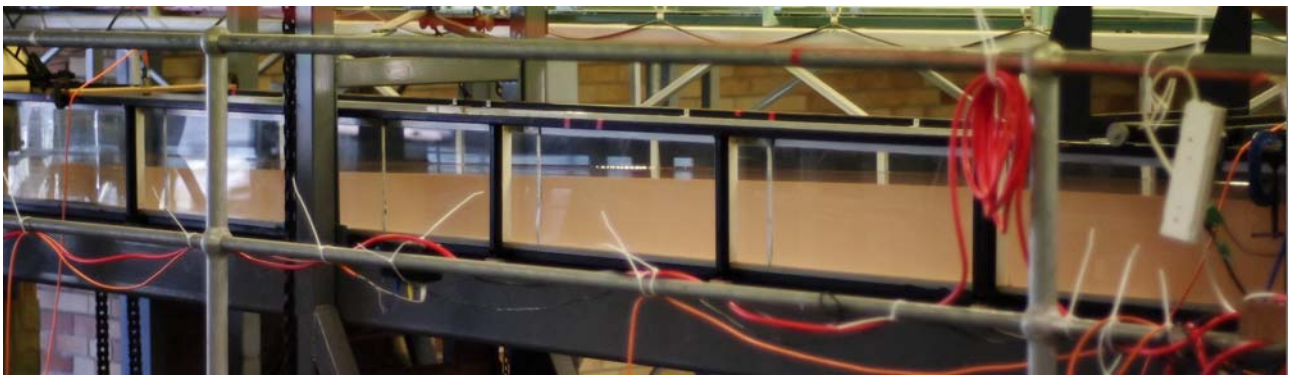

Fig. A-2 - Negative surge propagating upstream (from left to right) - Initial flow conditions: Q = 0.020 m^3/s, h = 0.030 m - From Top to Bottom, t = 0, 0.19, 0.38, 0.58, 0.77, 0.96, 1.15, 1.35, 1.54, 1.73, 1.92, 2.12, 2.31, 2.50, 2.69, 2.88, 3.08 s - The photograph covers 11 m > x > 6 m - The first photograph corresponds to the instant when the gate lower edge (far left) is just above the water surface - Lens: Voigtlander Nokton 58mm f1.4, shutter 1/1,000 s

APPENDIX B - PHYSICAL NEGATIVE SURGE EXPERIMENTS: INITIAL AND FINAL BOUNDARY CONDITIONS

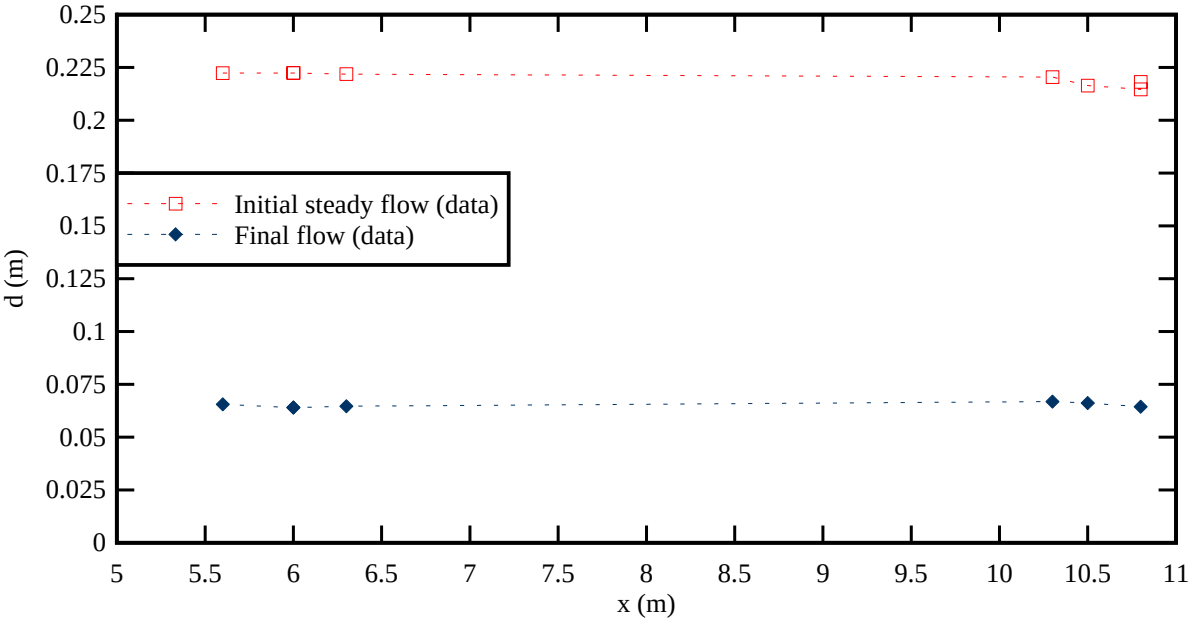

Fig. B-1 - Initial steady flow free-surface profile prior to negative surge and final free-surface profile after gate opening - Flow conditions: Q = 0.020 m^3/s, h = 0.030 m, steady flow direction from right to left

APPENDIX C - TURBULENT VELOCITY MEASUREMENTS BENEATH A NEGATIVE SURGE

C.1 PRESENTATION

In a turbulent flow, the instantaneous velocity may be separated into an average component plus a turbulent fluctuation:

$$V = \overline{V} + v \tag{D-1}$$

where V is the instantaneous velocity, $\overline{V}$ is the average velocity, and v is the instantaneous fluctuation. In steady flows, $\overline{V}$ is the time-averaged velocity. When the flow is unsteady, the time-average is meaningless, and the long-term and short-term turbulent fluctuations must be processed separately. In periodic flows, $\overline{V}$ may be taken as the phase-averaged velocity. In a transient flow, the mean motion is determined by ensemble-averaging (Bradshaw 1971, Schlichting and Gersten 2001). That is, the experiment is repeated N times and the ensemble-averaged velocity is:

$$\overline{V} = \frac{1}{N}\sum_{i-1}^{N} V_i \tag{D-2}$$

where the subscript i refers to the experimental run. When the number N of experiments is small, the ensemble-average is best replaced the ensemble median value. The turbulent velocity fluctuation v becomes the deviation of the instantaneous velocity V from the ensemble median $\overline{V}$.

Herein the turbulent velocity measurements were performed for the experimental flow conditions summarised in Table C-1. At each sampling location, 25 runs were repeated and the data were ensemble-averaged. The ensemble median was calculated as well as the standard deviation of the turbulent velocity fluctuation:

$$v' = \sqrt{\frac{1}{N}\sum_{i-1}^{N} (V_i - \overline{V})^2} \tag{D-3}$$

where $\overline{V}$ is the ensemble median.

Table C-1 - Experimental flow conditions for turbulent stress measurements in negative surges

Q	S_o	h	d_o	V_o	ADV location	
					x	z
(m^3/s)			(m)	(m/s)	(m)	(m)
(1)	(2)	(3)	(4)	(5)	(6)	(7)
0.020	0.000	0.030	0.22	0.18	6.0	0.00669, 0.12394, 0.1352
					10.5	0.00669, 0.02501, 0.12394, 0.1352

Notes: d_o initial flow depth at x = 6 m; Q: initial flow rate; S_o: bed slope; V_o initial flow velocity at x = 6 m; z: vertical elevation of sampling volume.

List of symbols

d	flow depth (m) measured normal to the invert;
d_o	initial flow depth (m) measured normal to the chute invert at x = 6 m;
g	gravity constant (m/s^2): g = 9.794 m/s^2 in Brisbane, Australia;
h	undershoot gate height (m) prior to sudden gate opening
Q	volume flow rate (m^3/s);
S_o	bed slope: $S_o = \sin\theta$;
V	instantaneous velocity component (m/s);
V_o	initial flow velocity (m/s) at x = 6 m;
v	instantaneous turbulent velocity fluctuation (m/s);
v'	standard deviation (m/s) of turbulent velocity fluctuation;
$\overline{V}$	ensemble-median velocity component (m/s).
x	longitudinal distance (m) measured from the channel upstream end, positive downstream;
z	distance (m) normal to the bed; it is the vertical distance (m) for a horizontal channel; for the fixed ravel bed, z is measured above the top of the gravel bed;
θ	bed slope angle with the horizontal, positive downwards;

Subscript

o	initial flow conditions: i.e., upstream of the negative surge leading edge;
x	longitudinal direction positive downstream;
y	transverse direction positive towards the left;
z	vertical direction positive upwards;
25	first quartile: i.e., value for which 25% of data are smaller;
75	third quartile: i.e., value for which 75% of data are smaller;

Abbreviations

EA	ensemble average.

C.2 RESULTS

The basic results are presented herein in terms of the median component calculated using an ensemble-averaging (EA) method (median value of 25 runs). The results are presented in Figures C-1 and C-2 for x = 6 m and x = 10.5 m respectively. The latter location was close to the gate while the former was 5.15 m upstream of the tainter gate. The gate was located at x = 1.15 m. Figures C-1

and C-2 show the median water depth, the ensemble median velocity component, the instantaneous velocity component during an experimental run (run 1) and the difference between the 3rd and 1st quartiles (V_{75}-V_{25}). For a Gaussian velocity distribution around the mean, the difference (V_{75}-V_{25}) would correspond to 0.7v' where v' is the standard deviation of the velocity component.

The experimental results showed a number of basic features at both locations. The longitudinal velocity measurements showed a acceleration of the flow beneath the negative surge (Fig. C1-1 & C-2). This was associated with some increase in all velocity component fluctuations, compared to the steady state. The transverse velocity component V_y showed quantitatively lesser fluctuations before, during and after surge formation than in the horizontal and vertical directions. Close to the free-surface (z/d_o = 0.56 & 0.62), the vertical velocity component was negative on average and its magnitude was comparable to the maximum vertical velocity of the free-surface: that is, $(\partial d/\partial z)_{max}$ = -0.303 and -0.045 m/s at x = 10.5 and 6 m respectively. The present data indicated that the negative surge flow was an unsteady three-dimensional turbulent process.

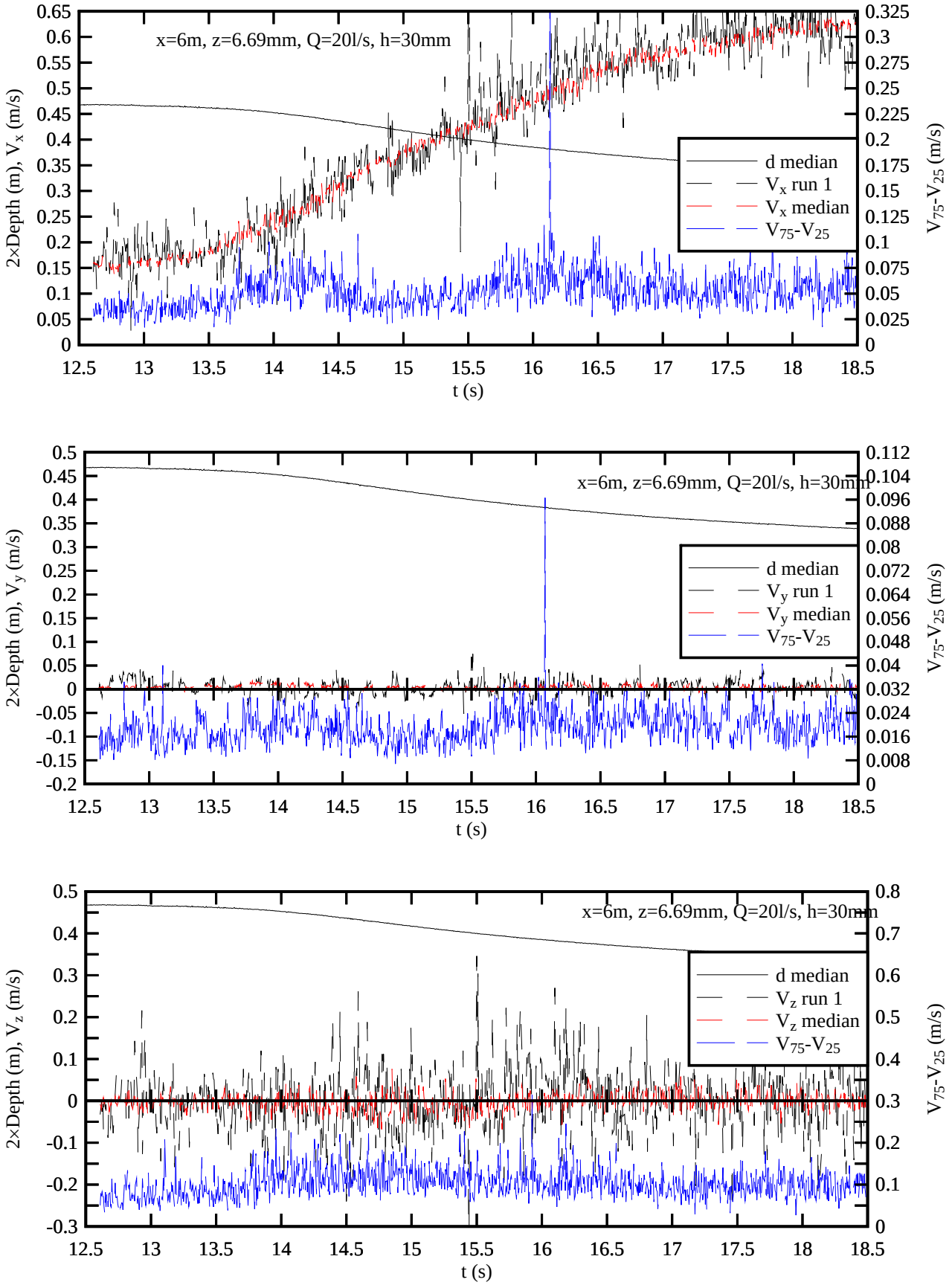
x=6m, z=6.69mm, Q=20l/s, h=30mm
2×Depth (m), Vx (m/s)
V75-V25 (m/s)
t (s)
d median
Vx run 1
Vx median
V75-V25
x=6m, z=6.69mm, Q=20l/s, h=30mm
2×Depth (m), Vy (m/s)
V75-V25 (m/s)
t (s)
d median
Vy run 1
Vy median
V75-V25
x=6m, z=6.69mm, Q=20l/s, h=30mm
2×Depth (m), Vz (m/s)
V75-V25 (m/s)
t (s)
d median
Vz run 1
Vz median
V75-V25

(A) $z/d_o = 0.030$

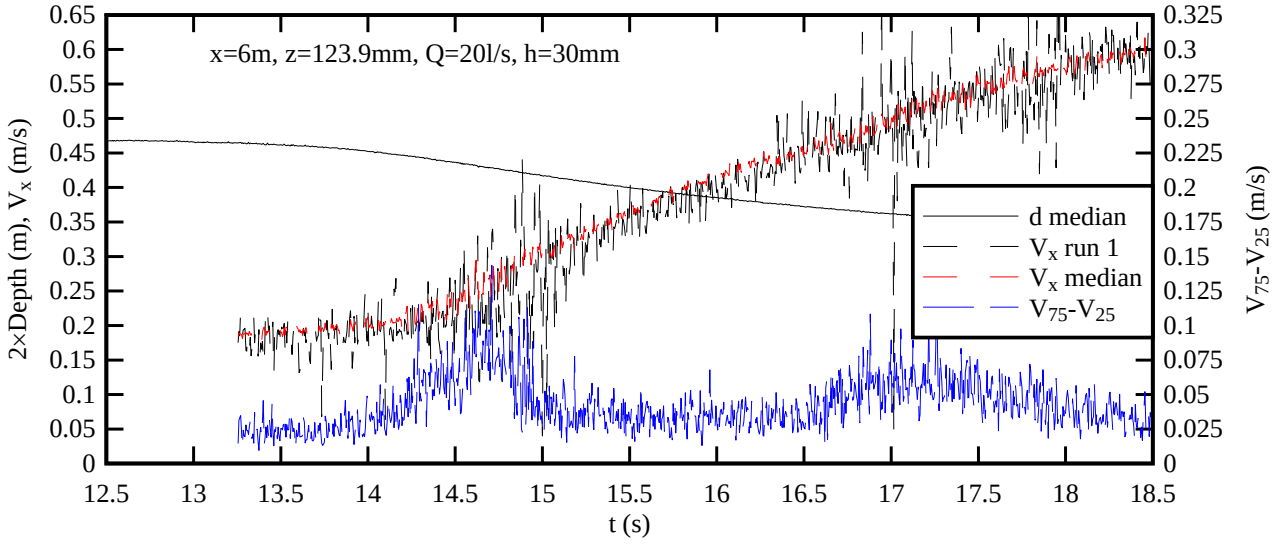
x=6m, z=123.9mm, Q=20l/s, h=30mm
2×Depth (m), Vx (m/s)
V75-V25 (m/s)
t (s)
d median
Vx run 1
Vx median
V75-V25

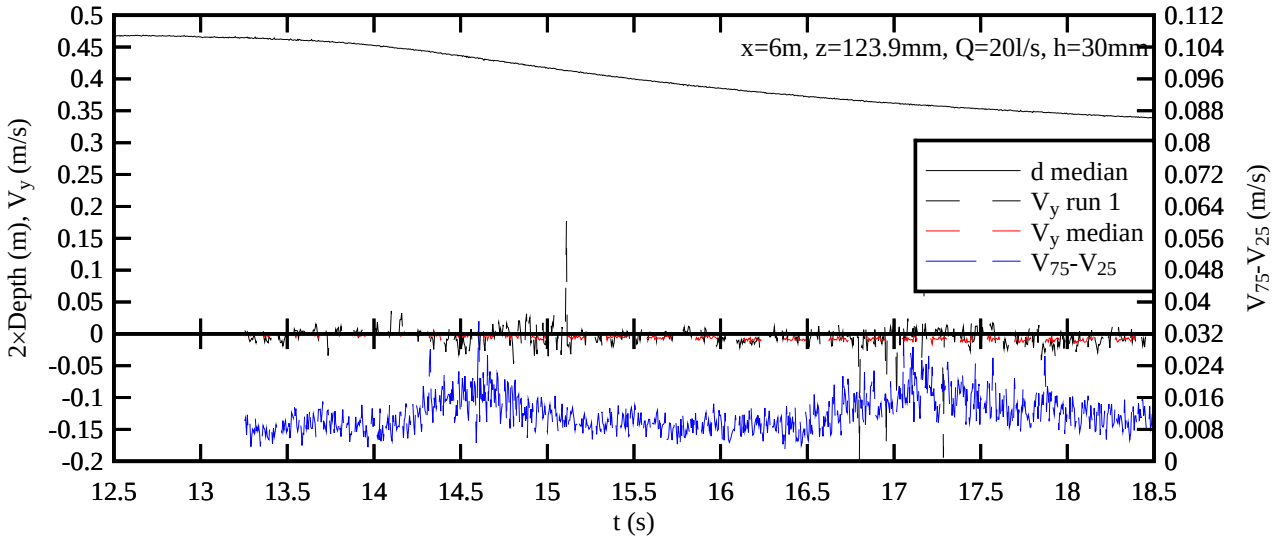
x=6m, z=123.9mm, Q=20l/s, h=30mm
2×Depth (m), Vy (m/s)
V75-V25 (m/s)
t (s)
d median
Vy run 1
Vy median
V75-V25

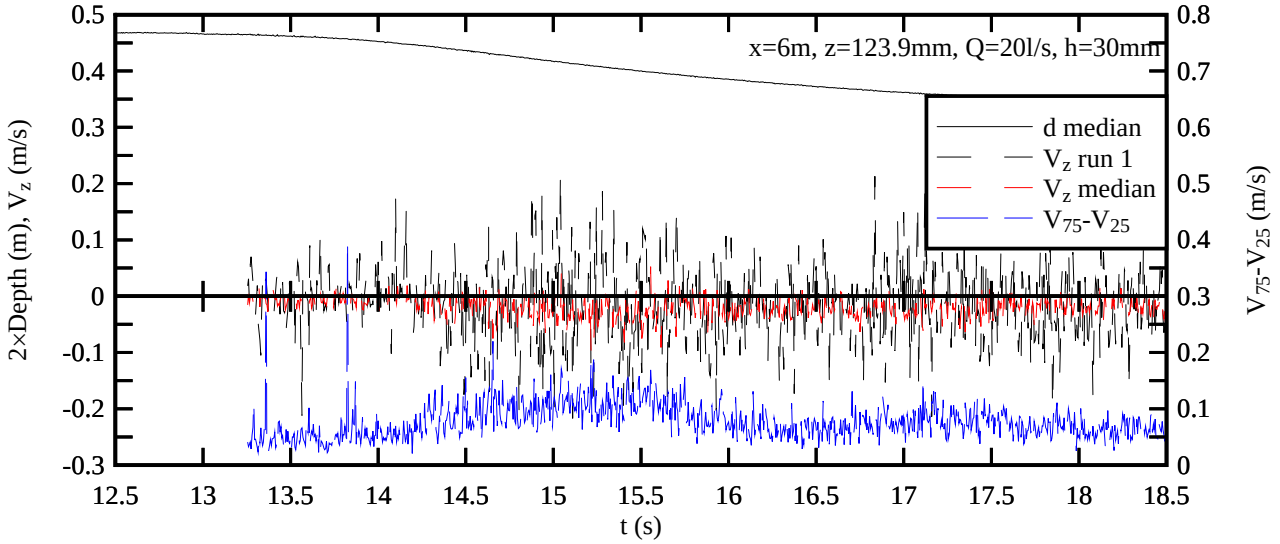
x=6m, z=123.9mm, Q=20l/s, h=30mm
2×Depth (m), Vz (m/s)
V75-V25 (m/s)
t (s)
d median
Vz run 1
Vz median
V75-V25

(B) $z/d_o = 0.563$

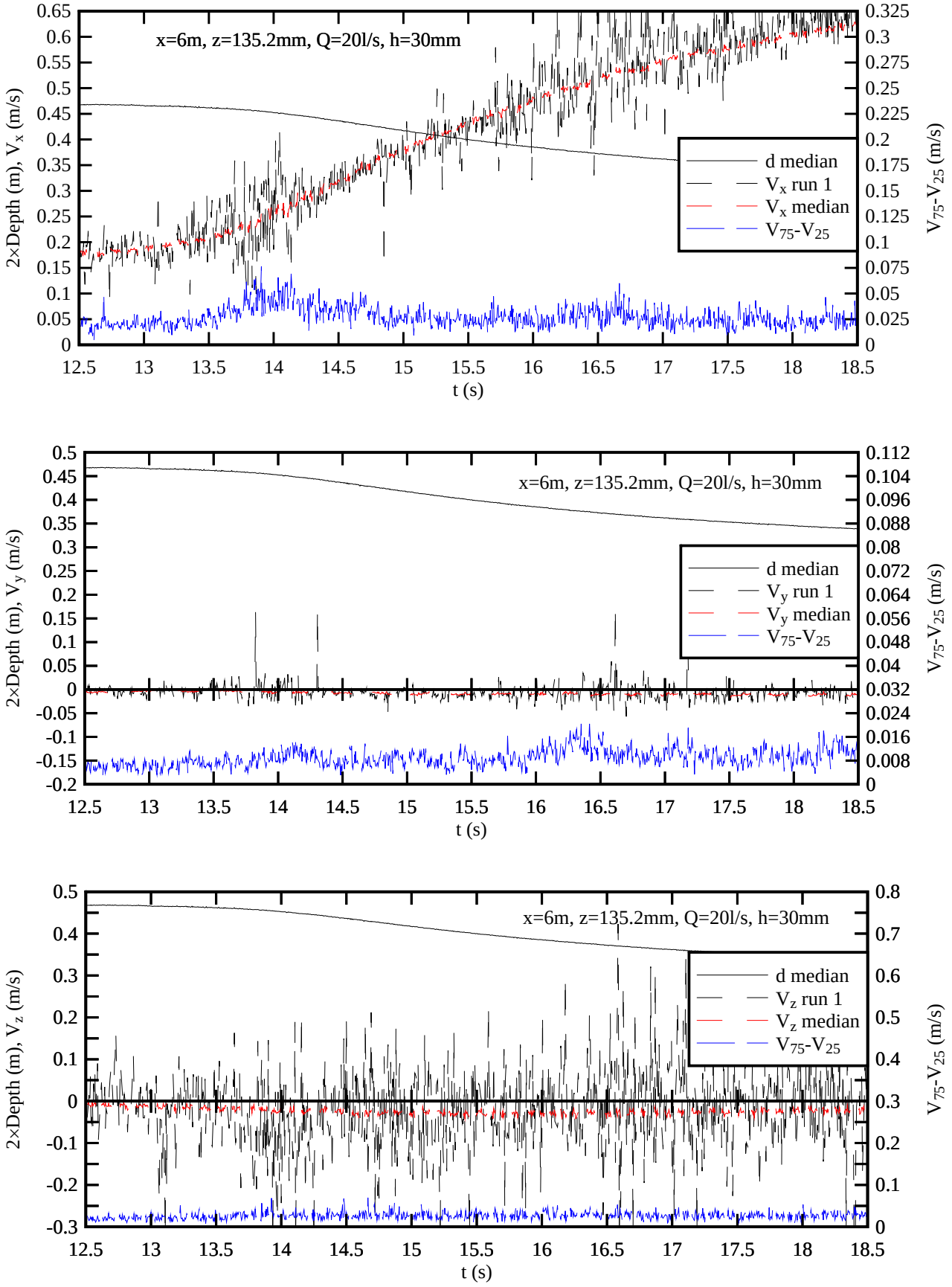

(D) $z/d_o = 0.615$

Fig. C-1 - Ensemble-median water depth d_{median}, median velocity components and difference between the 3rd and 1st quartiles (V_{75}-V_{25}) beneath a negative surge at x = 6 m (5.15 m upstream of

gate) - From top to bottom: V_x, V_y, V_z - Flow conditions: Q = 0.020 m^3/s, h = 0.030 m, x = 6.0 m

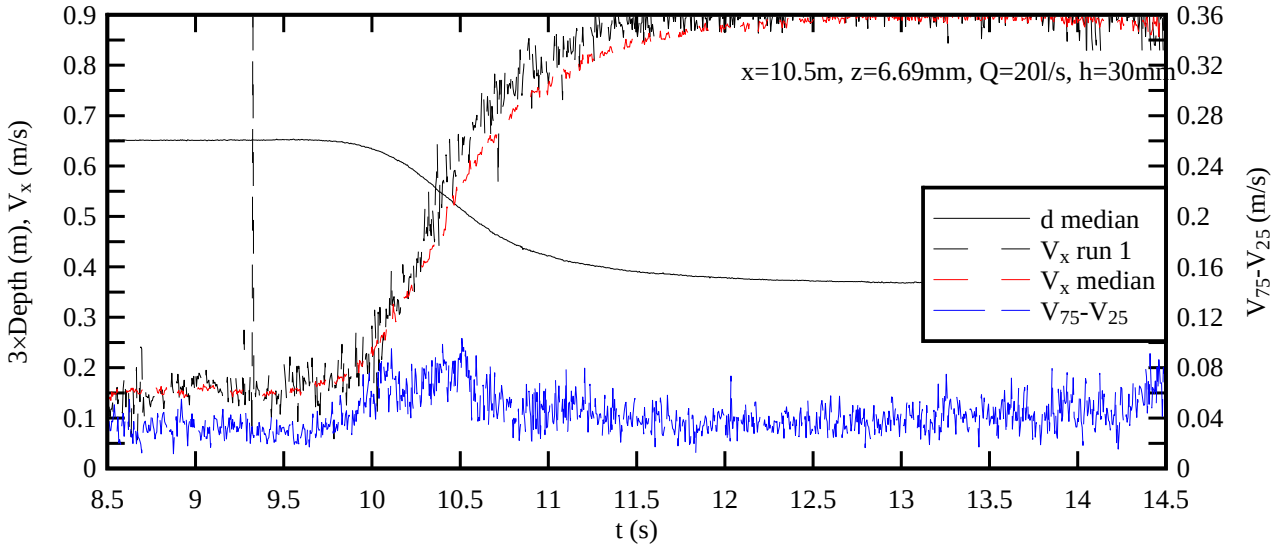

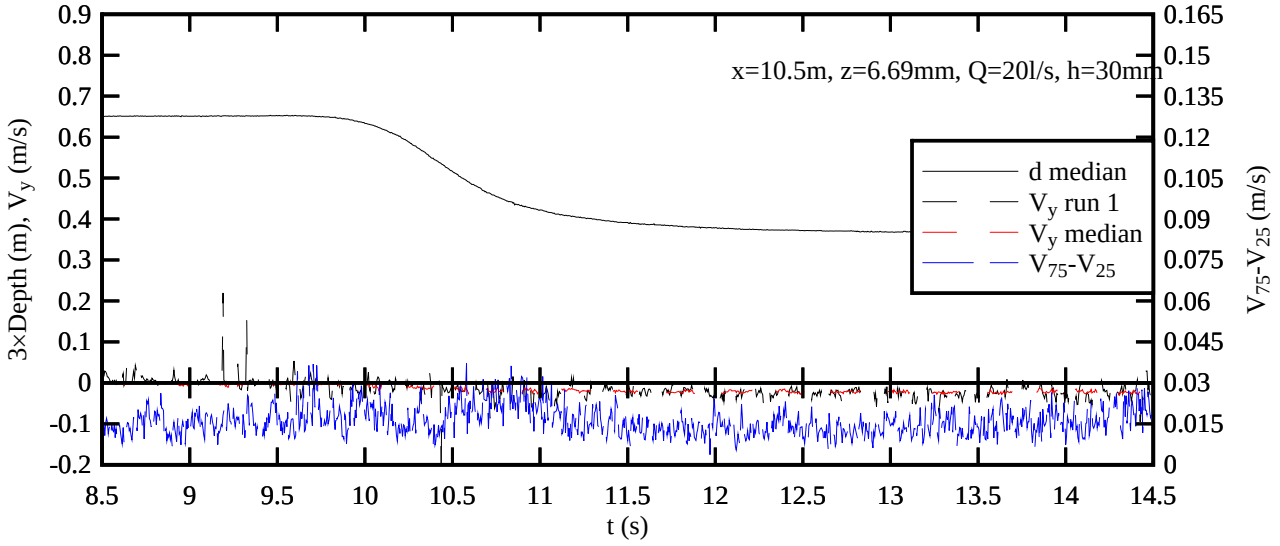

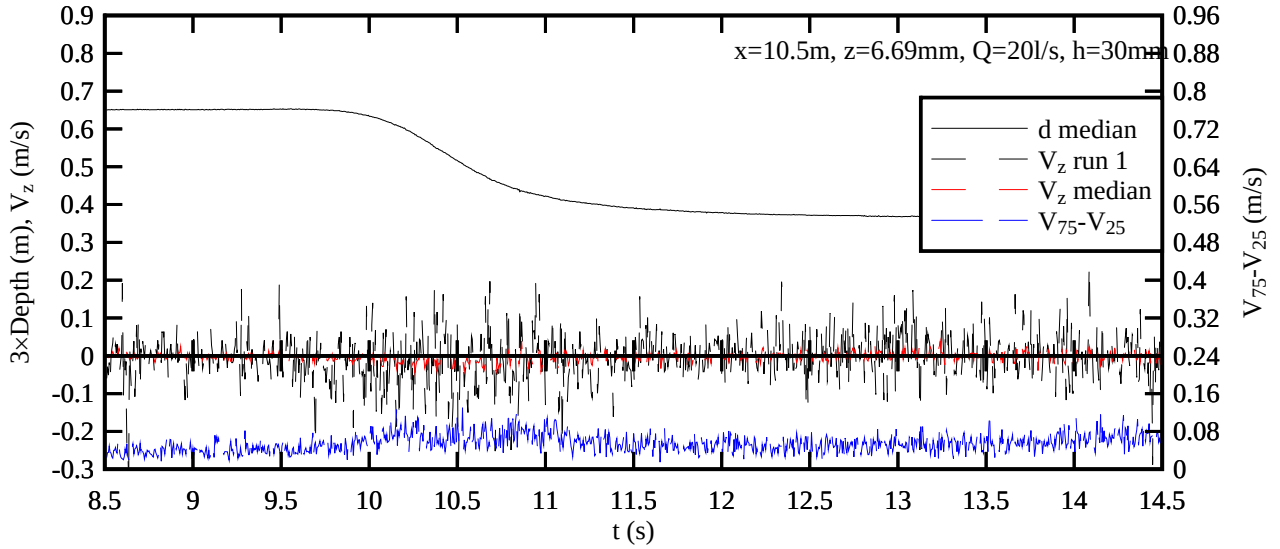

(A) $z/d_o = 0.030$

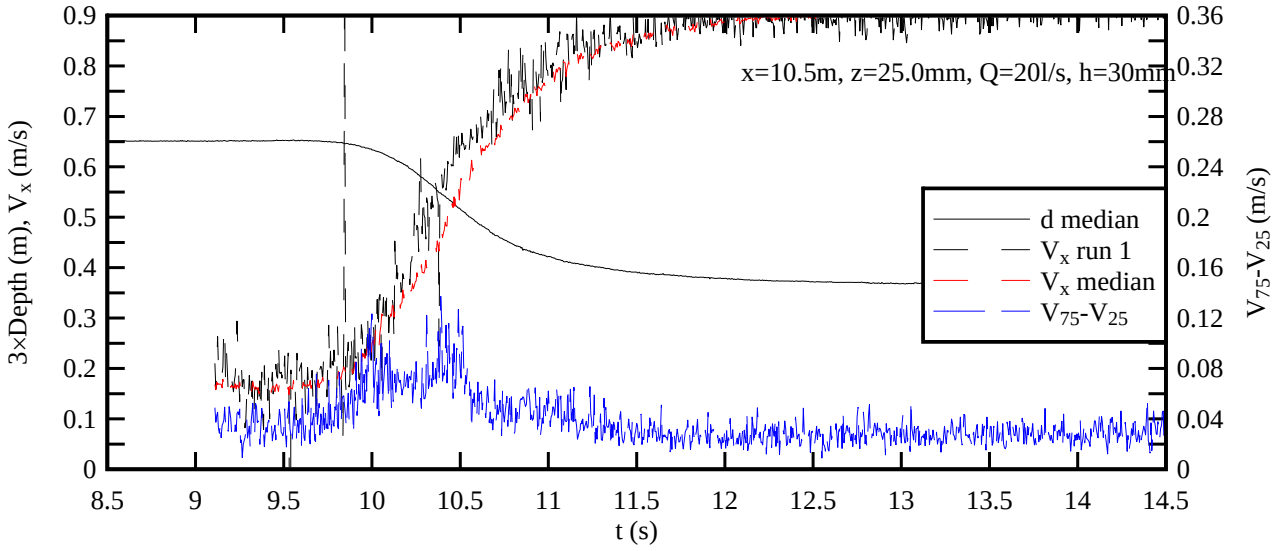
x=10.5m, z=25.0mm, Q=20l/s, h=30mm
3×Depth (m), V_x (m/s)
V_{75}-V_{25} (m/s)
t (s)
d median
V_x run 1
V_x median
V_{75}-V_{25}

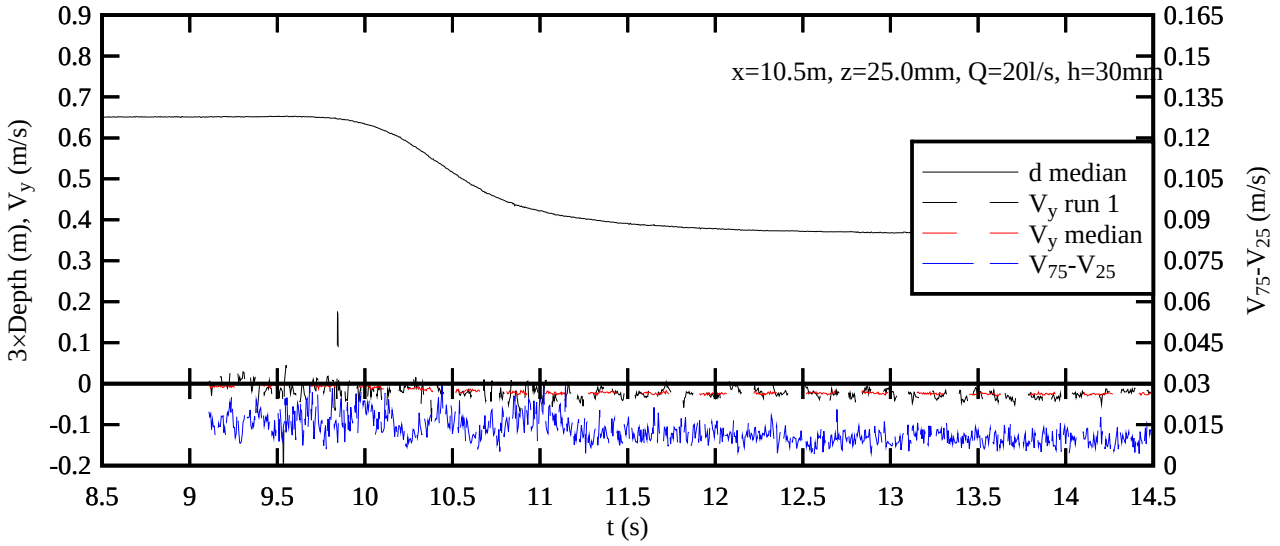
x=10.5m, z=25.0mm, Q=20l/s, h=30mm
3×Depth (m), V_y (m/s)
V_{75}-V_{25} (m/s)
t (s)
d median
V_y run 1
V_y median
V_{75}-V_{25}

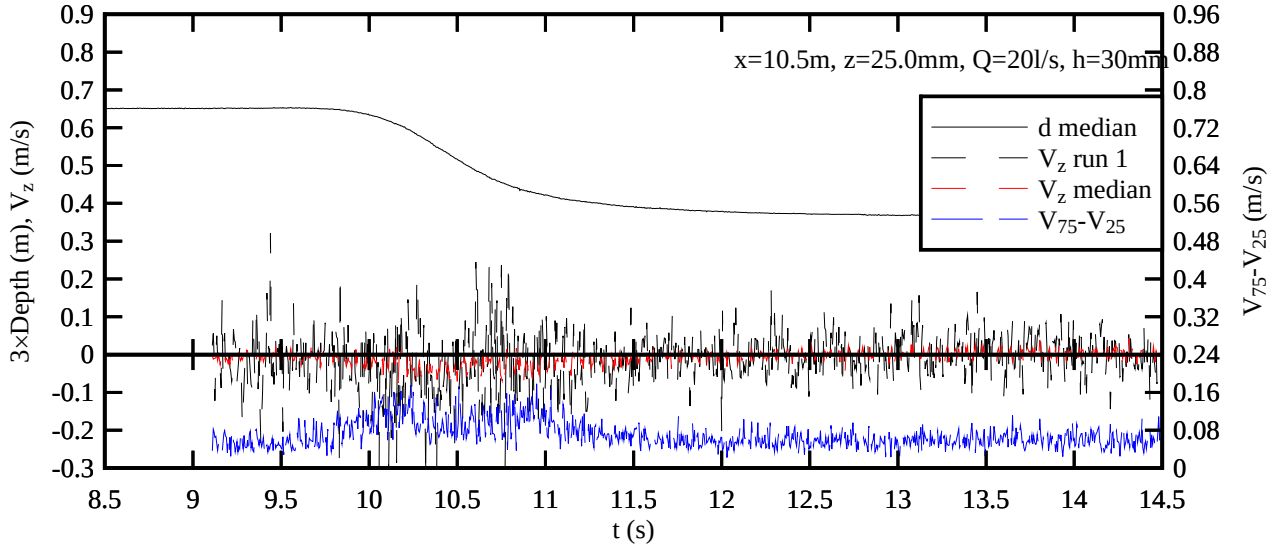
x=10.5m, z=25.0mm, Q=20l/s, h=30mm
3×Depth (m), V_z (m/s)
V_{75}-V_{25} (m/s)
t (s)
d median
V_z run 1
V_z median
V_{75}-V_{25}

(B) $z/d_o = 0.114$

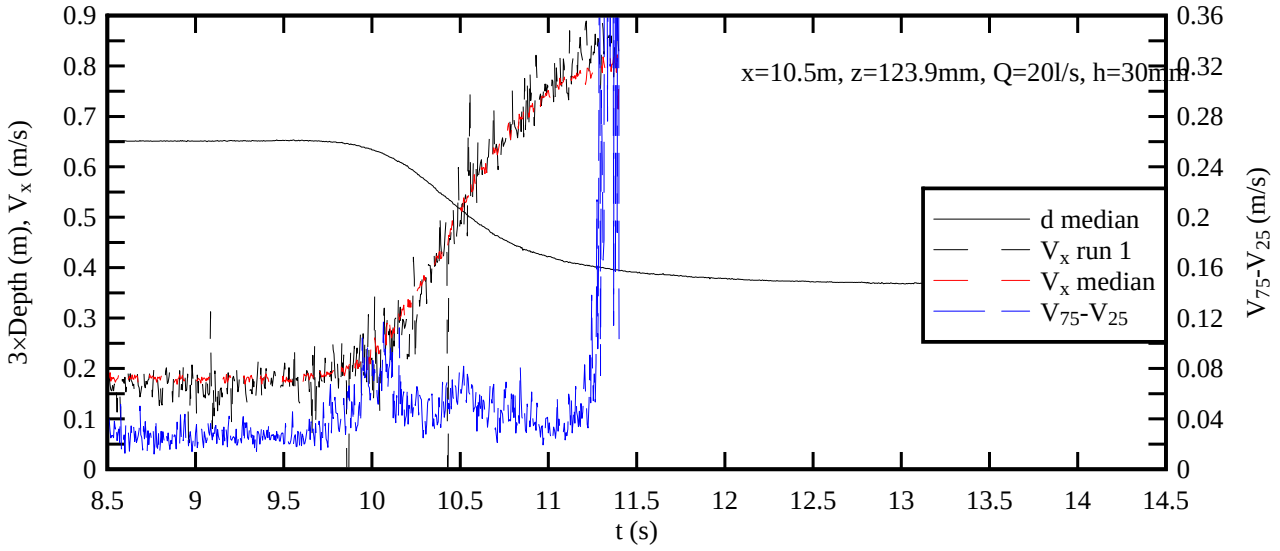

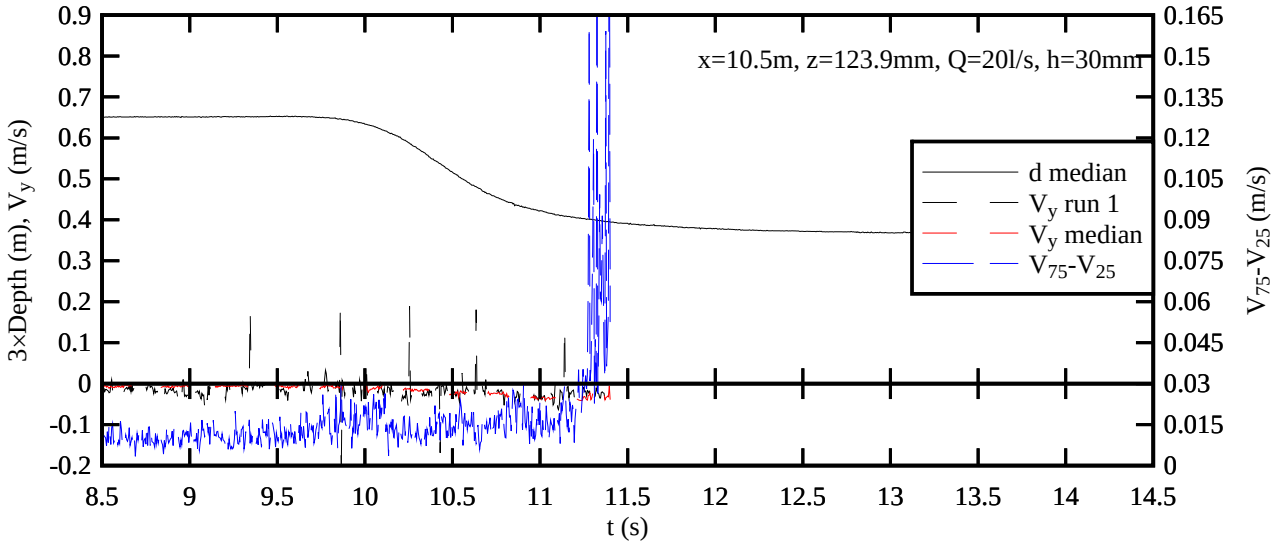

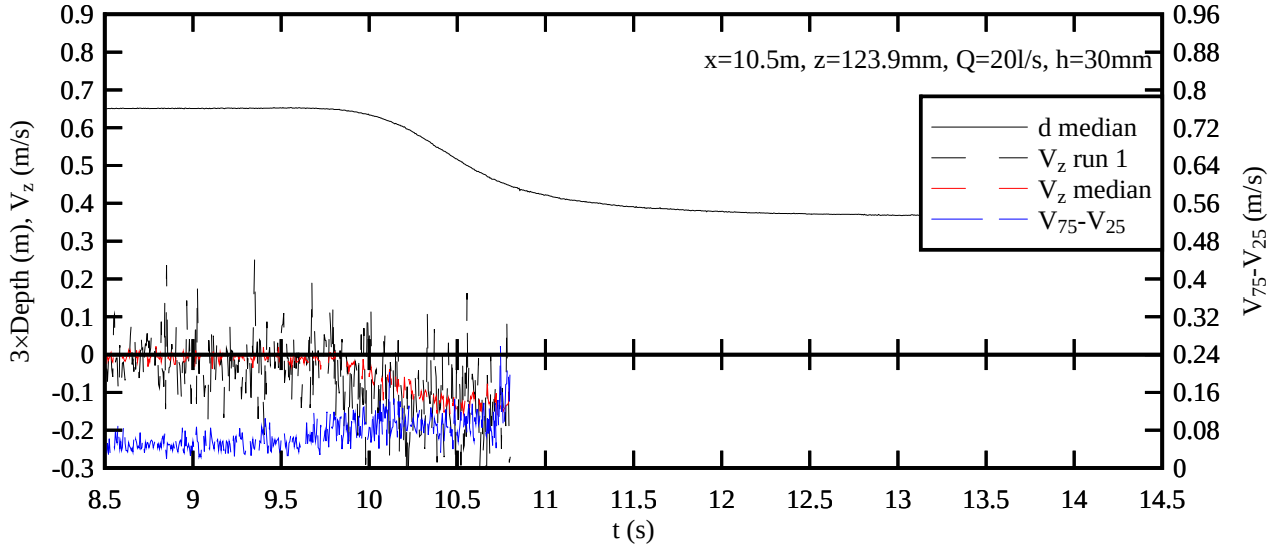

(C) z/d_o = 0.563 - Note that the probe was out of water for t > 10.8 to 11.4 s

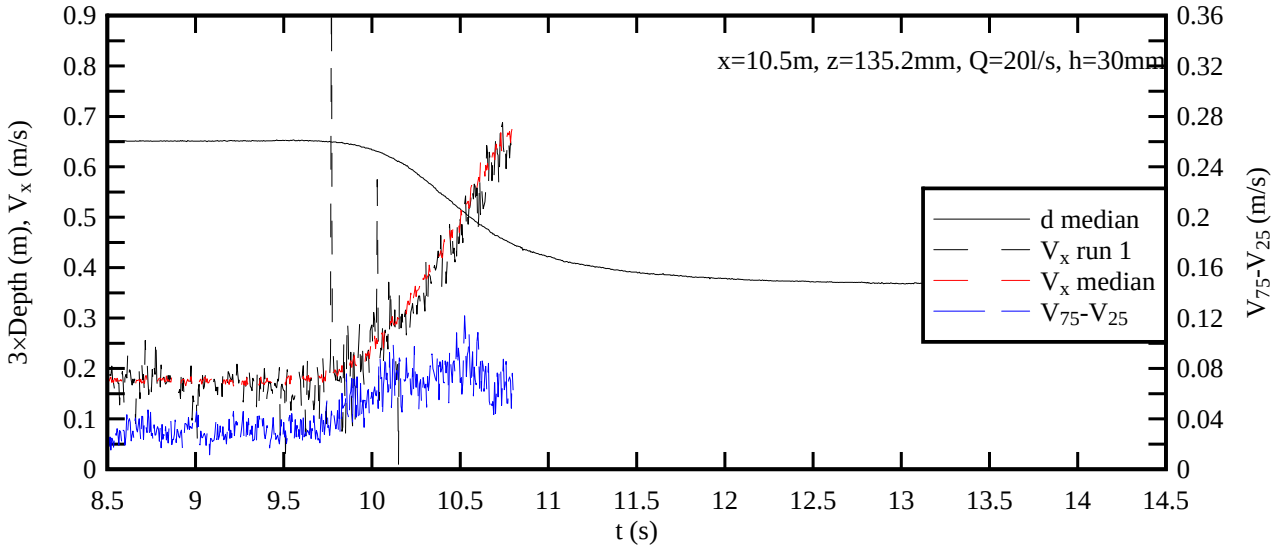

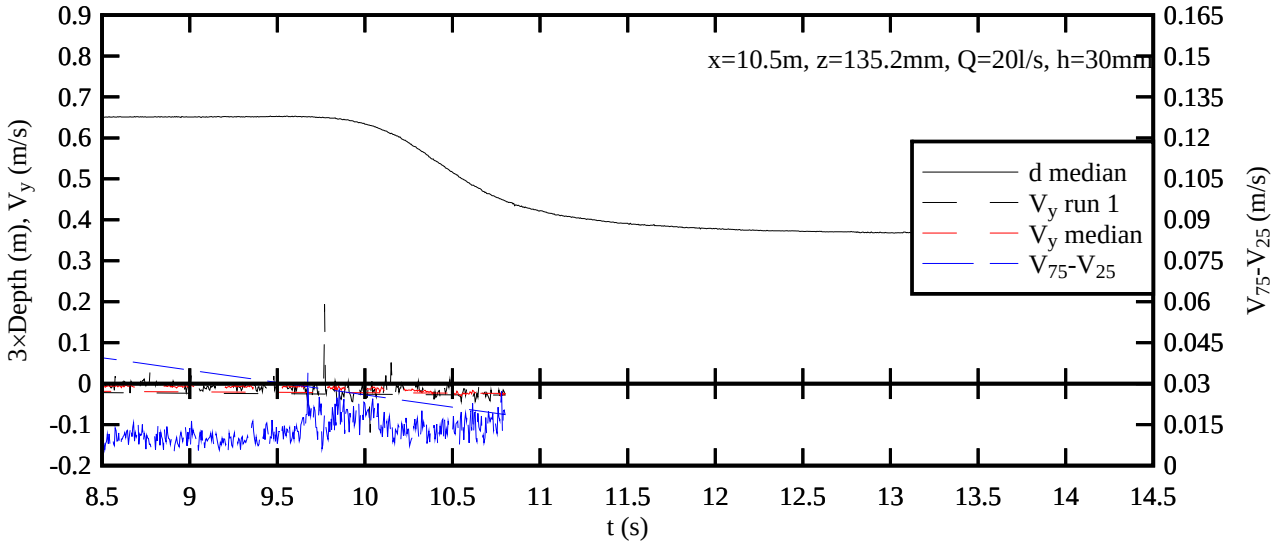

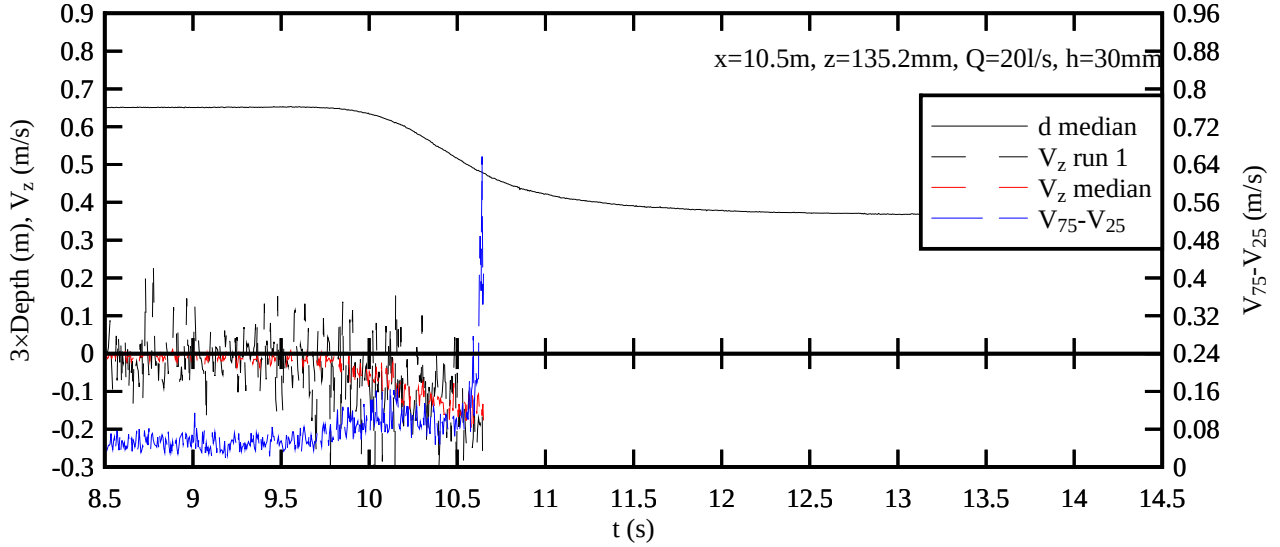

(D) z/d_o = 0.615 - Note that the probe was out of water for t > 10.65 to 10.8 s

Fig. D-2 - Ensemble-median water depth d_{median}, median velocity components and difference

between the 3rd and 1st quartiles (V_{75}-V_{25}) beneath a negative surge at x = 10.5 m (0.65 m upstream of gate) - From top to bottom: V_x, V_y, V_z - Flow conditions: Q = 0.020 m^3/s, h = 0.030 m, x = 10.5 m

APPENDIX D - TURBULENT REYNOLDS STRESS MEASUREMENTS IN A NEGATIVE SURGE

D.1 PRESENTATION

In a turbulent flow, the instantaneous velocity may be separated into an average component plus a turbulent fluctuation:

$$V = \overline{V} + v \tag{D-1}$$

where V is the instantaneous velocity, $\overline{V}$ is the average velocity, and v is the instantaneous fluctuation. In steady flows, $\overline{V}$ is the time-averaged velocity. When the flow is unsteady, the notion of time-average is meaningless. Instead the long-term and short-term turbulent fluctuations must be processed separately. In periodic flows, $\overline{V}$ may be taken as the phase-averaged velocity. In a transient flow, the mean motion is determined by ensemble-averaging (Bradshaw 1971, Schlichting and Gersten 2000). That is, the experiment is repeated N times and the ensemble-averaged velocity is:

$$\overline{V} = \frac{1}{N}\sum_{i-1}^{N} V_i \tag{D-2}$$

where the subscript i refers to the experimental run. When the number N of experiments is small, the ensemble-average is best replaced the ensemble median value. The turbulent velocity fluctuation v becomes the deviation of the instantaneous velocity V from the ensemble median $\overline{V}$.

In turbulent flows, the Reynolds stress tensor is a transport effect resulting from turbulent motion induced by velocity fluctuations with its subsequent increase of momentum exchange and of mixing (Piquet 1999). Herein the instantaneous turbulent Reynolds stresses were calculated using the ensemble-averaging (EA) technique for the experimental flow conditions summarised in Table D-1.

Table D-1 - Experimental flow conditions for turbulent stress measurements in negative surges

Q	S_o	h	d_o	V_o	ADV location	
					x	z
(m^3/s)			(m)	(m/s)	(m)	(m)
(1)	(2)	(3)	(4)	(5)	(6)	(7)
0.020	0.000	0.030	0.22	0.18	6.0	0.00669, 0.12394, 0.1352
					10.5	0.00669, 0.02501, 0.12394, 0.1352

Notes: d_o initial flow depth at x = 6 m; Q: initial flow rate; S_o: bed slope; V_o initial flow velocity at x = 6 m; z: vertical elevation of sampling volume.

List of symbols

d	flow depth (m) measured normal to the invert;
d_o	initial flow depth (m) measured normal to the chute invert at x = 6 m;
g	gravity constant (m/s^2): g = 9.794 m/s^2 in Brisbane, Australia;
h	undershoot gate height (m) prior to sudden gate opening
Q	volume flow rate (m^3/s);
S_o	bed slope: $S_o = \sin\theta$;
V	instantaneous velocity component (m/s);
V_o	initial flow velocity (m/s) at x = 6 m;
v	instantaneous turbulent velocity fluctuation (m/s);
$\overline{V}$	ensemble-median velocity component (m/s).
x	longitudinal distance (m) measured from the channel upstream end, positive downstream;
z	distance (m) normal to the bed; it is the vertical distance (m) for a horizontal channel; for the fixed ravel bed, z is measured above the top of the gravel bed;
θ	bed slope angle with the horizontal, positive downwards;
ρ	water density (kg/m^3);

Subscript

o	initial flow conditions: i.e., upstream of the negative surge leading edge;
x	longitudinal direction positive downstream;
y	transverse direction positive towards the left;
z	vertical direction positive upwards;

Abbreviations

EA	ensemble average.

D.2 RESULTS

The basic results are presented herein in terms of the median Reynolds stress components calculated using an ensemble-averaging (EA) method (median value of 25 runs). The results are presented in Figures D-1 and D-2 for x = 6 m and x = 10.5 m respectively. (The gate was located at x = 1.15 m.) The latter location was close to the gate while the former was 5.15 m upstream of the tainter gate.

The experimental results showed a number of basic features. Overall the turbulent stress data suggested that the passage of a negative surge was associated with large turbulent stresses at all vertical elevations. That is, the magnitude of turbulent Reynolds stress components was

significantly larger than in the initially steady flow and than in the final flow (after the passage of the surge). Note that the data presented some noise when the ADV receivers started to become out of water (z/d_o = 0.56 & 0.61). At these two upper locations, the signal was cut once the ADV head became out of water (Fig. D-2C & D2-D).

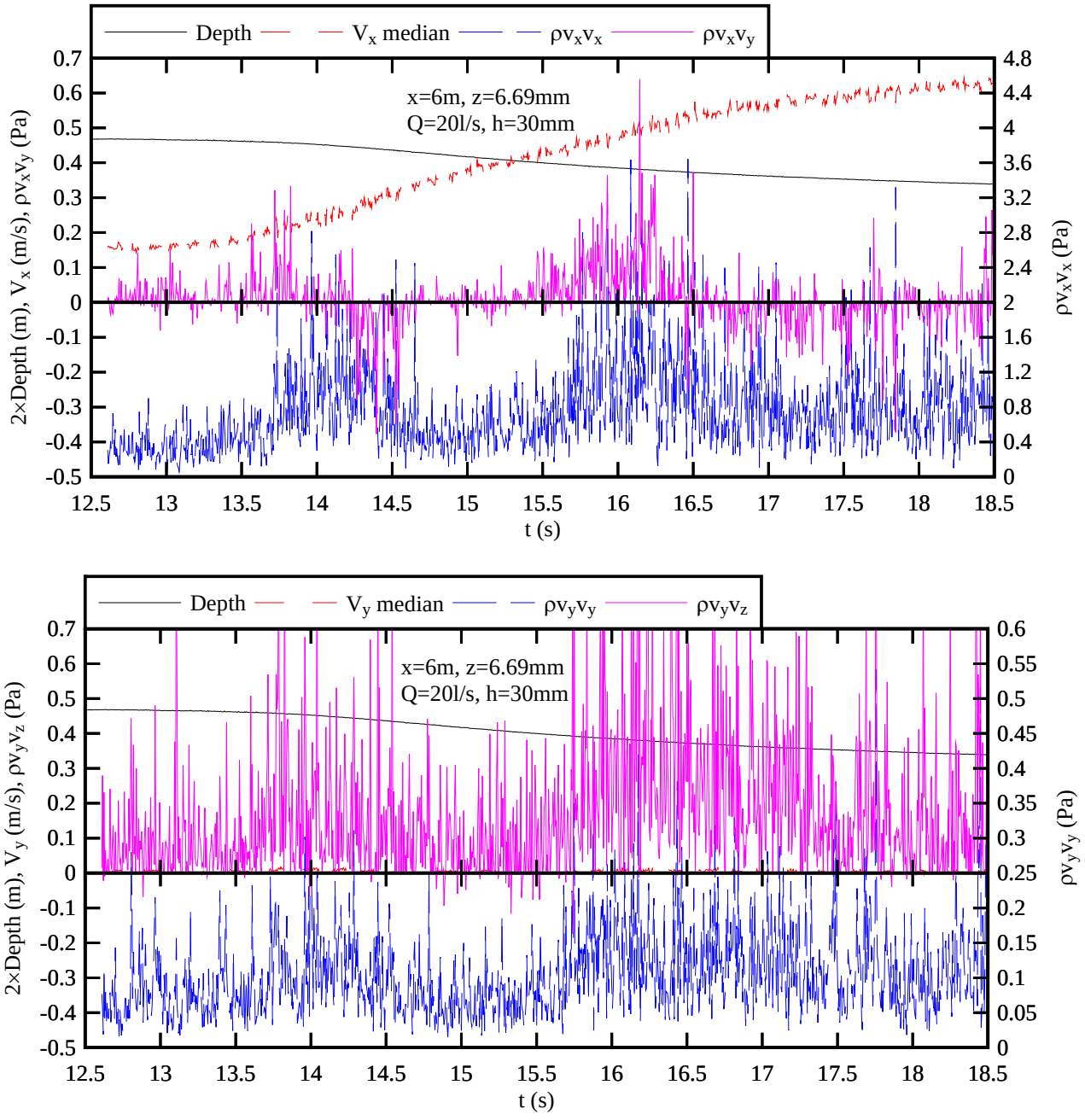

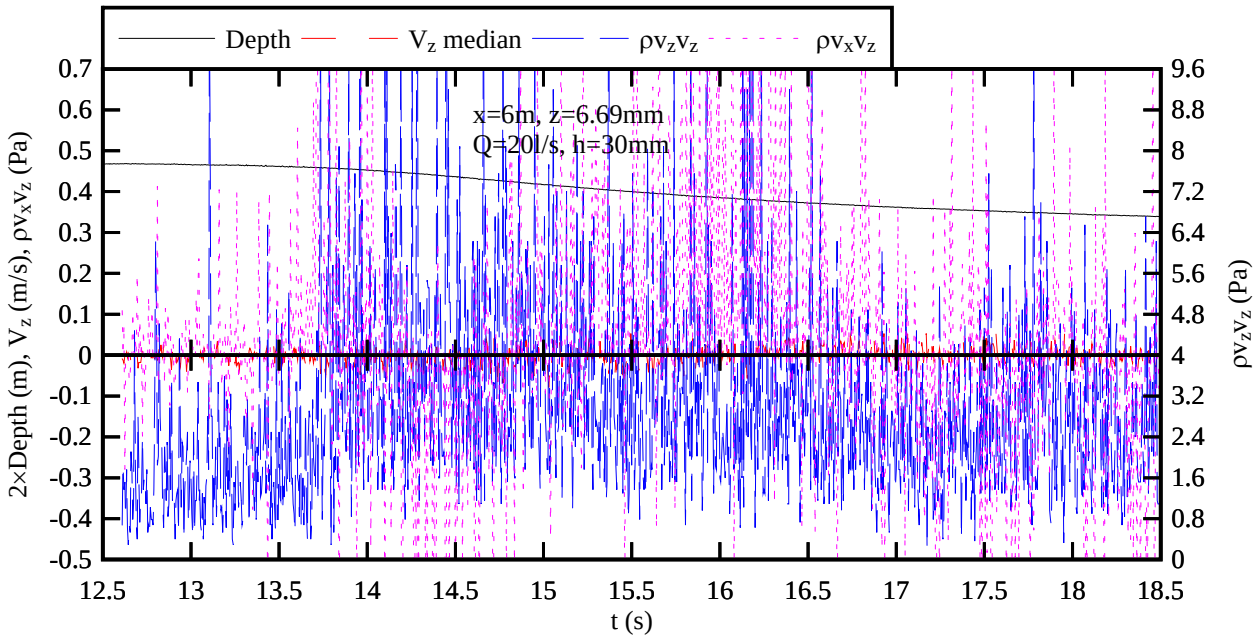
Depth
V_z median
$\rho v_z v_z$
$\rho v_x v_z$
x=6m, z=6.69mm
Q=20l/s, h=30mm
2×Depth (m), V_z (m/s), $\rho v_x v_z$ (Pa)
$\rho v_z v_z$ (Pa)
t (s)

(A) $z/d_o = 0.030$

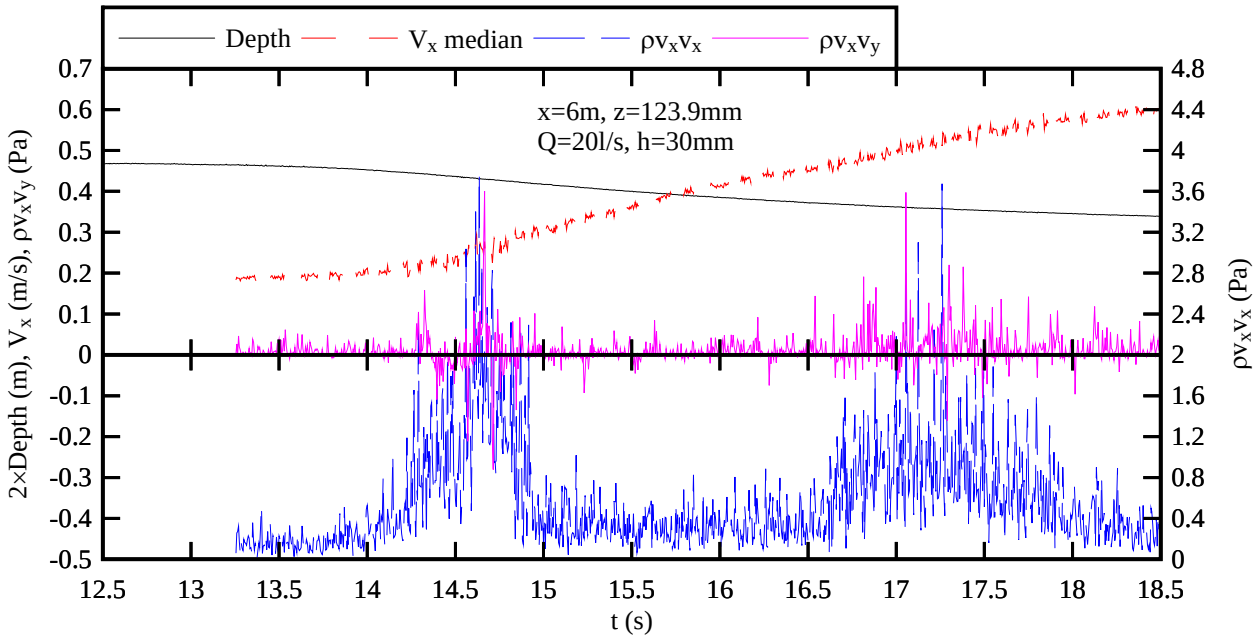
Depth
V_x median
$\rho v_x v_x$
$\rho v_x v_y$
x=6m, z=123.9mm
Q=20l/s, h=30mm
2×Depth (m), V_x (m/s), $\rho v_x v_y$ (Pa)
$\rho v_x v_x$ (Pa)
t (s)

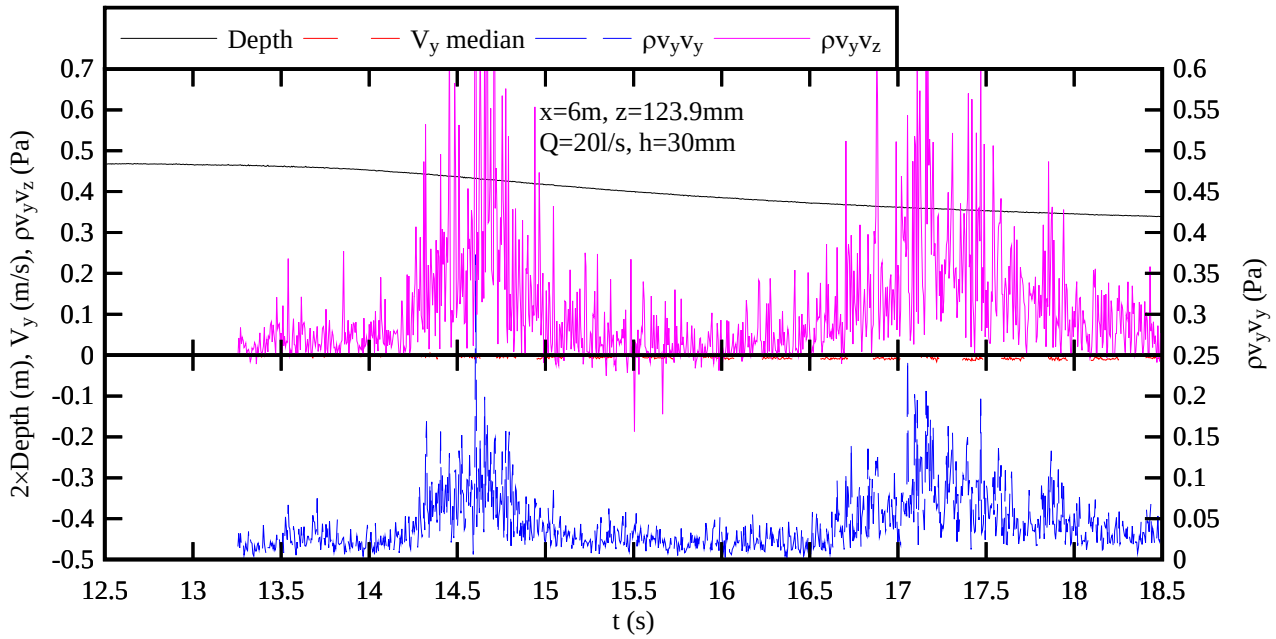
Depth
V_y median
$\rho v_y v_y$
$\rho v_y v_z$
x=6m, z=123.9mm
Q=20l/s, h=30mm
2×Depth (m), V_y (m/s), $\rho v_y v_z$ (Pa)
$\rho v_y v_y$ (Pa)
t (s)

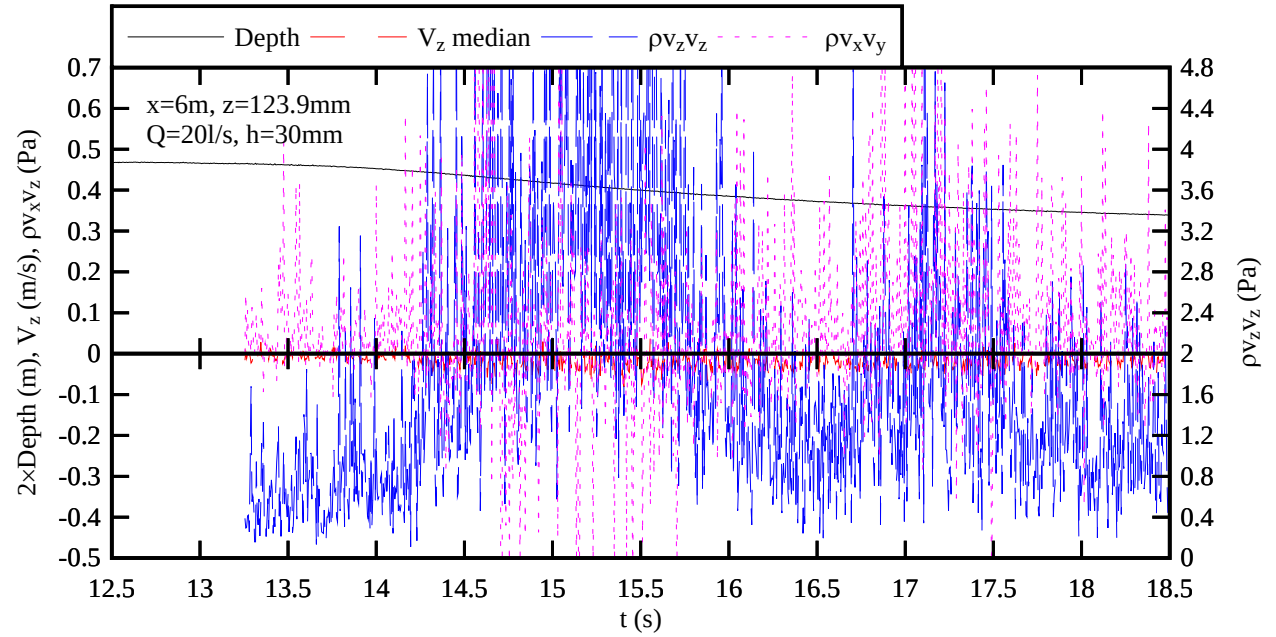
Depth
V_z median
$\rho v_z v_z$
$\rho v_x v_y$
x=6m, z=123.9mm
Q=20l/s, h=30mm
2×Depth (m), V_z (m/s), $\rho v_x v_z$ (Pa)
$\rho v_z v_z$ (Pa)
t (s)

(B) $z/d_o = 0.563$

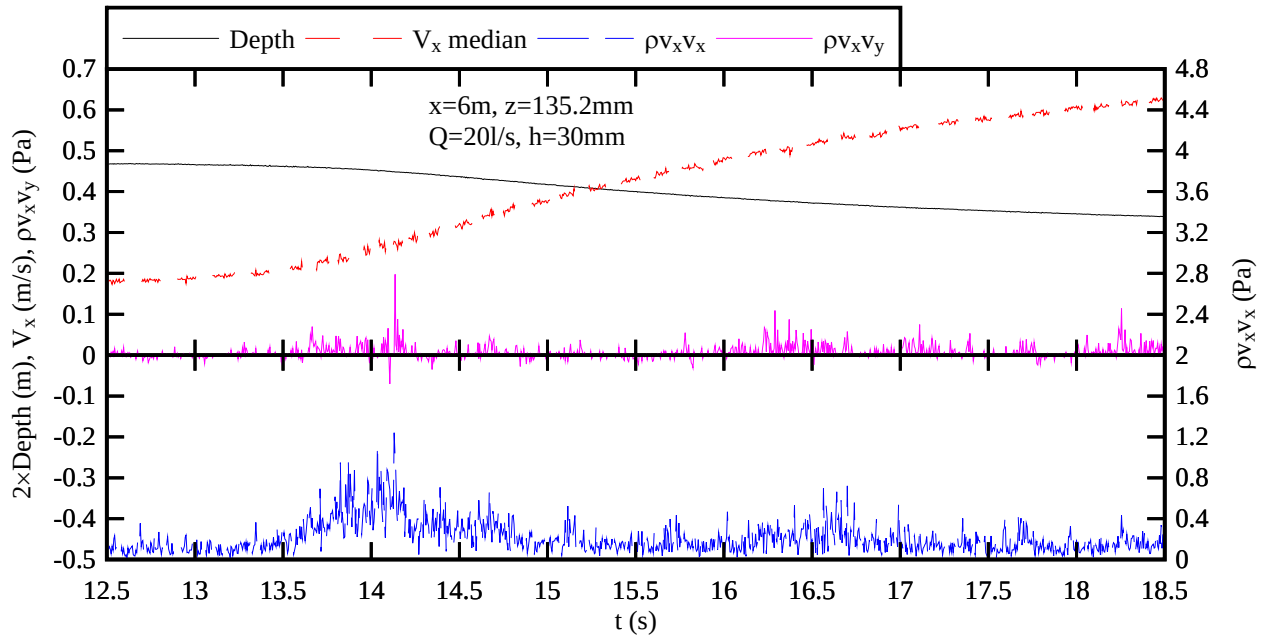
Depth
Vx median
ρvxvx
ρvxvy
x=6m, z=135.2mm
Q=20l/s, h=30mm
2×Depth (m), Vx (m/s), ρvxvy (Pa)
ρvxvx (Pa)
t (s)

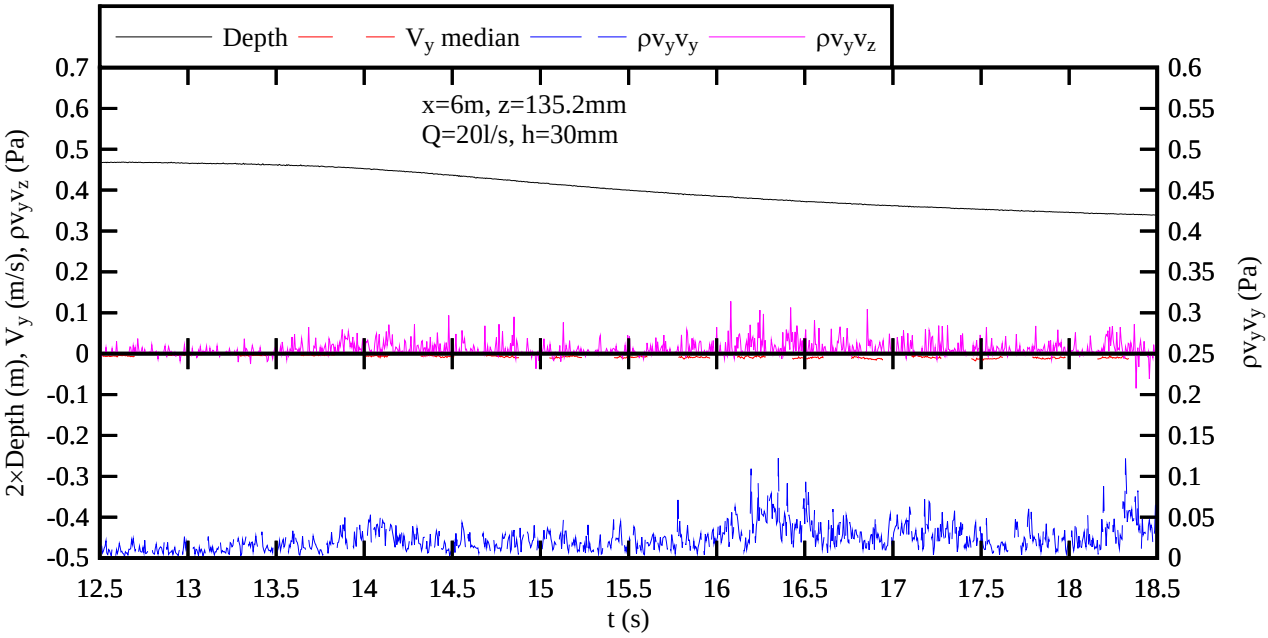
Depth
Vy median
ρvyvy
ρvyvz
x=6m, z=135.2mm
Q=20l/s, h=30mm
2×Depth (m), Vy (m/s), ρvyvz (Pa)
ρvyvy (Pa)
t (s)

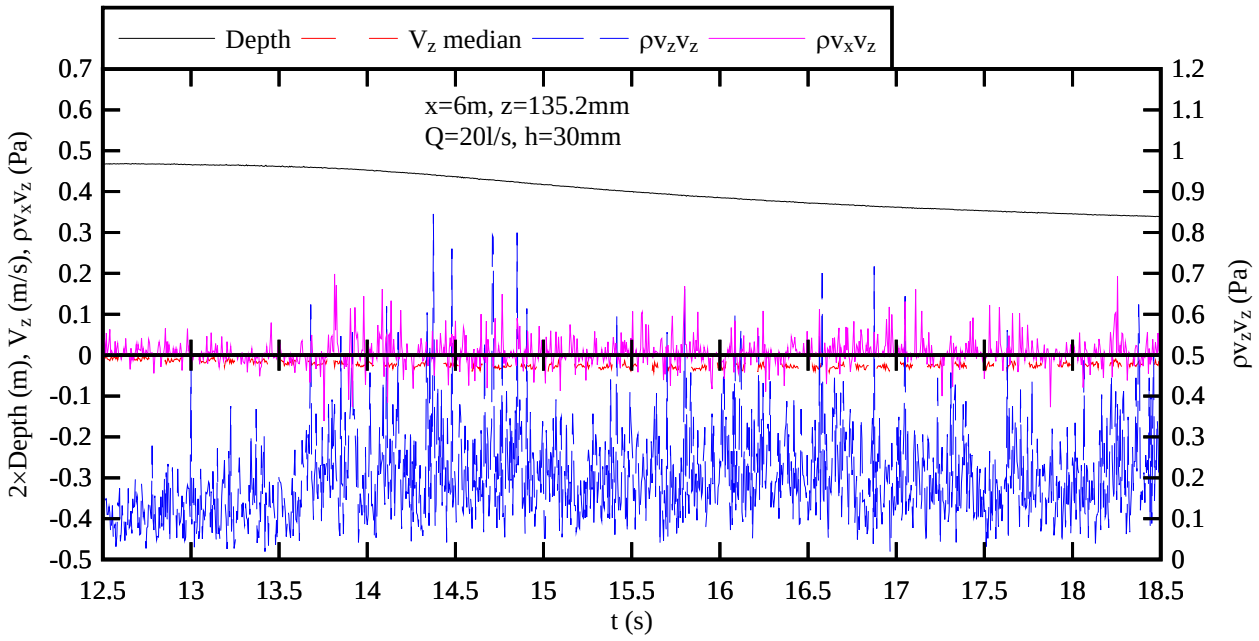

(D) $z/d_o = 0.615$

Fig. D-1 - Ensemble-median water depth d_{median} and velocity components, and median turbulent Reynolds stress tensor components beneath a negative surge at x = 6 m (5.15 m upstream of gate) - From top to bottom: (ρv_x^2, $\rho v_x v_y$), (ρv_y^2, $\rho v_y v_z$), (ρv_z^2, $\rho v_x v_z$) - Flow conditions: Q = 0.020 m^3/s, h = 0.030 m, x = 6.0 m

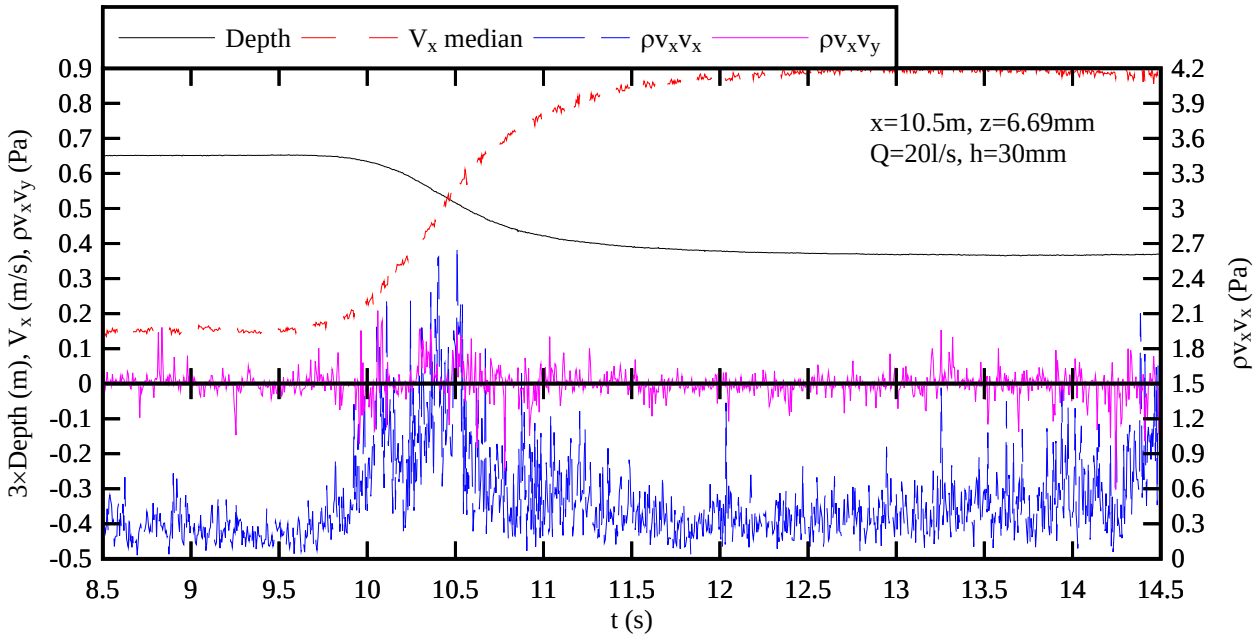

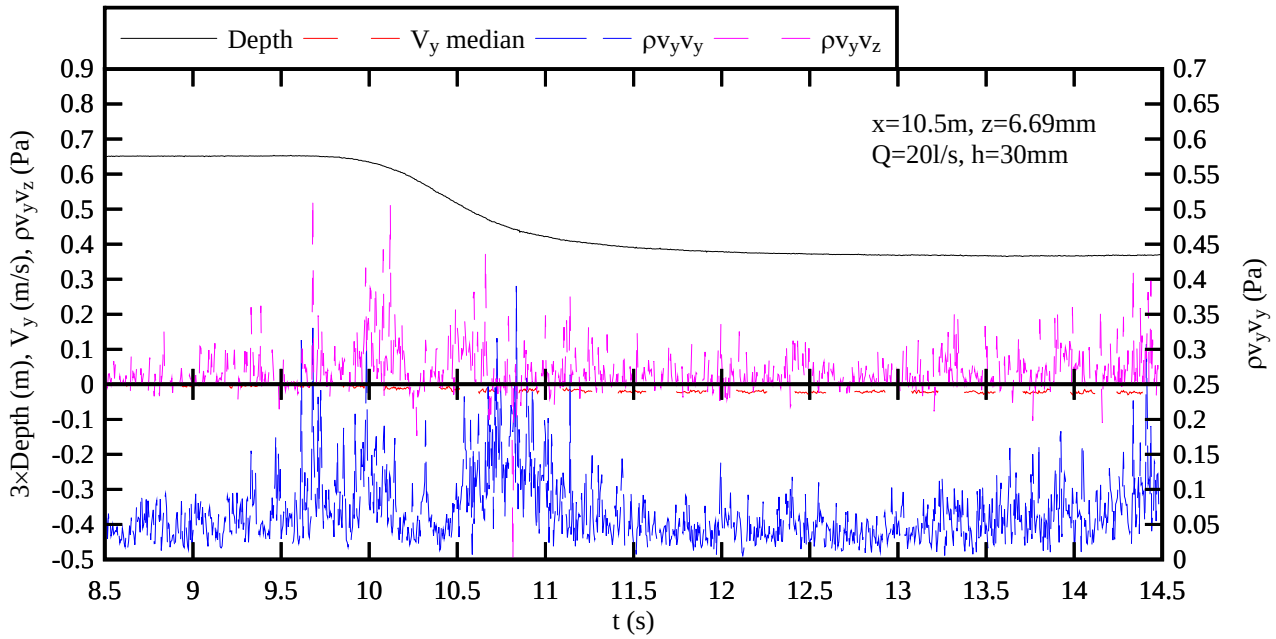
Depth
V_y median
$\rho v_y v_y$
$\rho v_y v_z$
x=10.5m, z=6.69mm
Q=20l/s, h=30mm
3×Depth (m), V_y (m/s), $\rho v_y v_z$ (Pa)
$\rho v_y v_y$ (Pa)
t (s)

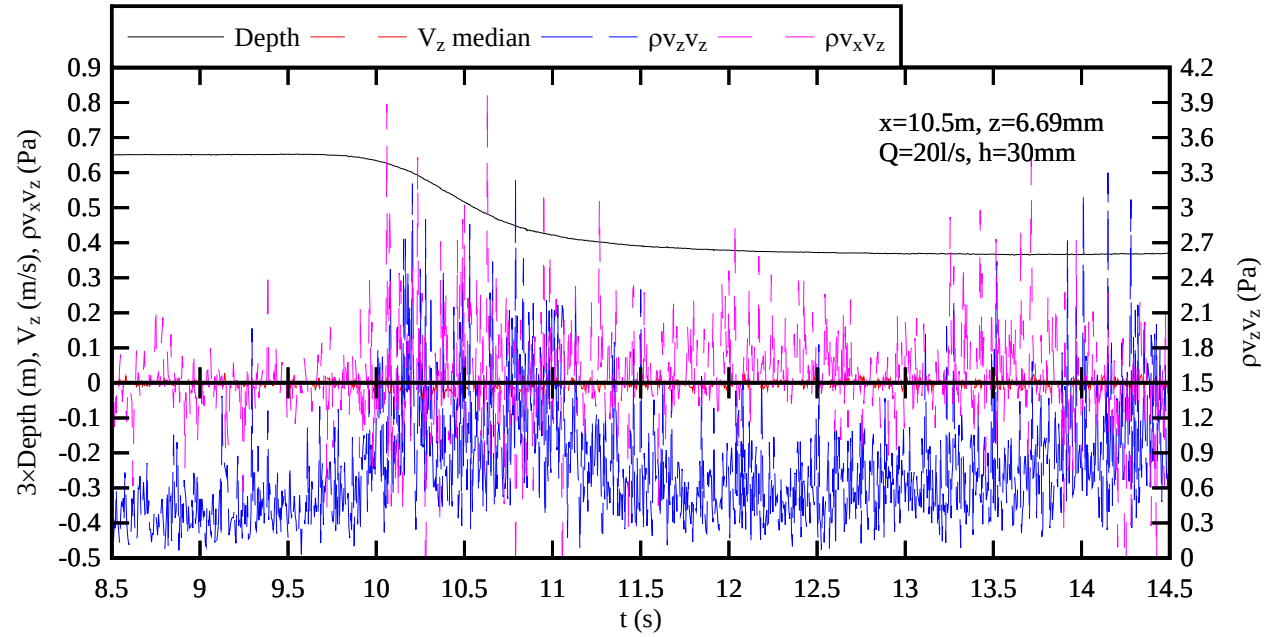
Depth
V_z median
$\rho v_z v_z$
$\rho v_x v_z$
x=10.5m, z=6.69mm
Q=20l/s, h=30mm
3×Depth (m), V_z (m/s), $\rho v_x v_z$ (Pa)
$\rho v_z v_z$ (Pa)
t (s)

(A) $z/d_o = 0.030$

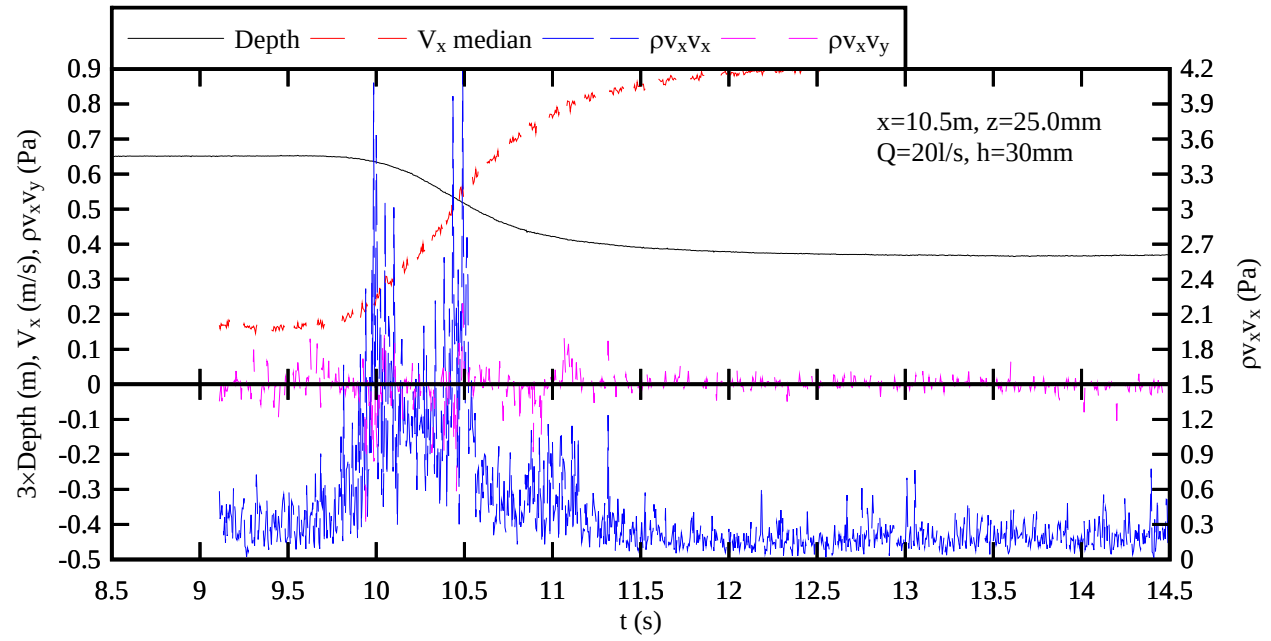
Depth
Vx median
ρvxvx
ρvxvy
x=10.5m, z=25.0mm
Q=20l/s, h=30mm
3×Depth (m), Vx (m/s), ρvxvy (Pa)
ρvxvx (Pa)
t (s)

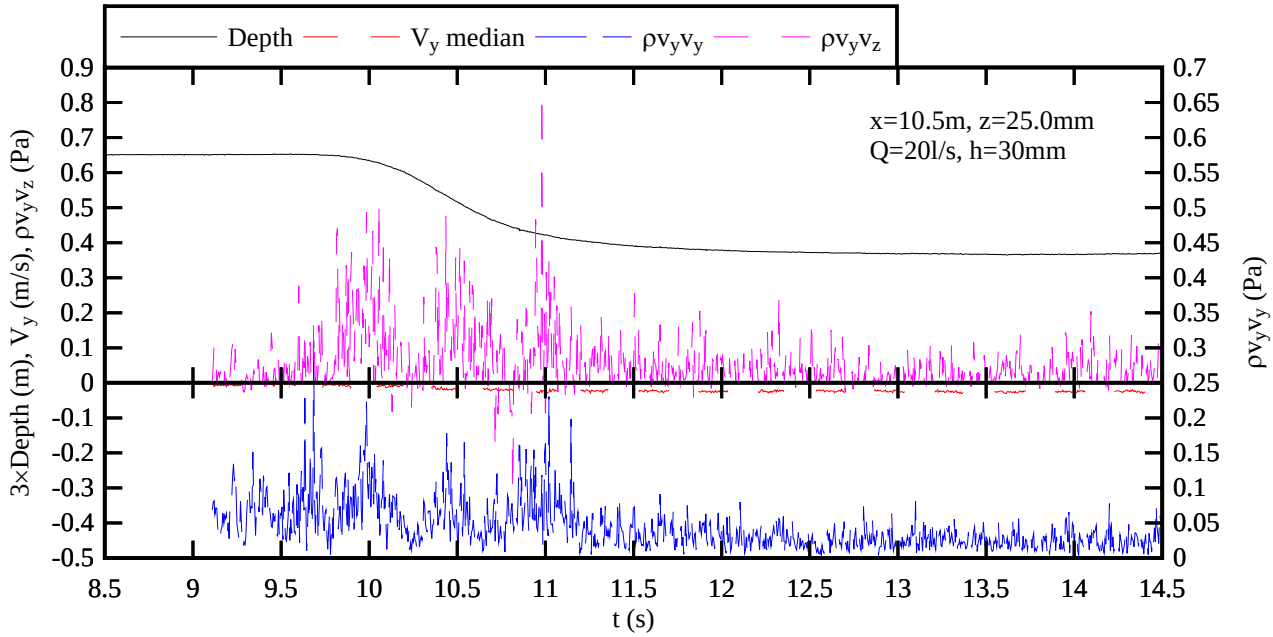
Depth
Vy median
ρvyvy
ρvyvz
x=10.5m, z=25.0mm
Q=20l/s, h=30mm
3×Depth (m), Vy (m/s), ρvyvz (Pa)
ρvyvy (Pa)
t (s)

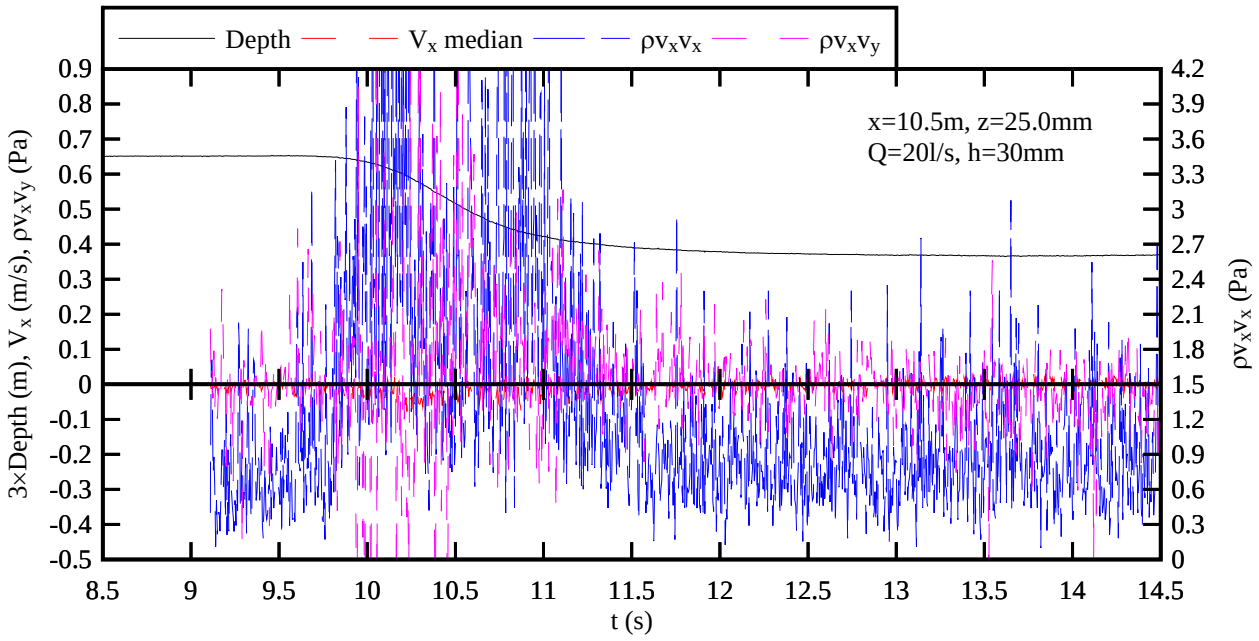
Depth
V_x median
$\rho v_x v_x$
$\rho v_x v_y$
x=10.5m, z=25.0mm
Q=20l/s, h=30mm
3×Depth (m), V_x (m/s), $\rho v_x v_y$ (Pa)
$\rho v_x v_x$ (Pa)
t (s)

(B) $z/d_o = 0.114$

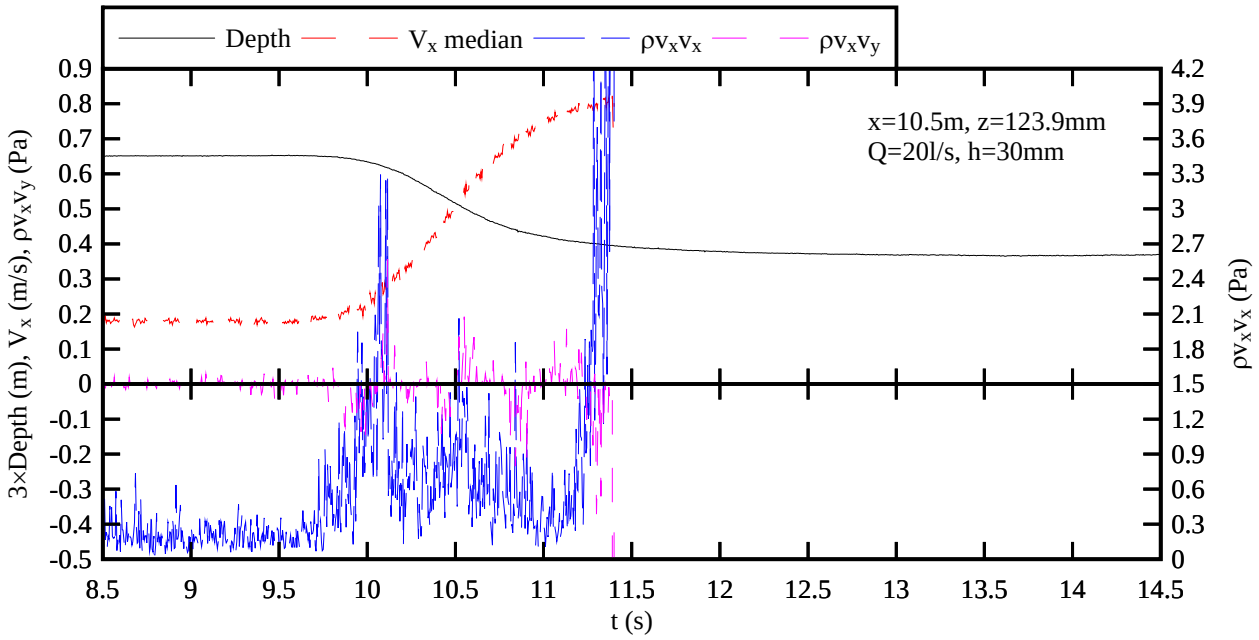
Depth
V_x median
$\rho v_x v_x$
$\rho v_x v_y$
x=10.5m, z=123.9mm
Q=20l/s, h=30mm
3×Depth (m), V_x (m/s), $\rho v_x v_y$ (Pa)
$\rho v_x v_x$ (Pa)
t (s)

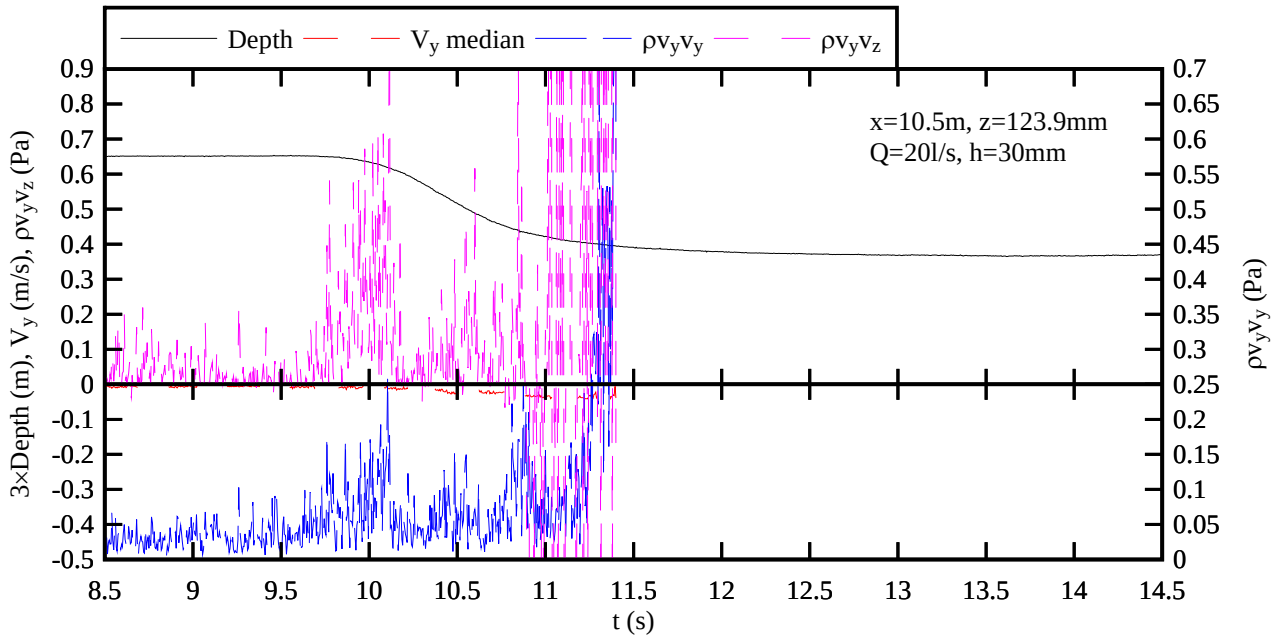

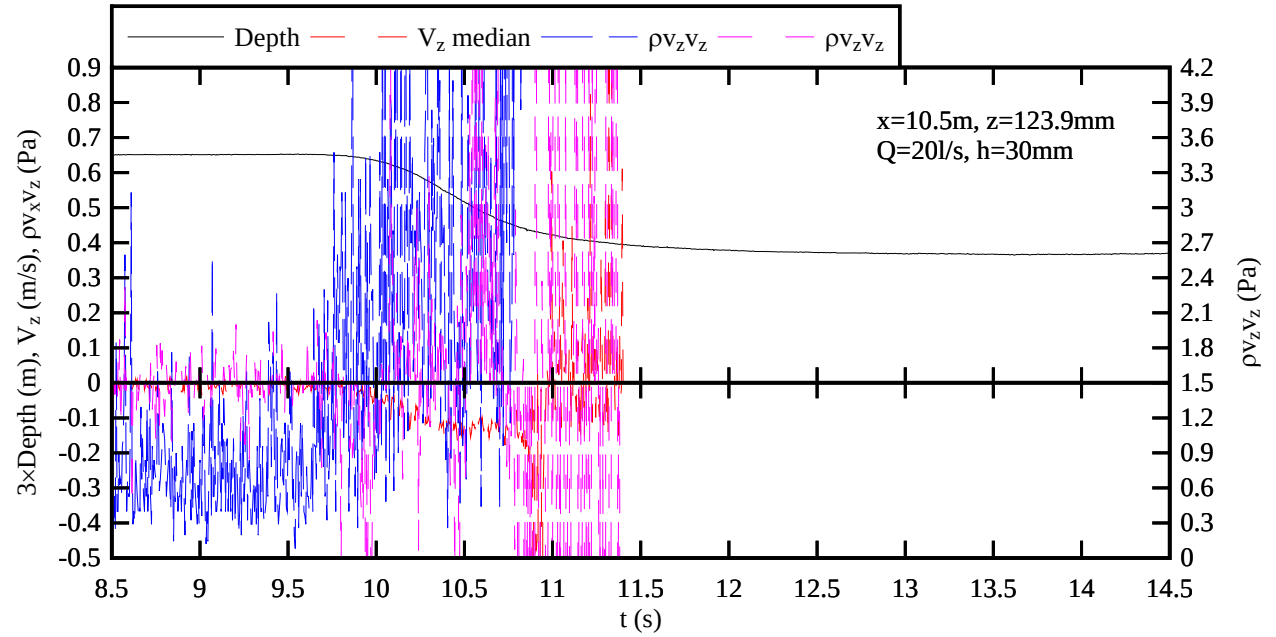

(C) z/d_o = 0.563 - Note that the probe was out of water for t > 10.8 to 11.4 s

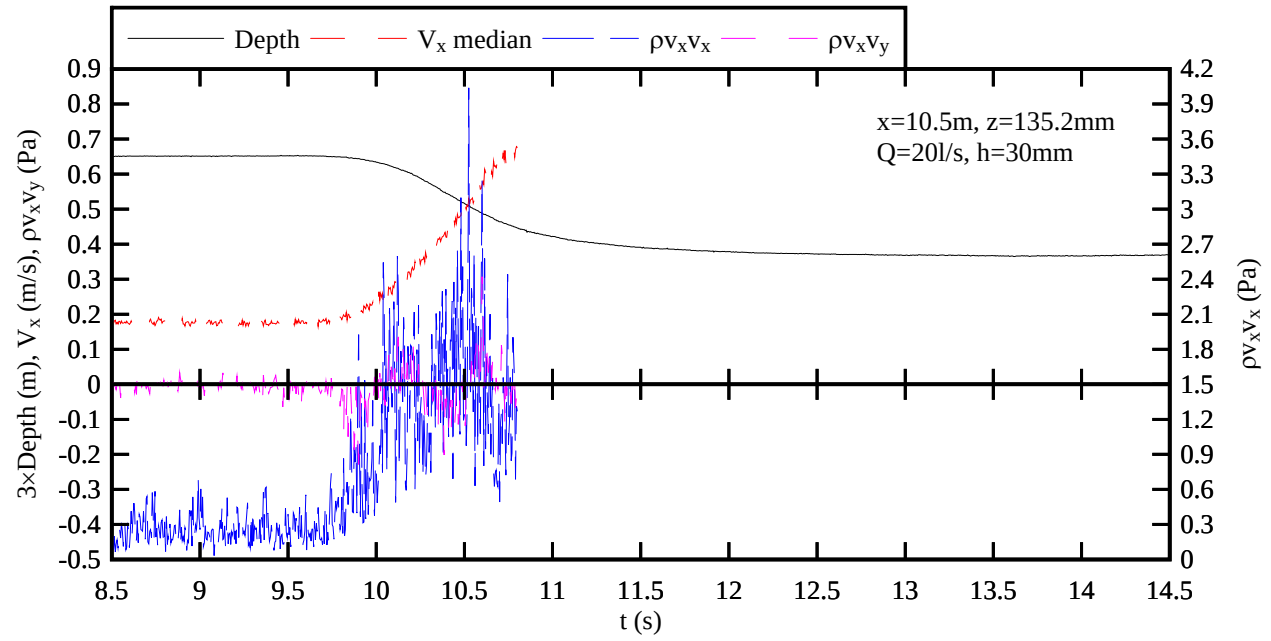
Depth
V_x median
$\rho v_x v_x$
$\rho v_x v_y$
x=10.5m, z=135.2mm
Q=20l/s, h=30mm
3×Depth (m), V_x (m/s), $\rho v_x v_y$ (Pa)
$\rho v_x v_x$ (Pa)
t (s)

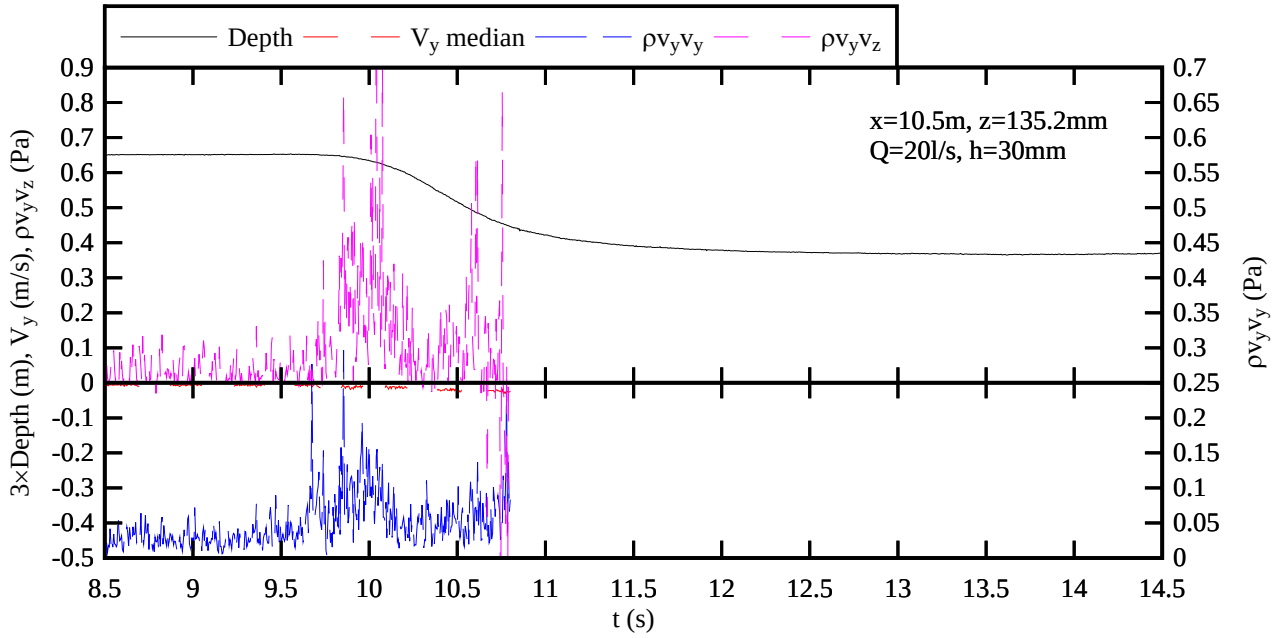
Depth
V_y median
$\rho v_y v_y$
$\rho v_y v_z$
x=10.5m, z=135.2mm
Q=20l/s, h=30mm
3×Depth (m), V_y (m/s), $\rho v_y v_z$ (Pa)
$\rho v_y v_y$ (Pa)
t (s)

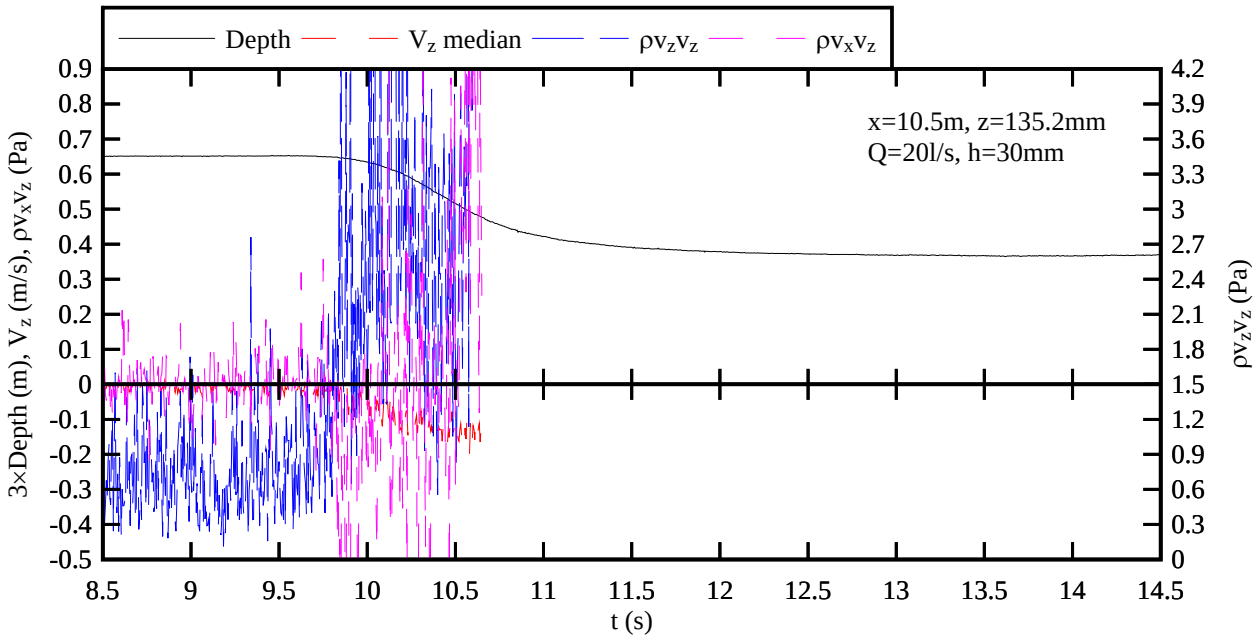

(D) z/d_o = 0.615 - Note that the probe was out of water for t > 10.65 to 10.8 s

Fig. D-2 - Ensemble-median water depth d_{median} and velocity components, and median turbulent Reynolds stress tensor components beneath a negative surge at x = 10.5 m (0.65 m upstream of gate) - From top to bottom: (ρv_x^2, $\rho v_x v_y$), (ρv_y^2, $\rho v_y v_z$), (ρv_z^2, $\rho v_x v_z$) - Flow conditions: Q = 0.020 m^3/s, h = 0.030 m, x = 10.5 m

APPENDIX E - NUMERICAL MODELLING OF A NEGATIVE SURGE WITH FLOW-3D™

E.1 PRESENTATION

Flow-3D™ is a computational fluid dynamics CFD model developed by Flow Science Inc. (Flow Science 2007). Flow-3D™ calculates the velocity components and pressure at the nodes of a orthogonal finite difference grid. The free surfaces are modelled with the Volume of Fluid (VOF) technique. The VOF method consists of a scheme to locate the surface, an algorithm to track the surface as a sharp interface moving through a computational grid, and a means of applying boundary conditions at the surface.

In the present study, the numerical model was set up using Flow-3D™ version 9.3. The model was set up with an incompressible fluid flow and a free surface. The fluid properties were set as air and water at 20 C for all calculations. The viscosity and turbulence options were selected with Newtonian viscosity and the renormalisation group (RNG) turbulence model that used a dynamically computed maximum turbulence mixing length.

The geometry for the model was a simple rectangular channel with the same width and depth as the experimental channel although the total length of the channel was extended by 0.8 m to reduce boundary effects. The channel was modelled in two dimensions (instead of three) to reduce simulation time. The gate was simulated using the general moving object (GMO). The GMO settings were set as prescribed motion with 6 degree of freedom (6-DOF). The initial location of the reference point was selected in the middle of the gate at x = 11.2 m, y = 0.25 m and z = 0.25 m. The gate was operated using the translational velocity component in the space system with a velocity of a non-sinusoidal movement in the z direction of +1 m/s for the negative surge. The gate opening was selected to maximise model stability. The gate movement for the simulations was vertical which is slightly different from the tainter gate operation in the physical model.

The Reynolds-averaged Navier-Stokes (RANS) equations are the fundamental underlying equations solved by Flow-3D™. The time steps were set as default except the initial time step which was adjusted down to 0.0002 s for initial model stability. A small initial time step was necessary for the simulations as the gate opening using the GMO application resulted in an initially less stable model environment. The time step size was controlled by stability and convergence. The pressure solver option was selected as implicit with automatic limited compressibility and the implicit solver option was generalised minimum residual (GMRES). The simulations were calculated using the explicit solver options. The difference between the explicit and implicit solver options are that the explicit solution is solved progressively at each computational cell by stepping trough time, while the time step is restricted to meet stability criteria. On the other hand the implicit solution is solved in each

time step using the information from a previous time step, which requires more complex interactive or matrix solution but does not impose time step restrictions. The models were run calculating both the momentum and continuity equation with a first order momentum advection.

E.2 DISCUSSION

An uniform mesh size was selected and a sensitivity analysis was performed using three different uniform mesh sizes of 5 mm, 15 mm and 30 mm to assess the impact of mesh size on the free-surface profile of the negative surge. Typical results are presented in Figure E-1.

The results indicated that the CFD model reproduced the physical data of negative surge qualitatively well. All the simulation with 5 mm, 15 mm and 30 mm mesh sizes showed that the water surface depth decreased more slowly than the experimental observations. The results with 5 mm uniform mesh size compared best with the data. The results for 15 mm and 30 mm mesh sizes yielded a lesser agreement with the observations, with little differences between 15 mm and 30 mm mesh size results (Fig. E-1). As a result, all calculations were performed with the 5 mm mesh size.

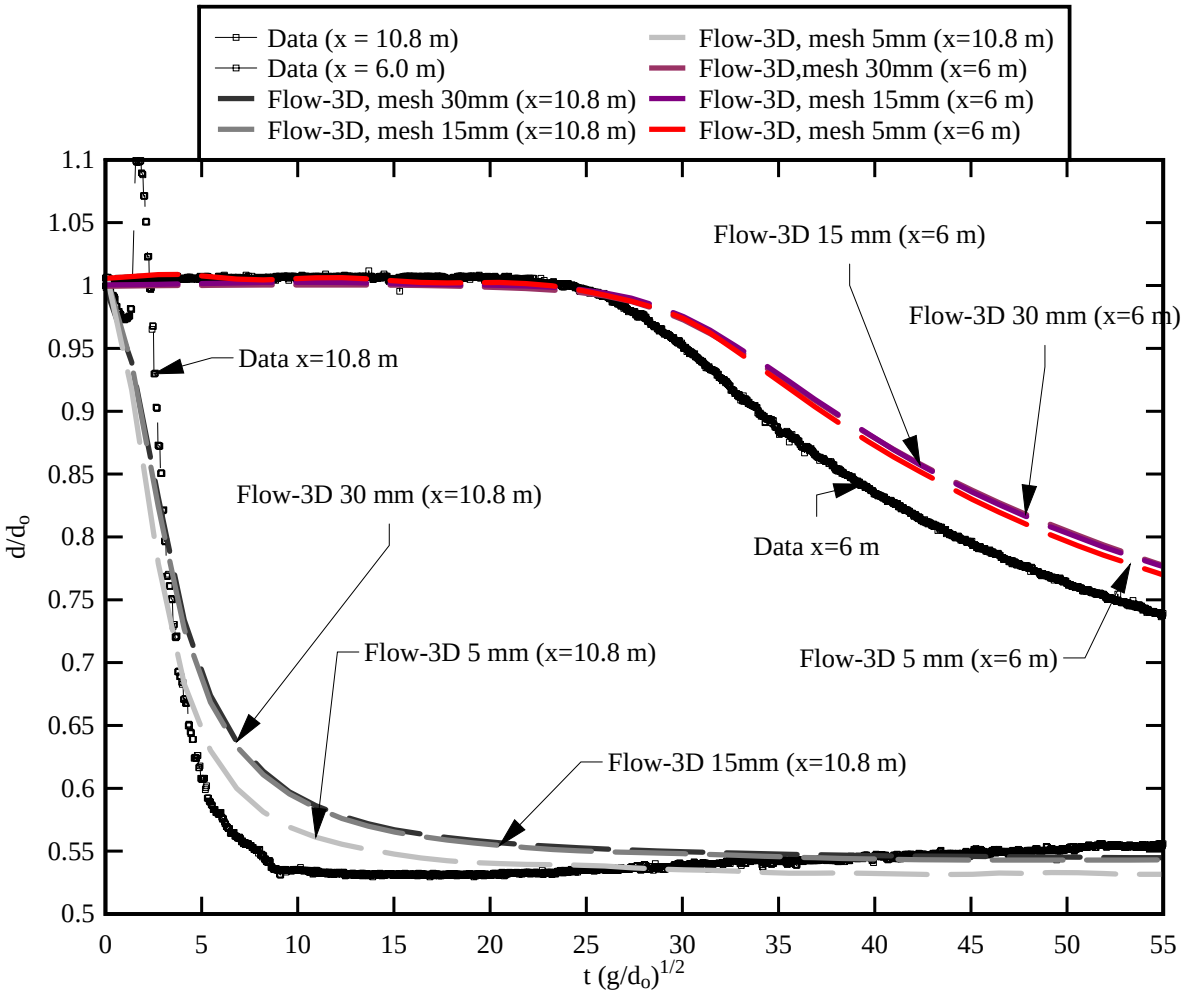

Fig. E-1 - Dimensionless free-surface profile during the negative surge: comparison between

physical and numerical data at x = 6 and 10. 8 m - Flow conditions: Q = 0.020 m^3/s, h = 0.030 m, x = 6.0 & 10.8 m

REFERENCES

Bradshaw, P. (1971). "An Introduction to Turbulence and its Measurement." *Pergamon Press*, Oxford, UK, The Commonwealth and International Library of Science and technology Engineering and Liberal Studies, Thermodynamics and Fluid Mechanics Division, 218 pages.

British Standard (1943). "Flow Measurement." *British Standard Code BS 1042:1943*, British Standard Institution, London.

Chanson, H. (1999). "The Hydraulics of Open Channel Flow: An Introduction." *Edward Arnold*, London, UK, 512 pages.

Chanson, H. (2004). "Environmental Hydraulics of Open Channel Flows." *Elsevier-Butterworth-Heinemann*, Oxford, UK, 483 pages.

Chanson, H. (2009). "Applied Hydrodynamics: An Introduction to Ideal and Real Fluid Flows." *CRC Press*, Taylor & Francis Group, Leiden, The Netherlands, 478 pages.

Courant, R., Isaacson, E., and Rees, M. (1952). "On the Solution of Non-Linear Hyperbolic Differential Equations byFinite Differences." *Comm. Pure Appl. Math.*, Vol. 5, pp. 243-255.

Favre, H. (1935). "Etude Théorique et Expérimentale des Ondes de Translation dans les Canaux Découverts." ('Theoretical and Experimental Study of Travelling Surges in Open Channels.') *Dunod*, Paris, France (in French).

Flow Science (2007). "Flow-3D User's Manuals." *Flow Science Inc.*, Version 9.2, Santa Fe NM, USA.

Graf, W.H. (1971). "Hydraulics of Sediment Transport". *McGraw-Hill*, New York, USA.

He, S., Ariyaratne, C., and Vardy, A.E. (2011). "Wall shear stress in accelerating turbulent pipe flow." *Jl Fluid Mech.*, Vol. 685, pp. 440-460 (DOI: 10.1017/jfm.2011.328).

Henderson, F.M. (1966). "Open Channel Flow." *MacMillan Company*, New York, USA.

Jaeger, C. (1956). "Engineering Fluid Mechanics." *Blackie & Son*, Glasgow, UK, 529 pages.

Johnson, T.V. (1991). "The Study of Unsteady Pipe Flow and Non-Uniform Channel Flow by the Use of Laser Doppler Anemometry." *Ph.D. thesis*, Dept of Civil Engineering, The University of Queensland, Brisbane, Australia.

Julien, P.Y. (1995). "Erosion and Sedimentation." *Cambridge University Press*, Cambridge, UK, 280 pages.

Koch, C., and Chanson, H. (2005). "An Experimental Study of Tidal Bores and Positive Surges: Hydrodynamics and Turbulence of the Bore Front." *Report No. CH56/05*, Dept. of Civil Engineering, The University of Queensland, Brisbane, Australia, July, 170 pages.

Koch, C., and Chanson, H. (2009). "Turbulence Measurements in Positive Surges and Bores." *Journal of Hydraulic Research*, IAHR, Vol. 47, No. 1, pp. 29-40 (DOI: 10.3826/jhr.2009.2954).

Lauber, G. (1997). "Experimente zur Talsperrenbruchwelle im glatten geneigten Rechteckkanal." ('Dam Break Wave Experiments in Rectangular Channels.') *Ph.D. thesis*, VAW-ETH, Zürich, Switzerland (in German). (also *Mitteilungen der Versuchsanstalt fur Wasserbau, Hydrologie und Glaziologie*, ETH-Zurich, Switzerland, No. 152).

Lauber, G., and Hager, W.H. (1998). "Experiments to Dambreak Wave: Horizontal Channel." *Jl of Hyd. Res.*, IAHR, Vol. 36, No. 3, pp. 291-307.

Montes, J.S. (1998). "Hydraulics of Open Channel Flow." *ASCE Press*, New-York, USA, 697 pages.

Montes, J.S., and Chanson, H. (1998). "Characteristics of Undular Hydraulic Jumps. Results and Calculations." *Journal of Hydraulic Engineering*, ASCE, Vol. 124, No. 2, pp. 192-205.

Nortek (2009). "Vectrino Velocimeter User Guide." *Nortek AS*, Norway, 42 pages.

Piquet, J. (1999). "Turbulent Flows. Models and Physics." *Springer*, Berlin, Germany, 761 pages.

Rijn, L.C. van (1984). "Sediment transport, Part II: Suspended load transport." *Journal of Hydraulic Engineering*, ASCE, Vol. 110, No. 11, pp. 1613–1641.

Rouse, H. (1946). "Elementary Mechanics of Fluids." *John Wiley & Sons*, New York, USA, 376 pages.

Schlichting, H., and Gersten, K. (2000). "Boundary Layer Theory." *Springer Verlag*, Berlin, Germany, 8th edition., 707 pages.

Stacey, M.T., Monismith, S.G., and Burau, J.R. (1999). "Observations of Turbulence in a Partially Stratified Estuary." *Jl Phys. Ocean.*, Vol. 29, Aug., pp. 1950-1970.

Sturm, T.W. (2001). "Open Channel Hydraulics." *McGraw Hill*, Boston, USA, Water Resources and Environmental Engineering Series, 493 pages.

Tan, L. and Chu, V.H. (2010). "Lauber and Hager's Dam-break Wave Data for Numerical Model Validation." *Jl of Hyd. Res.*, IAHR, Vol. 47, No.4, pp. 524-528.

Trevethan, M., Chanson, H., and Brown, R. (2008). "Turbulent Measurements in a Small Subtropical Estuary with Semi-Diurnal Tides." *Journal of Hydraulic Engineering*, ASCE, Vol. 134, No. 11, pp. 1665-1670 (DOI: 10.1061/(ASCE)0733-9429(2008)134:11(1665)).

Bibliography

Chanson, H., and Docherty, N.J. (2010). "Unsteady Turbulence in Tidal Bores: Ensemble-Average or VITA?" *Proc. 17th Australasian Fluid Mechanics Conference*, Auckland, New Zealand, 5-9 Dec., G.D. Mallinson and J.E. Cater Editors, Paper 034, 4 pages

Chanson, H., and Docherty, N.J. (2012). "Turbulent Velocity Measurements in Open Channel Bores." *European Journal of Mechanics B/Fluids*, Vol. 31 (DOI 10.1016/j.euromechflu.2011.10.001). (In print)

Reichstetter, M., and Chanson, H. (2011). "Negative Surge in Open Channel: Physical, Numerical and Analytical Modelling." *Proc. 34th IAHR World Congress*, Brisbane, Australia, 26 June-1 July, Engineers Australia Publication, Eric Valentine, Colin Apelt, James Ball, Hubert Chanson, Ron Cox, Rob Ettema, George Kuczera, Martin Lambert, Bruce Melville and Jane Sargison Editors, pp. 2306-2313.

Internet bibliography

Research papers in hydraulic engineering (open access)	{http://espace.library.uq.edu.au/list/author_id/193/}

Bibliographic reference of the Report CH84/11

The Hydraulic Model research report series CH is a refereed publication published by the School of Civil Engineering at the University of Queensland, Brisbane, Australia.

The bibliographic reference of the present report is:

REICHSTETTER, M., and CHANSON, H. (2011). "Physical and Numerical Modelling of Negative Surges in Open Channels." *Hydraulic Model Report No. CH84/11*, School of Civil Engineering, The University of Queensland, Brisbane, Australia, 82 pages (ISBN 9781742720388).

The Report CH84/11 is available, in the present form, as a PDF file on the Internet at UQeSpace:

http://espace.library.uq.edu.au/

It is listed at:

http://espace.library.uq.edu.au/list/author_id/193/

HYDRAULIC MODEL RESEARCH REPORT CH

The Hydraulic Model Report CH series is published by the School of Civil Engineering at the University of Queensland. Orders of any reprint(s) of the Hydraulic Model Reports should be addressed to the School Secretary.

School Secretary, School of Civil Engineering, The University of Queensland
Brisbane 4072, Australia - Tel.: (61 7) 3365 3619 - Fax : (61 7) 3365 4599
Url: http://www.eng.uq.edu.au/civil/ Email: hodciveng@uq.edu.au

Report CH	**Unit price**	Quantity	**Total price**
REICHSTETTER, M., and CHANSON, H. (2011). "Physical and Numerical Modelling of Negative Surges in Open Channels." *Hydraulic Model Report No. CH84/11*, School of Civil Engineering, The University of Queensland, Brisbane, Australia, 82 pages (ISBN 9781742720388).	AUD$60.00		
BROWN, R., CHANSON, H., McINTOSH, D., and MADHANI, J. (2011). "Turbulent Velocity and Suspended Sediment Concentration Measurements in an Urban Environment of the Brisbane River Flood Plain at Gardens Point on 12-13 January 2011." *Hydraulic Model Report No. CH83/11*, School of Civil Engineering, The University of Queensland, Brisbane, Australia, 120 pages (ISBN 9781742720272).	AUD$60.00		
CHANSON, H. "The 2010-2011 Floods in Queensland (Australia): Photographic Observations, Comments and Personal Experience." *Hydraulic Model Report No. CH82/11*, School of Civil Engineering, The University of Queensland, Brisbane, Australia, 127 pages (ISBN 9781742720234).	AUD$60.00		
MOUAZE, D., CHANSON, H., and SIMON, B. (2010). "Field Measurements in the Tidal Bore of the Sélune River in the Bay of Mont Saint Michel (September 2010)." *Hydraulic Model Report No. CH81/10*, School of Civil Engineering, The University of Queensland, Brisbane, Australia, 72 pages (ISBN 9781742720210).	AUD$60.00		
JANSSEN, R., and CHANSON, H. (2010). "Hydraulic Structures: Useful Water Harvesting Systems or Relics." *Proceedings of the Third International Junior Researcher and Engineer Workshop on Hydraulic Structures (IJREWHS'10)*, 2-3 May 2010, Edinburgh, Scotland, R. JANSSEN and H. CHANSON (Eds), Hydraulic Model Report CH80/10, School of Civil Engineering, The University of Queensland, Brisbane, Australia, 211 pages (ISBN 9781742720159).	AUD$60.00		
CHANSON, H., LUBIN, P., SIMON, B., and REUNGOAT, D. (2010). "Turbulence and Sediment Processes in the Tidal Bore of the Garonne River: First Observations." *Hydraulic Model Report No. CH79/10*, School of Civil Engineering, The University of Queensland, Brisbane, Australia, 97 pages (ISBN 9781742720104).	AUD$60.00		
CHACHEREAU, Y., and CHANSON, H., (2010). "Free-Surface Turbulent Fluctuations and Air-Water Flow Measurements in Hydraulics Jumps with Small Inflow Froude Numbers." *Hydraulic Model Report No. CH78/10*, School of Civil Engineering, The University of Queensland, Brisbane, Australia, 133 pages (ISBN 9781742720036).	AUD$60.00		

CHANSON, H., BROWN, R., and TREVETHAN, M. (2010). " Turbulence Measurements in a Small Subtropical Estuary under King Tide Conditions." *Hydraulic Model Report No. CH77/10*, School of Civil Engineering, The University of Queensland, Brisbane, Australia, 82 pages (ISBN 9781864999969).	AUD$60.00		
DOCHERTY, N.J., and CHANSON, H. (2010). "Characterisation of Unsteady Turbulence in Breaking Tidal Bores including the Effects of Bed Roughness." *Hydraulic Model Report No. CH76/10*, School of Civil Engineering, The University of Queensland, Brisbane, Australia, 112 pages (ISBN 9781864999884).	AUD$60.00		
CHANSON, H. (2009). "Advective Diffusion of Air Bubbles in Hydraulic Jumps with Large Froude Numbers: an Experimental Study." *Hydraulic Model Report No. CH75/09*, School of Civil Engineering, The University of Queensland, Brisbane, Australia, 89 pages & 3 videos (ISBN 9781864999730).	AUD$60.00		
CHANSON, H. (2009). "An Experimental Study of Tidal Bore Propagation: the Impact of Bridge Piers and Channel Constriction." *Hydraulic Model Report No. CH74/09*, School of Civil Engineering, The University of Queensland, Brisbane, Australia, 110 pages and 5 movies (ISBN 9781864999600).	AUD$60.00		
CHANSON, H. (2008). "Jean-Baptiste Charles Joseph BÉLANGER (1790-1874), the Backwater Equation and the Bélanger Equation." *Hydraulic Model Report No. CH69/08*, Div. of Civil Engineering, The University of Queensland, Brisbane, Australia, 40 pages (ISBN 9781864999211).	AUD$60.00		
GOURLAY, M.R., and HACKER, J. (2008). "Reef-Top Currents in Vicinity of Heron Island Boat Harbour, Great Barrier Reef, Australia: 2. Specific Influences of Tides Meteorological Events and Waves." *Hydraulic Model Report No. CH73/08*, Div. of Civil Engineering, The University of Queensland, Brisbane, Australia, 331 pages (ISBN 9781864999365).	AUD$60.00		
GOURLAY, M.R., and HACKER, J. (2008). "Reef Top Currents in Vicinity of Heron Island Boat Harbour Great Barrier Reef, Australia: 1. Overall influence of Tides, Winds, and Waves." *Hydraulic Model Report CH72/08*, Div. of Civil Engineering, The University of Queensland, Brisbane, Australia, 201 pages (ISBN 9781864999358).	AUD$60.00		
LARRARTE, F., and CHANSON, H. (2008). "Experiences and Challenges in Sewers: Measurements and Hydrodynamics." *Proceedings of the International Meeting on Measurements and Hydraulics of Sewers*, Summer School GEMCEA/LCPC, 19-21 Aug. 2008, Bouguenais, Hydraulic Model Report No. CH70/08, Div. of Civil Engineering, The University of Queensland, Brisbane, Australia (ISBN 9781864999280).	AUD$60.00		
CHANSON, H. (2008). "Photographic Observations of Tidal Bores (Mascarets) in France." *Hydraulic Model Report No. CH71/08*, Div. of Civil Engineering, The University of Queensland, Brisbane, Australia, 104 pages, 1 movie and 2 audio files (ISBN 9781864999303).	AUD$60.00		
CHANSON, H. (2008). "Turbulence in Positive Surges and Tidal Bores. Effects of Bed Roughness and Adverse Bed Slopes." *Hydraulic Model Report No. CH68/08*, Div. of Civil Engineering, The University of Queensland, Brisbane, Australia, 121 pages & 5 movie files (ISBN 9781864999198)	AUD$70.00		
FURUYAMA, S., and CHANSON, H. (2008). "A Numerical Study of Open Channel Flow Hydrodynamics and Turbulence of the Tidal Bore and Dam-Break Flows." *Report No. CH66/08*, Div. of Civil Engineering, The University of Queensland, Brisbane, Australia, May, 88 pages (ISBN 9781864999068).	AUD$60.00		
GUARD, P., MACPHERSON, K., and MOHOUPT, J. (2008). "A Field Investigation into the Groundwater Dynamics of Raine Island." *Report No. CH67/08*, Div. of Civil Engineering, The University of Queensland, Brisbane, Australia, February, 21 pages (ISBN 9781864999075).	AUD$40.00		

FELDER, S., and CHANSON, H. (2008). "Turbulence and Turbulent Length and Time Scales in Skimming Flows on a Stepped Spillway. Dynamic Similarity, Physical Modelling and Scale Effects." *Report No. CH64/07*, Div. of Civil Engineering, The University of Queensland, Brisbane, Australia, March, 217 pages (ISBN 9781864998870).	AUD$60.00		
TREVETHAN, M., CHANSON, H., and BROWN, R.J. (2007). "Turbulence and Turbulent Flux Events in a Small Subtropical Estuary." Report No. CH65/07, Div. of Civil Engineering, The University of Queensland, Brisbane, Australia, November, 67 pages (ISBN 9781864998993)	AUD$60.00		
MURZYN, F., and CHANSON, H. (2007). "Free Surface, Bubbly flow and Turbulence Measurements in Hydraulic Jumps." *Report CH63/07*, Div. of Civil Engineering, The University of Queensland, Brisbane, Australia, August, 116 pages (ISBN 9781864998917).	AUD$60.00		
KUCUKALI, S., and CHANSON, H. (2007). "Turbulence in Hydraulic Jumps: Experimental Measurements." *Report No. CH62/07*, Div. of Civil Engineering, The University of Queensland, Brisbane, Australia, July, 96 pages (ISBN 9781864998825).	AUD$60.00		
CHANSON, H., TAKEUCHI, M, and TREVETHAN, M. (2006). "Using Turbidity and Acoustic Backscatter Intensity as Surrogate Measures of Suspended Sediment Concentration. Application to a Sub-Tropical Estuary (Eprapah Creek)." *Report No. CH60/06*, Div. of Civil Engineering, The University of Queensland, Brisbane, Australia, July, 142 pages (ISBN 1864998628).	AUD$60.00		
CAROSI, G., and CHANSON, H. (2006). "Air-Water Time and Length Scales in Skimming Flows on a Stepped Spillway. Application to the Spray Characterisation." *Report No. CH59/06*, Div. of Civil Engineering, The University of Queensland, Brisbane, Australia, July (ISBN 1864998601).	AUD$60.00		
TREVETHAN, M., CHANSON, H., and BROWN, R. (2006). "Two Series of Detailed Turbulence Measurements in a Small Sub-Tropical Estuarine System." *Report No. CH58/06*, Div. of Civil Engineering, The University of Queensland, Brisbane, Australia, Mar. (ISBN 1864998520).	AUD$60.00		
KOCH, C., and CHANSON, H. (2005). "An Experimental Study of Tidal Bores and Positive Surges: Hydrodynamics and Turbulence of the Bore Front." *Report No. CH56/05*, Dept. of Civil Engineering, The University of Queensland, Brisbane, Australia, July (ISBN 1864998245).	AUD$60.00		
CHANSON, H. (2005). "Applications of the Saint-Venant Equations and Method of Characteristics to the Dam Break Wave Problem." *Report No. CH55/05*, Dept. of Civil Engineering, The University of Queensland, Brisbane, Australia, May (ISBN 1864997966).	AUD$60.00		
CHANSON, H., COUSSOT, P., JARNY, S., and TOQUER, L. (2004). "A Study of Dam Break Wave of Thixotropic Fluid: Bentonite Surges down an Inclined plane." *Report No. CH54/04*, Dept. of Civil Engineering, The University of Queensland, Brisbane, Australia, June, 90 pages (ISBN 1864997710).	AUD$60.00		
CHANSON, H. (2003). "A Hydraulic, Environmental and Ecological Assessment of a Sub-tropical Stream in Eastern Australia: Eprapah Creek, Victoria Point QLD on 4 April 2003." *Report No. CH52/03*, Dept. of Civil Engineering, The University of Queensland, Brisbane, Australia, June, 189 pages (ISBN 1864997044).	AUD$90.00		
CHANSON, H. (2003). "Sudden Flood Release down a Stepped Cascade. Unsteady Air-Water Flow Measurements. Applications to Wave Run-up, Flash Flood and Dam Break Wave." *Report CH51/03*, Dept of Civil Eng., Univ. of Queensland, Brisbane, Australia, 142 pages (ISBN 1864996552).	AUD$60.00		
CHANSON, H,. (2002). "An Experimental Study of Roman Dropshaft Operation : Hydraulics, Two-Phase Flow, Acoustics." *Report CH50/02*, Dept of Civil Eng., Univ. of Queensland, Brisbane, Australia, 99 pages (ISBN 1864996544).	AUD$60.00		

CHANSON, H., and BRATTBERG, T. (1997). "Experimental Investigations of Air Bubble Entrainment in Developing Shear Layers." *Report CH48/97*, Dept. of Civil Engineering, University of Queensland, Australia, Oct., 309 pages (ISBN 0 86776 748 0).	AUD$90.00		
CHANSON, H. (1996). "Some Hydraulic Aspects during Overflow above Inflatable Flexible Membrane Dam." *Report CH47/96*, Dept. of Civil Engineering, University of Queensland, Australia, May, 60 pages (ISBN 0 86776 644 1).	AUD$60.00		
CHANSON, H. (1995). "Flow Characteristics of Undular Hydraulic Jumps. Comparison with Near-Critical Flows." *Report CH45/95*, Dept. of Civil Engineering, University of Queensland, Australia, June, 202 pages (ISBN 0 86776 612 3).	AUD$60.00		
CHANSON, H. (1995). "Air Bubble Entrainment in Free-surface Turbulent Flows. Experimental Investigations." *Report CH46/95*, Dept. of Civil Engineering, University of Queensland, Australia, June, 368 pages (ISBN 0 86776 611 5).	AUD$80.00		
CHANSON, H. (1994). "Hydraulic Design of Stepped Channels and Spillways." *Report CH43/94*, Dept. of Civil Engineering, University of Queensland, Australia, Feb., 169 pages (ISBN 0 86776 560 7).	AUD$60.00		
POSTAGE & HANDLING (per report)	AUD$10.00		
GRAND TOTAL			

OTHER HYDRAULIC RESEARCH REPORTS

Reports/Theses	Unit price	Quantity	Total price
TREVETHAN, M. (2008). "A Fundamental Study of Turbulence and Turbulent Mixing in a Small Subtropical Estuary." Ph.D. thesis, Div. of Civil Engineering, The University of Queensland, 342 pages.	AUD$100.00		
GONZALEZ, C.A. (2005). "An Experimental Study of Free-Surface Aeration on Embankment Stepped Chutes." *Ph.D. thesis*, Dept of Civil Engineering, The University of Queensland, Brisbane, Australia, 240 pages.	AUD$80.00		
TOOMBES, L. (2002). "Experimental Study of Air-Water Flow Properties on Low-Gradient Stepped Cascades." *Ph.D. thesis*, Dept of Civil Engineering, The University of Queensland, Brisbane, Australia.	AUD$100.00		
CHANSON, H. (1988). "A Study of Air Entrainment and Aeration Devices on a Spillway Model." *Ph.D. thesis*, University of Canterbury, New Zealand.	AUD$60.00		
POSTAGE & HANDLING (per report)	AUD$10.00		
GRAND TOTAL			

CIVIL ENGINEERING RESEARCH REPORT CE

The Civil Engineering Research Report CE series is published by the School of Civil Engineering at the University of Queensland. Orders of any of the Civil Engineering Research Report CE should be addressed to the School Secretary.

School Secretary, School of Civil Engineering, The University of Queensland
Brisbane 4072, Australia
Tel.: (61 7) 3365 3619 Fax : (61 7) 3365 4599
Url: http://www.eng.uq.edu.au/civil/ Email: hodciveng@uq.edu.au

Recent Research Report CE	Unit price	Quantity	Total price
CALLAGHAN, D.P., NIELSEN, P., and CARTWRIGHT, N. (2006). "Data and Analysis Report: Manihiki and Rakahanga, Northern Cook Islands - For February and October/November 2004 Research Trips." *Research Report CE161*, Division of Civil Engineering, The University of Queensland (ISBN No. 1864998318).	AUD$10.00		
GONZALEZ, C.A., TAKAHASHI, M., and CHANSON, H. (2005). "Effects of Step Roughness in Skimming Flows: an Experimental Study." *Research Report No. CE160*, Dept. of Civil Engineering, The University of Queensland, Brisbane, Australia, July (ISBN 1864998105).	AUD$10.00		
CHANSON, H., and TOOMBES, L. (2001). "Experimental Investigations of Air Entrainment in Transition and Skimming Flows down a Stepped Chute. Application to Embankment Overflow Stepped Spillways." *Research Report No. CE158*, Dept. of Civil Engineering, The University of Queensland, Brisbane, Australia, July, 74 pages (ISBN 1 864995297).	AUD$10.00		
HANDLING (per order)	AUD$10.00		
GRAND TOTAL			

Note: Prices include postages and processing.

PAYMENT INFORMATION

1- VISA Card

Name on the card :	
Visa card number :	

Expiry date :	
Amount :	AUD$ .....

2- Cheque/remittance payable to: THE UNIVERSITY OF QUEENSLAND and crossed "Not Negotiable".

N.B. For overseas buyers, cheque payable in Australian Dollars drawn on an office in Australia of a bank operating in Australia, payable to: THE UNIVERSITY OF QUEENSLAND and crossed "Not Negotiable".

Orders of any Research Report should be addressed to the School Secretary.

School Secretary, School of Civil Engineering, The University of Queensland
Brisbane 4072, Australia - Tel.: (61 7) 3365 3619 - Fax : (61 7) 3365 4599
Url: http://www.eng.uq.edu.au/civil/ Email: hodciveng@uq.edu.au